2013

Redox-Initiated Adiabatic Emulsion Polymerization

Shi Wang
Lehigh University

REDOX-INITIATED ADIABATIC EMULSION POLYMERIZATION

By

SHI WANG

A Dissertation
Presented to the Graduate and Research Committee
of Lehigh University
in Candidacy for the Degree of
Doctor of Philosophy

in

Chemical Engineering

Lehigh University

(January 2013)

Certificate of Approval

Approved and recommended for acceptance as a dissertation in partial fulfillment of the requirements for the degree of Doctor of Philosophy.

_____
Date

_____
Accepted Date

_____
Professor Andrew Klein
Dissertation Director

Committee Members:

_____
Professor Andrew Klein
Committee Chair and Advisor

_____
Professor Mohamed S. El-Aasser
Co-Advisor

_____
Dr. Eric S. Daniels
Co-Advisor

_____
Professor Hugo S. Caram

_____
Professor Do Ik Lee

ACKNOWLEDGEMENTS

I would like to express my sincere gratitude and appreciation to the following persons for their contribution during six years of my Ph.D. study.

Professor A. Klein and Professor M. S. El-Aasser for their thoughtful advice, comments, guidance, encouragement and support throughout my study.

Dr. E. S. Daniels and Dr. E. D. Sudol for their suggestions, discussions and support for this project and correction of the GRPR reports and ARM presentations.

Professor D. I. Lee and Professor H. S. Caram for their valuable suggestions and discussions during this study and for serving as my committee members.

Dr. Z. Song, Dr. Y. Yang and Dr. L. Liu for their help with SEM and TEM.

Other EPI staff and students for their help and friendship.

My wife, Dr. A. Xiang, my son and my parents for their continuous support.

Financial support from the Emulsion Polymers Industrial Liaison Program, Dynalene Inc., U. S. Department of Energy, and the Ben Franklin Technology Center.

DEDICATION

To my beloved wife Aishuang Xiang, my son Elwin, and my parents

Table of Contents

List of Figures

List of Tables

Abstract

Emulsion polymerizations are usually carried out under isothermal conditions at relatively high temperatures (e.g., 70 °C) for the production of commercial latex products. However, this process incurs significant energy costs. To reduce energy costs, redox-initiated 'adiabatic' emulsion polymerization processes are being evaluated as a 'green' process since the polymerization can be initiated at a low temperature and the reaction heat can be efficiently utilized. The advantage in using redox initiators is to initiate the polymerization at lower temperatures to save energy. In addition, the redox initiators generate much higher radical flux compared to thermal initiators, which can make the latex particle size much smaller. The smaller latex particles have higher surface area and higher particle number, which have many potential applications. In this dissertation research, *n*-butyl methacrylate (BMA) was used as the monomer in a model system employing redox initiators (ascorbic acid and H_2O_2) with sodium lauryl sulfate (SLS) as surfactant. A Mettler RC1 reactor calorimeter was used to study the reaction under isothermal and adiabatic conditions.

First, isothermal potassium persulfate (KPS)-initiated as well as redox-initiated batch emulsion polymerization processes were carried out to study the influence of different initiators as well as that of other conditions on the kinetics of emulsion polymerization. In the redox-initiated process, 7 mM of sodium chloride (NaCl) was added to increase the electrolyte concentration in the emulsion system, which controls

the viscosity of the latex, and ferrous sulfate ($FeSO_4$) was used as catalyst to enhance the radical generation rate.

The high radical flux resulting from the use of redox initiators (25 ºC) leads to the formation of latexes with much smaller particle size, lower molecular weight and faster reaction rate compared with KPS-initiated thermal emulsion polymerizations (70 ºC). Furthermore, in Interval II of the emulsion polymerization process, the reaction rate continued to increase in the case of redox-initiated polymerization, and the reaction rate is constant for the KPS-initiated emulsion polymerization. Those differences are due to the high radical flux induced by the redox initiators. Particle size is increased with lower surfactant concentration and lower initiator concentration. Molecular weight is higher with higher surfactant concentration and lower initiator concentration, and is not influenced significantly by changes in the solids content. TEM imaging in conjunction with a negative staining technique was used for particle sizing. Based on the reaction rates and the relationships between particle number and surfactant/initiator concentrations and solids contents, it has been demonstrated that micellar nucleation is the main nucleation mechanism for the KPS-initiated system, and both micellar nucleation and homogeneous nucleation play important roles in the redox-initiated system, which is further proved by the observed increase in particle number during the polymerization in the redox-initiated system. Homogenous nucleation rates were calculated based on the Fitch-Tsai theory and the Ugelstad-Hansen theory. The Fuchs stability factor for latex particles during the polymerization and the oligmer radical concentration in water were calculated and agree with the

Fitch-Tsai theory. However, that is not good agreement with the Ugelstad-Hansen theory for the redox-initiated system, due to the inaccuracy in the value of the Fuchs stability factor for a charged radical colliding with a latex particle.

Miniemulsion polymerizations were then carried out to study the influence of the high radical flux resulting from the redox initiator system. Droplet nucleation is the main nucleation mechanism in miniemulsion polymerization and high radical flux has little influence on the nucleation process.

Further, the surface tension of the aqueous phase obtained from the redox-initiated and KPS-initiated latex systems was measured by the Du Nuoy ring method. The free SLS concentration in the aqueous phase can be calculated from surface tension by using a calibration curve (surface tension vs. SLS concentration). The fractional surface coverage by SLS surfactant can be calculated. The high particle number in the redox-initiated latex results in lower free SLS concentration in the aqueous phase and lower fractional surface coverage compared with the KPS-intiated latex. The fractional surface coverage is higher with higher SLS concentration, lower initiatior concentration and lower solids contents in the recipe. Due to the significant difference of the fractional surface coverage between redox-initiated and KPS-initiated latex, the mechanical stability of the latex was studied using a blender test. The redox-initiated latex particles require less surfactant surface coverage compared to the KPS-initiated latex particles to maintain a similar mechanical stability, which results from

the presence of extra hydrophilic hydroxyl groups introduced by the high radical flux from the redox initiator.

'Adiabatic' batch emulsion polymerization was then carried out in a Mettler RC1 reaction calorimeter under distillation mode, and the reaction heat was utilized to increase the reactor temperature and shorten the cycle time. Under 'adiabatic' conditions, the latex exhibits a larger particle size without significant change in molecular weight compared with the latex produced using redox initiator under isothermal conditions at the same starting temperatures. Seeded semi-batch polymerizations were carried out to study the influence of redox/KPS initiators and isothermal/adiabatic conditions. The particle size and conversion increased during the monomer feed process, with a high fractional conversion during the polymerization. The particle number remains constant during the polymerization, showing that secondary nucleation is eliminated.

Chapter 1

Introduction

1.1 General Introduction

Emulsion polymerization is an important method to produce latex polymers in industry. Many commodity polymers are prepared by the emulsion polymerization process, such as synthetic rubber, latex paints, paper coatings, adhesives and binders for non-woven fabrics [1]. World demand for emulsion polymers is forecast to rise 5.2 percent per year to 12.8 million metric tons in 2014 [2]. In recent years, the field of polymer colloids has expanded rapidly in many applications, such as biotechnology, medicine, sensors, printing, catalysts, etc[3]. In conventional thermally-initiated emulsion polymerization, the particle size can range from 50 to 500 nm. However, for many novel applications, smaller particle size and monodispersity result in better performance. Therefore, high surfactant concentration, low solids and some radiation methods (microwave) can be used to synthesize latex particles that are smaller than 50 nm [4], but those have limitations in larger scale latex production. To use conventional emulsion polymerization methods to synthesize monodisperse latex particles that are smaller than 50 nm, a redox initiator system was considered. Compared with the slow radical generation rate of thermal initiators, redox initiators can have a high radical flux from the reduction-oxidation reaction to initiate the polymerization and result in

the formation of small particles at low surfactant concentrations and high solids content. In addition, redox initiators can generate radicals at room temperature without high reaction temperature constraints. In conventional thermally-initiated emulsion polymerization, high-temperature isothermal emulsion polymerization processes are usually employed to maintain process stability and reproducibility and to reduce the polymerization cycle time. The energy used in commercial-scale processes is large and the cost is huge. The cost of electricity has increased more than 30% in the last ten years (as shown in Figure 1.1) [5], and is expected to continue increasing in the future. Heating of the reactor contents also takes a significant amount of time. In addition, heating equipment and heat transfer systems are expensive. By using redox initiator, the reaction can be carried out at room temperature, where energy costs, equipment costs and reaction time can be reduced. Polymerization reactions are highly exothermic and the heat of reaction can be utilized to decrease the amount of external heat needed to carry out the polymerization. Therefore, the use of a redox-initiated emulsion polymerization combined with an ‘adiabatic’ process is being evaluated to synthesize smaller polymer particles (less than 50 nm); and save energy with a low starting polymerization temperature, and shorten the reaction time by utilizing the heat of polymerization under adiabatic conditions.

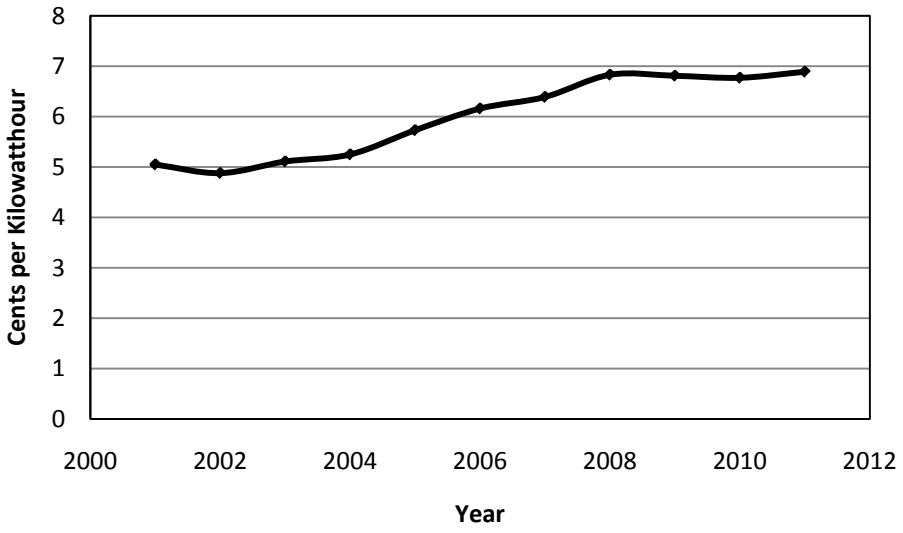

Figure 1.1 *Average retail price of electricity for the industrial sector from 2001 to 2012*

1.2 Polymer Nanoparticles

Polymer nanoparticles can be defined as solid, colloidal polymer particles with particle size in the range of 10 to 100 nm. The polymer particle surface area and particle number increases generally with decreasing particle size. Therefore, the properties of nanoparticles, such as their thermal properties, reactivity, surface charge density, etc., can be directly influenced by particle size. In many applications, including medical diagnostics, drug release, catalysts, biosensors, etc., the use of monodisperse polymer nanoparticles can result in more consistent and uniform properties.

Emulsion polymerization, miniemulsion polymerization and microemulsion polymerization are the common methods utilized to synthesize polymer

nanoparticles[4]. For the miniemulsion polymerization [6, 7], the particle size is in the range of 50 to 500 nm, which needs high shear forces (homogenizer or sonicator) to break up the monomer droplets. For the microemulsion polymerization [8], the particle size can be as small as 20 nm; however, an excessive amount of surfactant and costabilizer and low solids content used in the polymerization limit the application of this technique. Conventional emulsion polymerization gives latexes in a particle size ranging from 50 to 500 nm. Microwave [9] and ultrasonic [10] radiations have been used to prepare latex particle smaller than 50 nm, but they have limitations in larger scale production. Therefore, the use of conventional emulsion polymerization with a redox initiator system was developed to produce monodisperse polymer nanoparticles.

1.3 Emulsion Polymerization

Emulsion polymerization is a free radical-initiated chain polymerization process, which usually starts with an emulsion incorporating water, initiator, monomer, and surfactant to form a product, known as a latex. Emulsion polymerization has developed into a widely used process for the production of synthetic latexes since its first introduction on an industrial scale in the 1930s [1].

The emulsion polymerization process has several distinct advantages. High latex polymer molecular weight can be obtained at a high polymerization rate, which is different than bulk or solution polymerization. Moreover, this polymerization can proceed at a high rate due to good heat transfer of the continuous aqueous phase with

good heat removal. The viscosity of latex products is low and independent of molecular weight. On the other hand, there are some disadvantages of this process. For example, the structure of polymer chains are not easy to control, compared with bulk and solution polymerizations, and the presence of surfactants in latexes may affect the final products' quality.

A number of emulsion polymerization books have been published [1,11,12], and theories concerning the kinetics of emulsion polymerization is well explained in these books. In an emulsion polymerization system, a hydrophobic monomer can be present in the micelles, when the surfactant concentration is above its critical micelle concentration (cmc). According to Harkins' mechanism [13], conventional micellar nucleation emulsion polymerization can be divided into three intervals, which are the particle nucleation stage (Interval I) and particle growth stages (Intervals II and III). In this theory, monomer-swollen micelles are the main location of particle nucleation. During Interval I, free radicals generated in the aqueous phase enter monomer-swollen micelles to initiate polymerization (micellar nucleation). However, aqueous phase radicals can also initiate polymerization of dissolved monomer in the aqueous phase to form oligomers, which can continue to grow and then precipitate out [14, 15]. Homogenous nucleation is the main nucleation mechanism for emulsion polymerization when the surfactant concentration is below the cmc, and also plays an important role when using hydrophilic monomer. In conventional emulsion polymerization, droplet nucleation is quite limited, due to the relatively small interfacial area of the large monomer droplets. During nucleation, the monomer

diffuses from the monomer droplets through the aqueous phase and polymerizes in the monomer-swollen nuclei. Free surfactant molecules are adsorbed on the existing particles and stabilize the growing particles. Both the particle number and polymerization rate increase with time. This stage ends when the micelles disappear. During Interval II, the particle number remains constant and the monomer droplets act as reservoirs to supply the required monomer to the growing polymer particles via diffusion through the aqueous phase. This process maintains saturation swelling in the particles and supports the propagation reaction. The particle number and the polymerization rate are classically considered to be constant in Interval II. The monomer droplets disappear at the end of Interval II, which is around 40% conversion. In Interval III, the reaction continues until the monomer in the monomer-swollen particles is consumed by conversion to polymer. During this final stage, the particle number also remains constant and the polymerization rate decreases due to the decrease in the monomer concentration in the particles.

A quantitative model to describe this micellar nucleation mechanism was developed by Smith and Ewart [16] and further modified by others [17,18]. The expression for the general rate of polymerization is shown in Eq. (1-1).

$$R_p = \frac{k_p \bar{n} [M]_p N_p}{N_A} \tag{1-1}$$

where k_p is the propagation rate constant, $\bar{n}$ is the average number of radicals per particle, $[M]_p$ is the monomer concentration in the particles, N_p is the total number of particles and N_A is Avogadro's number (6.022×10^{23} mol^{-1}). Smith and Ewart described

three cases depending on the value of $\overline{n}$ which were determined by the radical desorption rate from the particles, particle size, modes of termination, and the rates of initiation and termination relative to each other [19]. During the propagation, small particles can contain either only one growing radical or no radical: "zero-one" kinetics applies. Thus, the value of $\overline{n}$ can be considered as 0.5 in Eq. (1-1) used to calculate R_p. The relationship between particle number and surfactant concentration/initiator concentration is expressed in Eq. (1-2).

$$N_p \propto [E]^a [I]^b \tag{1-2}$$

where [E] is the surfactant concentration and [I] is the initiator concentration. For emulsion polymerization of styrene using SLS as surfactant, the values of a and b are equal to 0.6 and 0.4 [16], respectively.

1.4 Miniemulsion Polymerization

Conventional and miniemulsion polymerization techniques have many similarities. However, differences are apparent in their particle nucleation and mass transport phenomena. In conventional emulsion polymerization, particle nucleation takes place either through radical entry into monomer-swollen micelles or via homogenous nucleation in the aqueous phase. The monomer droplets act as reservoirs to supply monomer to the growing particles. In contrast, miniemulsion polymerizations begin with relatively stable monomer droplets, which are prepared by applying high shear force (sonification) in an emulsification process [20]. The droplets are stabilized against coalescence by using both surfactant and a co-stabilizer, such as

hexadecane. Particle nucleation occurs primarily by the entry of radicals into the monomer droplets. Monomer transport during the polymerization is less important in miniemulsion polymerization, compared to emulsion polymerization, since the presence of co-stabilizer in miniemulsion polymerization retards the monomer transport from Ostwald ripening.

1.5 Initiators

Both thermal initiators and redox initiators are widely used to generate free radicals in emulsion polymerization. Potassium persulfate (KPS) is commonly used as a thermal initiator with sodium bicarbonate as a buffer to control the pH in order to maintain a constant decomposition rate of KPS. Above ~ 50°C, the persulfate ion breaks up into sulfate radical ions. The KPS radical generation equation is presented in Eq (1-3) and the half-life of KPS, $t_{1/2}$, at the reaction temperature of 70 ºC is about 8.6 h [21].

$$S_2O_8^{2-} \rightarrow 2\ SO_4^{2-} \bullet \qquad (1\text{-}3)$$

Free radical polymerization using redox initiation systems was first reported by Bacon [22], Mogan [23] and Baxendale [24]. In their studies, redox-initiated polymerization can be carried at a much lower temperature compared to systems using thermal initiators. The radicals are produced by the reactions between redox pairs. Trace quantities of certain transition metals, especially ferrous ion, have an accelerating catalysis effect in many systems. Fenton's reagent [25], hydrogen peroxide (H_2O_2) and ferrous salt ($FeSO_4$), have been extensively used as the redox initiation system in a

number of emulsion polymerizations [26, 27]. The mechanism of the reaction involves a one-electron transfer from the ferrous ion (Fe^{2+}) to the hydrogen peroxide with the dissociation of the oxygen-oxygen bond and the generation of one hydroxyl radical and one hydroxyl ion [28-30] (Eq. 1-4). The reducing agent (ascorbic acid) is used to regenerate Fe^{2+} from Fe^{3+} in order to maintain the generation of radicals [31]. However, the mechanism of this redox reaction is very complicated [32].

$$Fe^{2+} + H_2O_2 \rightarrow Fe^{3+} + OH^- + \bullet OH \qquad (1\text{-}4)$$

In some cases, the chelated Fe^{2+}, instead of ferrous salt, acts as a reservoir which regulates the Fe^{2+} concentration in the polymerization system and preventes premature precipitation of iron [33, 34]. Other persulfate (potassium persulfate) and peroxide (t-butyl hydroperoxide) initiators with other reductants, such as sodium metabisulfite, are also widely used as redox initiator systems in emulsion polymerization [35, 36].

1.6 Adiabatic Polymerization

High temperature isothermal conditions are widely used for emulsion polymerization in industry. However, it is hard to maintain isothermal conditions in a large scale reactor, where the surface to volume ratio limits the heat transfer. During the reaction, reactor temperature profile is difficult to maintain same during the scale-up and a great deal of energy is needed for this isothermal process. An ‘adiabatic’ (i.e., with negligible heat flow to or from the surroundings) emulsion polymerization process has been considered as an alternative to the conventional isothermal process[37].

An ‘adiabatic’ process can utilize the heat of polymerization to increase the reactor temperature, whereby a faster reaction rate is achieved and the cycle time is reduced. In this way, the polymerization time and the energy costs of heating the reactor can be reduced. The adiabatic process can therefore be regarded as a ‘green’ process resulting in a smaller environmental impact compared to the conventional isothermal process [36]. The adiabatic process could be used not only to synthesize the latex by a batch process, but also to prepare a seed latex, followed by semi-continuous monomer addition. The advantage of this latter process is that the polymerization could start at ambient temperature and continue at higher temperature, with no need for initial heat up of the reaction contents and only employing some cooling in order to remove the excess heat generated from polymerization for safety reasons.

1.7 Calorimetric Techniques and Mettler RC1 Reaction Calorimeter

A heat flow reaction calorimeter can be used to measure the instantaneous heat evolved during a reaction as a function of time. Making an energy balance around the system, the heat of reaction is calculated by measuring the reactor and jacket temperatures, and other reactor parameters such as the heat transfer coefficient and the heat transfer area. A monomer to polymer conversion curve can be obtained as a function of time by integration of the heat of reaction curve. By measuring the heat released in a polymerization reaction, it is possible to continuously obtain the rate of reaction on-line, which gives immediate insight into the polymerization process. With the calorimetric technique, the rate of polymerization is calculated directly from the

heat evolved from the reaction, which is independent of the conversion. Therefore, an instantaneous polymerization rate is measured, which is an advantage compared with other techniques.

Figure 1.2 *Set-up of the Mettler RC1 reaction calorimeter (RC1)*

One of the commercial heat flow reaction calorimeters is the Mettler RC1 reaction calorimeter (RC1), which is a lab scale calorimeter, developed based on the work of Regenass [38]. The working principles of this reactor have been described in the literature [39-41]. With this reactor, it is possible to run experiments in one of three modes: (1) isothermal mode, in which the desired reaction temperature is set at a constant value and the jacket temperature (T_j) changes automatically to maintain the reactor temperature (T_r) at the specific value; (2) adiabatic mode, in which the T_j is adjusted to be as same as T_r, and in such a manner the heat of reaction is conserved (heat transfer through the wall of reactor is limited due to the small difference of T_r and T_j); and (3) isoperibolic mode, where T_j is kept at a specific constant value. There are several advantages in using the RC1 to perform kinetic studies in emulsion polymerization: (1) the rate of polymerization is obtained directly from the reaction heat, with the conversion calculated from the integral of the heat of reaction curve, (2) data is collected every 2 seconds, where nearly continuous information for the polymerization is obtained. With this information, a detailed examination of the polymerization process can be made for a kinetics study. According to Eq. (1-5), the rate of heat evolution, Q_r ($J \cdot s^{-1}$) during exothermic polymerization is proportional to the rate of polymerization R_p ($mol \cdot dm^{-3} \cdot S^{-1}$) [42-44], where the molar heat of polymerization ΔH_p ($J \cdot mol^{-1}$) is obtained using Eq. (1-6)

$$R_p = \frac{Q_r}{\Delta H_p V_w} \tag{1-5}$$

The rate of polymerization is the moles of monomer converted per unit time per unit volume of water in the reactor and V_w (dm^3) is the volume of water in the recipe.

$$\Delta H_{\mathrm{p}} = \frac{M_0 \int_0^t Q_{\mathrm{r}} \mathrm{d}t}{m x_t} \tag{1-6}$$

where m (g) is the initial mass of monomer in the recipe, x_t is the monomer conversion after time t (s) of the reaction, M_0 (g/mol) is the molecular weight of the monomer, and the integral can be evaluated from the rate of heat evolution measured by the reaction calorimeter.

1.8 Research Objectives and Organization

The objectives of this research program are to investigate redox-initiated adiabatic emulsion polymerization as a process to produce latex (or seed latex), where the reaction can begin at room temperature and then utilize the reaction heat to accelerate the polymerization process. *n*-Butyl methacrylate was used as the model monomer, due to its relatively high reaction rate and low water solubility. The redox-initiated emulsion polymerizations under isothermal conditions were first studied and compared with conventional KPS-initiated processes. The Mettler RC1 reactor calorimeter was used to study the reaction rate by precisely measuring the reaction heat, and TEM imaging with a negative staining technique was used for particle sizing. The influence of the high radical flux generated from reaction of redox initiator system on the particle size, reaction rate and molecular weight was studied. The particle size and reaction rate obtained as a function of the emulsion polymerization time were used to study the nucleation mechanism. The different influences of redox initiator and KPS initiator on both batch emulsion polymerizations and batch

miniemulsion polymerizations were studied. A blender test [45] was used as a means of investigating the mechanical stability of the latex. Adiabatic conditions were employed for batch and semibatch polymerizations to compare with the isothermal polymerizations. The materials and the characterization techniques used in this work are described in Chapter 2.

In Chapter 3, the results of screening experiments are reported. In redox-initiated systems, electrolyte concentration is important to maintain the viscosity of latex. 7.2 mM NaCl was used as electrolyte in the later recipes to maintain low viscosity. A high mixing efficiency impeller was needed in the semi-batch process to ensure good mass transfer. Dynamic light scattering **(**DLS, Nicomp 370) and capillary hydrodynamic fractionation (CHDF 2000) were initially used for particle sizing. Due to the limitation of signal intensity of the samples for DLS and limitation of accuracy of CHDF below 50 nm, accurate particle size could not be obtained by those two equipments. Therefore, TEM imaging with a negative staining technique was used for particle sizing.

In Chapter 4, comparisons between redox-initiated (25 ºC) and KPS-initiated (70 ºC) isothermal emulsion polymerizations were investigated to study the influence of different initiators. The different influence of redox initiator and KPS initiator on the nucleation mechanism and kinetics of emulsion polymerization were studied. In redox-initiated systems, the reaction rate is significantly higher than the reaction rate in KPS-initiated systems, which is caused by the higher particle number present in the

redox-initiated system. Based on the reaction rates and the relationships between particle number and surfactant/initiator concentration and solids content, it has been demonstrated that micellar nucleation is the main mechanism in the KPS-initiated system, and both micellar nucleation and homogeneous nucleation play important roles in the redox-initiated system. Homogenous nucleation during redox-initiated emulsion polymerization was further confirmed by the increase in particle number and reaction rates. The homogeneous nucleation process was further investigated in Chapter 5. The Fitch-Tsai theory and the Ugelstad-Hansen theory were employed to investigate the homogeneous nucleation process. The Fuchs stability factor for latex particles during the polymerization and the oligmer radicals concentration in water are calculated based on the experiment data.

In Chapter 6, the influence of redox initiator and KPS initiator on the nucleation mechanism and kinetics of miniemulsion polymerization are described. Droplet nucleation was the main mechanism in miniemulsion polymerization for both redox and KPS initiators.

In Chapter 7, the mechanical stability of the corresponding latexes was studied by an ASTM blender test. Fractional surfactant surface coverage, which is an important factor affecting latex stability, was then calculated and correlated with the mechanical stability. The latex particles prepared with redox initiator require less surfactant surface coverage than KPS-initiated latex particles in order to maintain the

same mechanical stability, as a result of the extra hydroxyl group introduced by redox initiator.

In Chapters 8 and 9, 'Adiabatic' processes were carried out in the Mettler RC1 reactor. In Chapter 8, the redox-initiated batch process was first investigated under adiabatic conditions and was then compared to batch polymerization processes carried out under isothermal conditions. The adiabatic process has minimal heat loss and a shorter reaction time. In Chapter 9, the semi-batch emulsion polymerization process was investigated under adiabatic conditions and compared with isothermal conditions. The reaction rate was well controlled by the monomer-starved feed process and secondary nucleation is negligible. Finally, the conclusion of this research and future recommendations are listed in Chapter 10.

1.9 References

1 El-Aasser, M. S., Sudol, E. D., in *Emulsion Polymerization and Emulsion Polymers*, Lovell, P. A. and El-Aasser, M. S. Ed., John Wiley and Son, Chichester, p 38-41, (1997)

2 The Freedonia Group, in *World Emulsion Polymers: Industry Study with Forecasts for 2014 & 2019*, www.freedoniagroup.com, p 4 (2010)

3 Hosokawa, M., Nogi, K., Naito, M., and Yokoyama, T., *Nanoparticle Technology Handbook*, Elsevier, Netherlands, Amsterdam, (2007)

4 Rao, J. P. and Geckeler, K. E., *Prog. Polym. Sci.*, **36**, 887 (2011)

5 http://www.eia.doe.gov/

6 Choi, Y. T., El-Aasser, M. S., Sudol, E. D. and Vanderhoff, J. W., *J. Polym. Sci. Polym. Chem.*, **23**, 2973 (1985)

7 Wang, S. Wang, X. and Zhang, Z., *Eur. Polym. J.*, **43**, 178 (2007)

8 Jiang, W., Yang, W. Zeng, X. and Fu, S., *J. Polym. Sci. Polym. Chem.*, **42**, 733 (2004)

9 Gao, J. and Wu, C., *Langmuir*, **21**, 782 (2005)

10 Zhang, J. Cao, Y. and He, Y., *J. Appl. Polym. Sci.*, **94**, 763 (2004)

11 Gilbert, R. G., *Emulsion Polymerization: A Mechanistic Approach*, Academic Press, London (1995)

12 Fitch, R. M., *Polymer colloids: a comprehensive introduction*, Academic Press, San Diego (1997)

13 Harkins, W. D., *J. Am. Chem. Soc*., **69**, 1428 (1947)

14 Fitch, R.M. and Tsai, Ch. H., Homogeneous nucleation of polymer colloids, In *Polymer colloids*, Fitch, R.M., Plenum press, New York, p 73-102 (1971)

15 Fitch, R. M. Br. Polym. J. **5**, 467-483, (1973)

16 Smith, W. V. and Ewart, R. H., *J. Chem. Phys*., **16**, 592 (1948)

17 Stockmayer, W. H., *J. Polym. Sci*., **24**, 314 (1957)

18 Van der Hoff, B. M. E., in *Emulsion Polymerization*, K. Shinoda, Ed., Dekker (1967)

19 Odian, G., *Principles of Polymerization*, John Wiley and Sons, Inc., New York (1991)

20 Sudol, E. D. and El-Aasser, M. S., in *Emulsion Polymerization and Emulsion* Polymers, Lovell, P. A. and El-Aasser, M. S. Ed., John Wiley and Son, Chichester, p 707, (1997)

21 Gilbert, R. G. Emulsion polymerization: A Mechanistic Approach, Academic Press: London, p 28 (1995)

22 Bacon, R. G. R., *Trans. Faraday Soc*., **42**, 140 (1946)

23 Morgan, L. B., *Trans. Faraday Soc*., **42**, 169 (1946)

24 Baxendale, J. H., Evans, M. G. and Kilham, J. K., *Trans. Faraday Soc*., **42**, 155 (1946)

25 Fenton H.J.H. *J. Chem. Soc., Trans.* **65**, 899–911 (1894)

26 Boro, W. G., Baxendale, J. H., George, P. and Hargrave, K., *Trans. Faraday Soc*., **47**, 462 (1946)

27 Dainton, F. S., *J. Phys. Colloid Chem*., **52**, 490 (1948)

28 Jellinek, H. G., *Pure Appl. Chem*., **4**, 419 (1962)

29 Warson, H. *Per-Compounds and Persalts in Polymer Processes*, 54 (1980)

30 Daniels, E. S., Dimonie, V. L., El-Aasser, M. S. and Vanderhoff, J. W., *J. Appl. Polym. Sci.*, **41**, 2463 (1990)

31 Schildknecht, C. E., *Vinyl and Related Polymers*, John Wiley, 93-97 and 102-111 (1952)

32 Deutsch, J. C., Anal. Biochem., **255**, 1(1998)

33 Wang, C. C., Yu, N. S., Chen, C. Y. and Kuo, J. F., *J. Appl. Polym. Sci*., **60**, 493 (1996)

34 Liu Z., Han, Y., Zhou C., Zhang M., Li W., Zhang H., Liu F., and Liu W., *Ind. Eng. Chem. Res.* **49**, 7152–7158 (2010)

35 Sarac, A. S., *Prog. Polym. Sci*., **24**, 1149 (1999)

36 Goikoetxea, M., Heijungs, R., Barandiaran M. J. and Asua, J. M., *Macromol. React. Eng*., **2**, 90 (2008)

37 Nomura, M., Tobita, H., Suzuki, K., and Lee, D. I., *Polymeric Microspheres: Science and Technology*, Kyoto University Press, Kyoto, Japan, p. 181 (2007)

38 Regenass, W. *ACS Symp*. Ser. **65**, 37 (1978)

39 Manyasek, Z. and Rezabek, A. *J. Polym. Sci*., **56**, 47 (1962)

40 Andersen, H. M. *J. Polym. Sci*., **4**, 783 (1966)

41 Andersen, H. M. *J. Polym. Sci*., **7**, 2289 (1969)

42 Varela de la Rosa, L., Sudol, E. D., El-Aasser, M. S. and Klein, A. *J. Polym. Sci*., **34**, 461-473 (1996)

43 Varela de la Rosa, L. Ph.D. Dissertation, Lehigh University (1996)

44 Barrett, K. E. J., Thomas, H. R. *Br. Polym, J*., **2** , 45-48 (1970)

45 American *Standard Test Method* D1417-03D

Chapter 2

Materials, Instrumentation and Characterization

2.1 Materials

n-Butyl methacrylate (BMA, Acros) inhibited by 10 ppm monomethyl ether of hydroquinone was used as the monomer. The monomer was distilled in the presence of cuprous chloride at 40 mm Hg and 70 ºC to remove any residual inhibitor and oligomers. Sodium lauryl sulfate (SLS, MP Biomedicals) was used as the surfactant. Sodium bicarbonate ($NaHCO_3$, Mallinckrodt Chemicals) was used as the buffer. Potassium persulfate (KPS, Sigma-Aldrich) was used as the thermal initiator. Hydrogen peroxide 30% (Mallinckrodt Chemicals) and L-ascorbic acid (Sigma-Aldrich) were used as the redox initiators. Ferrous sulfate (Fisher) was used as the catalyst for redox initiators. Sodium chloride (Sigma-Aldrich) was used to control the ionic strength for redox-initiated polymerization. Hydroquinone (HQ, Sigma-Aldrich) was used as the inhibitor to terminate polymerization. Hexadecane (HD, Sigma-Aldrich) was used as the costabilizer for miniemulsion polymerization. Deionized water (DI water) having a conductivity below 0.8 μs, was obtained from a Barnstead NANO pure II system. Tetrahydrofuran (THF, J. T. Baker) was used for preparing the eluant for GPC and as a solvent to dissolve the polymer. All of the chemicals except for BMA were used as received.

2.2 Instrumentation and Characterization

2.2.1 Capillary Hydrodynamic Fractionation (CHDF)

CHDF 2000 (Matec Applied Sciences) was used to measure the particle size of the latex. The principle of CHDF is based on the particle separation by size due to the radial velocity profile occurring when a fluid flows though a capillary in laminar flow. The larger particles will not be able to approach the wall of capillary as closely as the smaller particles, and therefore, will experience fluid streamlines of higher velocity. Hence, particles are fractionated by the order of decreasing size passing through system[1]. The C-570 cartridge, which can measure particle size between 15 nm and 600 nm, was used in CHDF for particle sizing. The 1X-GR-500 solution was diluted to 10% (w/w) with DI water and used as eluant. The latex samples were diluted to a solids content between 1 % and 3 % prior to analysis. Approximately 45 µL of diluted latex samples were injected into the system.

2.2.2 Dynamic Light Scattering (DLS, Nicomp)

A Nicomp 370 (5 mW laser) was used to determine the latex particle size using dynamic light scattering. The latex was diluted with DI water to achieve an average intensity of the signal of DLS ~ 300 kHz. A monochromatic beam of light from a laser is focused onto the diluted suspension of particles and the scattering intensity is

measured at an angle θ (90º) by a detector. The phase and polarization of the scattered light depends on the position and orientation of each scatterer. The instruments analyze the intensity fluctuations and frequency fluctuations, which are caused by the diffusion of the particles [2]. The diffusion coefficient (D) can be obtained, which gives the value of the particle diameter (d) by the Stokes-Einstein equation:

$$D = \frac{k_B T}{3\pi\eta d} \tag{3-1}$$

where k_B (J/K) is the Boltzmann constant, T (K) is the temperature, and η (Pa·S) is the viscosity of the medium.

2.2.3 Transmission Electron Microscopy (TEM)

Transmission electron microscopy (TEM) (JEOL 2000) was used to obtain images of the latex particles. First, copper grids (Ernest F. Fullam, Inc.), covered with a film of Formvar polymer on one side, were prepared. One drop of formvar solution (in ethylene dichloride, 0.5 wt %) was added on the surface of DI water in a 4 liter beaker. The drop spread on the water surface to form a thin polymer film. The copper grids (with two sides, shiny side and dull side) were gently deposited on the film (with the shiny side up). Then the copper grids were scooped out of the beaker with a glass slide. The copper grids, with the formvar film on the dull side, were dull side up on the glass slide. The glass slides with copper grids present were dried in room temperature. Carbon was vapor-deposited next, in a vacuum chamber, on top of the formvar film. The latex samples were diluted as one drop of latex in 15 gram DI water. Then 15

drops of 2 wt % phosphotungstic acid negative stain were added. A drop of diluted and stained latex was added on the copper grid and dried at room temperature. The copper grid with the dried latex sample present was placed in the sample holder of the TEM. An electron beam with an accelerating voltage of 200 kV was used. Magnifications from 50 k× to 200 k× were used.

For the TEM images, ~ 1000 particles were counted to obtain the statistical results of the particle size and particle size distribution for each sample. The number-average diameter (D_n), volume-average diameter (D_v), surface average-diameter (D_s), and weight average-diameter (D_w) [3] were calculated from Eq. (2-1) to Eq. (2-4). The standard deviation was calculated from Eq. (2-5) and the particle size polydispersity index (PDI) was calculated from Eq. (2-6).

$$D_n = \frac{\sum n_i D_i}{\sum n_i} \tag{2-1}$$

$$D_w = \frac{\sum n_i D_i^4}{\sum n_i D_i^3} \tag{2-2}$$

$$D_s = \frac{\sum n_i D_i^3}{\sum n_i D_i^2} \tag{2-3}$$

$$D_v = \left[\frac{\sum n_i D_i^3}{\sum n_i} \right]^{1/3} \tag{2-4}$$

$$\sigma^2 = \frac{\sum n_i \left| D_i - D_n \right|^2}{\left(\sum n_i \right) - 1} \tag{2-5}$$

$$\text{PDI} = \frac{D_w}{D_n} \tag{2-6}$$

2.2.4 Gel Permeation Chromatography (GPC)

Molecular weight and molecular weight distribution were measured by gel permeation chromatography (GPC) using a Waters 515 HPLC Pump, Waters 410 differential refractometer detector (2487 Dual λ Absorbance Detector) and Waters Styragel columns (HR3, HR4 and HR6). The latex was dried in the oven (70 ºC) for 48 hours, and then dissolved in THF (1.5 wt %). The polymer solution was filtered with a 0.45 μm PTFE filter before injection into GPC. THF was used as the eluant at a flow rate of 1 ml/min. Narrow molecular weight polystyrene standards (590 g/mol, 1,680 g/mol, 3,250 g/mol, 10,100 g/mol, 28,500 g/mol, 66,000 g/mol, 156,000 g/mol, 560,000 g/mol, 2,880,000 g/mol and 3,800,000 g/mol) were used for calibration. The number-average molecular weight (M_n), weight-average molecular weight (M_w), and polydispersity index (PDI) were obtained.

2.2.5 Mettler RC1 Reaction Calorimeter (RC1)

The experimental setup for the Mettler RC1 reaction calorimeter consists of a 1 dm^3 medium pressure glass reactor rated at 10 bar pressure (MP10). The reactor has a cylindrical body and a hemispherical bottom. The temperature of the metal lid of the reactor is maintained by heated water flow through the lid, which minimizes the heat

loss. The reactor was equipped with a stainless steel baffle (14 cm long and 1.5 cm wide), a temperature sensor and a 25 watt calibration heater. The impeller used was a pitched blade impeller (four blades pitched at 45º to the axis with the diameter of 4.5 cm and blade width of 1.5 cm). Ten minutes of nitrogen purging at room temperature was carried out before the reaction was begun in order to eliminate oxygen from the reactor. The reaction kinetics was followed by operating the reaction in an isothermal mode (T_r) or in adiabatic mode (distillation mode) (D_i), using Mettler RC1's Quick Cal ™ procedure for calibration before and after the reaction. The operation and experimental configuration are given elsewhere [4, 5]. In the polymerization, the rate of reaction (R_p) and the fractional conversion (x_t) at any time can be calculated from the heat of reaction (Q_r), as shown in Eq. (2-7) and (2-8),

$$R_p = \frac{Q_r}{\Delta H_p V_w} \tag{2-7}$$

$$x_t = \frac{M_0 \int_0^t Q_r \mathrm{d}t}{\Delta H_p m} \tag{2-8}$$

where ΔH_p is the heat of polymerization (J/mol), V_w is the volume of water in the RC1 reactor (dm^3), M_0 (g/mol) is the molecular weight of the monomer, and m (g) is the initial mass of monomer in the recipe.

2.2.6 Surface Tension

The surface tension was measured by Du Nuoy ring method (Fisher model 215 autotensiomat surface tension analyzer, Fisher Scientific). Suppression was selected at

0 and the ring moving speed was selected to be 4 (0.5 in/min). The ring is a platinum-iridium ring (Fisher Scientific) with a circumference of 6.015 cm. The equipment was calibrated at 0 with the ring only and at 72 by the surface tension of DI water. The maximum value of the tension before the ring detached from the aqueous surface was recorded as the surface tension. Each sample was measured three times and the average value of three measurements was used as the surface tension. Surface tensions at various SLS concentrations and different electrolyte (KPS and $NaHCO_3$, or NaCl and AA) concentrations in DI water were measured and a calibration curve (surface tension vs. SLS concentration) was obtained. The aqueous phase of a latex sample was obtained using a serum replacement cell with 50 nm membrane and the surface tension of that aqueous phase was measured.

2.2.7 Surfactant Surface Coverage

Fractional surfactant surface coverage (θ), which represents the degree of surface saturation of surfactant on a latex polymer particle, is an important factor which can affect latex stability. The surface coverage of the PBMA particles with the adsorbed SLS surfactant molecules was calculated as follows. First, the aqueous phase of a latex sample was obtained using a serum replacement cell with a 50 nm membrane. A latex sample was put inside the serum replacement cell with magnetic mixing at room temperature. The aqueous phase without latex particles present flows through the membrane and the latex particles remaine inside the cell. The surface tension of the aqueous phase was measured by the Du Nouy ring method. The free

SLS concentration ($[SLS]_{free}$) in the aqueous phase can be calculated from surface tension by using a calibration curve (surface tension vs. SLS concentration). Then, the amount of SLS adsorbed on the surfaces of the latex polymer particles ($[SLS]_p$) can be calculated based on a mass balance using Eq. (2-9).

$$[SLS]_p = [SLS]_{total} - [SLS]_{free} \tag{2-9}$$

where $[SLS]_{total}$ is the total SLS concentration which was calculated from the recipes. Second, the particle number, N_p (no. per dm^3 water), and the total surface area of the particles, A_{tp} ($Å^2$), were calculated using Eq. (2-10) and (2-11).

$$N_p = \left(\frac{mx}{w}\right)\left(\frac{\rho_w}{\rho_p}\right)\left(\frac{6\times10^{24}}{\pi D_v^3}\right) \tag{2-10}$$

$$A_{tp} = N_p \pi D_s^2 \tag{2-11}$$

where m (g) is the mass of monomer used in the recipe, x is the gravimetric conversion, w (g) is the mass of water used in the recipe, ρ_w (g/cm^3) is the density of water, ρ_p (g/cm^3) is the density of polymer (PBMA: 1.05 g/cm^3) [6]. D_v and D_s are the volume-average and surface-average particle diameters, respectively, which were determined by counting at least 1000 particles from the TEM images. Third, the packing area (the area occupied by one SLS surfactant molecule at a monolayer on latex polymer particle surface), a ($Å^2$/molecule), was calculated using Eq. (2-12).

$$\alpha = \frac{A_{tp}}{[SLS]_p N_A} \tag{2-12}$$

Finally, the area covered per SLS surfactant molecule at surface saturation, a_s ($Å^2$/molecule), which was around 54 $Å^2$/molecule in the PBMA-SLS system [7, 8], was used to calculate the fractional surface coverage through Eq. (2-13).

$$\theta = \frac{a_s}{a} \tag{2-13}$$

2.2.8 Blender Test

A standard test used to determine the mechanical stability of a latex is given in American Standard Test Methods (ASTM) (D1417-03D) [9]: "A sample of latex is subjected to mechanical shear by the use of a high-speed stirrer. The amount of coagulum formed after a given time of agitation is considered a measure of latex stability". Based on this description, a blender test was used to analyze the mechanical stability of different latex samples. A Hamilton Beach Blender was used to run the blender test. The rotational speed was around 8000 rpm at the highest setting (HI MIX). 250 g of the latex sample was directly used for this test. At the beginning of the blender test, the temperature of the latex was 25 ºC. After 5 minutes of the blender test, the temperature rose to around 40 ºC and the experiment was stopped. A 100 µm mesh was used to filter the coagulum out of the latex. 1 liter of DI water was used to wash the foam, coagulum and the blender during the filtration. The coagulum held by the mesh was then placed in aluminum pan and put in an oven (90 ºC) for 48 h to dry and remove entrapped water, and the weight of the dried coagulum was measured. The percent coagulum of these samples was calculated based on the weight of dried coagulum and the weight of the total polymer in the latex samples.

2.2.9 Brookfield Viscometer

Viscosity was measured using a Brookfield viscometer (MV 4-speed). There are 7 spindles with different sizes and shapes, and each with different scales and factors which fit different ranges of viscosity. The 4 speeds of rotation are 20 rpm, 10 rpm, 4 rpm and 2 rpm. A 250 ml beaker was filled with latex and spindle (#1) with a speed of 20 rpm was used to measure the latex viscosity.

2.2.10 Differential Scanning Calorimetry (DSC)

Differential scanning calorimetry (DSC) is an analytical thermal technique, where the difference in the amount of heat required for increasing the temperature of a sample and reference is measured as a function of temperature. DSC is used widely for examining polymers to determine the composition, melting points and glass transition temperatures.

The glass transition temperature (T_g) of PBMA was measured with a TA instruments 2920 differential scanning calorimetry (DSC). Polymer samples of 10-20 mg were cut and sealed in aluminum pans and heated from 0 ºC to 80 ºC at a rate of 10 ºC/min.

2.3 References

1 Dos Ramos, J. G., Silebi, C. A., *Polymer International*, **30**, 445 (1993)

2 Collins, E. A. In *Emulsion Polymerization and Emulsion Polymers*, Lovell, P. A., El-Aasser, M. S., Eds., John Wiley and Sons: Chichester, U. K., p 385 (1997)

3 Collins, E. A. In Emulsion *Polymerization and Emulsion Polymers*; Lovell, P. A., El-Aasser, M. S. Eds.; John Wiley and Sons: Chichester, U. K., p 391 (1997)

4 Mettler RC1 User's Manual, Mettler Instrument Corporation

5 Varela de la Rosa, L. Ph.D. Dissertation, Lehigh University (1996)

6 Bicerano, J. In *Prediction of Polymer Properties*, 2nd ed.; Marcel Dekker, New York, p 71 (1996)

7 Sutterlin, N. in *Polymer Colloids II*, R. M. Fitch, Eds., Plenum, New York (1980)

8 Krishnan, S. *Ph.D. Dissertation*, Lehigh University (2002)

9 American *Standard Test Method* D1417-03D

Chapter 3

Screening of Redox-initiated Emulsion Polymerization Recipes, Mixing Conditions and Characterization Methods

3.1 Introduction

In conventional emulsion polymerization, water-soluble thermal initiator is widely used under high-temperature isothermal conditions to produce latex. The activation energy of thermal initiators is on the order of 120-170 $kJ \cdot mol^{-1}$. This activation energy brings a strong temperature dependence of the initiator dissociation, where reactions are usually carried out at 60 ºC - 90 ºC. The energy cost for this process is huge. For example, a 10 m^3 reactor will need at least 2×10^6 kJ to increase the temperature from 25 °C to 70 °C for the reactants themselves. To eliminate the heating process and save energy, redox initiators are considered. A lower activation energy (40-80 $kJ \cdot mol^{-1}$) of redox initiators allows the redox-initiated polymerization to take place at a much lower temperature compared to the thermal-initiated systems [1-3]. Smaller particle size can also be achieved due to high radical flux from decomposition of redox initiators.

Hydrogen peroxide (H_2O_2) and ascorbic acid (AA), in conjunction with metal ion (i.e., Fe^{2+}), have been used as the redox initiator system in the polymerization of

vinyl monomers [4-8]. However, the initiation mechanism, as well as the polymerization kinetics obtained using the redox initiator, is not well known. In this research program, H_2O_2/AA as redox initiator with ferrous sulfate ($FeSO_4$) as the catalyst metal ion is used. Different recipes were tested to find suitable recipes to study the nucleation mechanism and kinetics of redox-initiated emulsion polymerization.

n-Butyl methacrylate (BMA), a monomer widely used in industry as well as in research [9,10], was selected as the model monomer. This monomer has high propagation rate constant [11], k_p, (1241.6 $dm^3mol^{-1}s^{-1}$ at 70 °C and 369.7 $dm^3mol^{-1}s^{-1}$ at 25 °C), which can be calculated from Eq. (3-1). The faster propagation rate constant results in a shorter reaction time, which can minimize heat loss during the reaction, which is good for an adiabatic study.

$$k_p = 10^{6.58}\,\mathrm{L\cdot mol^{-1}\cdot s^{-1}} \exp\left(\frac{-22.9\mathrm{kJ\cdot mol^{-1}}}{RT}\right) \quad (3\text{-}1)$$

where the ideal gas constant R is 8.314 J mol^{-1} K^{-1} and T is the absolute temperature (K). The BMA water solubility is low [12] (3.2×10^{-3} mol/L at 70 °C and 2.9×10^{-3} mol/L at 25 °C), which can be calculated from Eq. (3-2).

$$M_{sat} = 2.781 + 6.55\times10^{-3}\,T \quad (3\text{-}2)$$

where M_{sat} (10^{-3} mol/L) is the aqueous concentration in monomer saturated water and T (degree Celsius) is the temperature. Therefore, BMA was used as the monomer for this research program.

The initial batch recipe was formulated for 25% solids content with sodium lauryl sulfate (SLS) surfactant, concentration above its cmc (7.8 mM) [13], which is a classic recipe for emulsion polymerization. The electrolyte concentration is important to control the thickness of the electrical double layer in the redox-initiated system, and thus to keep the viscosity of the latex constant at a low value. In the semi-batch emulsion polymerization process, different types of impellors were used to study the influence of shear force on the polymerization rate. Batch redox-initiated emulsion polymerizations at different surfactant and initiator concentrations was then carried out to study the nucleation process. Various particle sizing methods, such as DLS, CHDF and TEM imaging, were used and compared to obtain accurate results.

3.2 Experimental

Redox-initiated Emulsion Polymerization of BMA

The redox-initiated emulsion polymerization recipes for screening emulsion polymerization studies are shown in Tables 3.1, 3.2, 3.3 and 3.4. In the redox-initiated system, BMA was used as monomer; SLS was used as surfactant; ascorbic acid (A A) and H_2O_2 were used as redox initiator components and $FeSO_4$ was used as initiator catalyst. All ingredients except for the redox initiator components were weighed and poured into a 500 mL beaker, and then stirred with a magnetic stir bar for 5 minutes. Then the emulsion was poured into the reactor which purged with nitrogen gas for 10 minutes before the reaction started. The reactor was flushed with nitrogen during the

polymerization to prevent O_2 inhibition. At the end of the reaction, 1% hydroquinone solution (5 g) was added into the reactor to stop any further polymerization.

The recipes used in the initial recipe study under isothermal conditions at 25 ºC are shown in Table 3.1. The experiments were carried out in a 500 mL round bottom flask with a half-moon impeller. The solutions of redox initiator components (ascorbic acid and H_2O_2) were separately fed into the reactor with syringe pump over a 20 minutes feeding time. The adiabatic emulsion polymerizations (shown in Table 3.2) were carried out in a metal thermos sealed with a rubber stopper. Different impellers (half-moon, pitched-blade and Rushton impellers) were used to study the influence of shear force on the conversion of semi-batch redox-initiated emulsion polymerization. In reaction E0, the redox initiator was fed into the reactor over a one-hour period, as the batch process to be compared to the semi-batch processes. In in-situ semi-batch reactions E1, E2, and E3, the redox initiators were fed into the reactor by a syringe pump over 3 hours. The monomer (BMA) feed was begun after 40 minutes, when there was no more increase in the reactor temperature and the seed stage reaction was finished. The monomer feeding tubing was located beneath the solution surface and near the impeller. The monomer was fed into the reactor with a syringe pump over 2 hours. The stirring speed was around 175 rpm. A half-moon impeller was used in reaction E0 and E1, while a pitched-blade impeller was used in reaction E2, and a Rushton impeller was used in reaction E3. Different impellers were used to study the influence of mixing efficiency. The initial temperature was around 25 ºC. The

temperature of the reaction was measured during the polymerization by a thermocouple (Omega Engineering, DP460).

Table 3.1: Recipes Used for Batch Redox-initiated Emulsion Polymerizations under Isothermal Conditions (25 ºC)

Reaction		**A1**	**A2**	**A3**
BMA (g)		100	100	100
DI water (g)		290	290	290
SLS (g) *		1.20 (13.9 mM)	2.20 (25.4 mM)	2.19 (25.4 mM)
$FeSO_4$ (g) *		0.03 (0.35 mM)	0.01 (0.12 mM)	0.01 (0.12 mM)
NaCl (g) *		-	-	0.12 (7.2 mM)
Feed	AA (g)	0.42	0.03	0.03
	H_2O_2 (g)	2.0	0.2	0.2
	DI water (g)	10	10	10

*Molar concentrations based on water

Table 3.2: Recipes Used for 'Adiabatic' Semi-batch Redox-initiated Emulsion Polymerizations with Electrolyte (NaCl) (Starting Temperature: 25 ºC)

Reaction		**E0**	**E1**	**E2**	**E3**
BMA (g)		90	30		
DI water (g)		260			
SLS (g) *		1.0 (12.8 mM)			
$FeSO_4$ (g) *		0.006 (0.08 mM)			
NaCl (g) *		0.12 (7.6 mM)			
Feed	BMA (g)	N/A	60		
	AA (g)	0.05	0.15		
	H_2O_2 (g)	0.05	0.15		
	DI water (g)	10	10		
	Time (h)	1	3		
Impeller		Half-moon	Half-moon	Pitched-blade	Rushton

*Molar concentrations based on water

The recipes used to study the nucleation mechanism of redox-initiated emulsion polymerization are shown in Tables 3.3 and 3.4. The experiments were carried out in a 250 mL round bottom flask with a half-moon impeller at 25 ºC. One redox initiator component solution (H_2O_2) was fed into the flask as one shot first and the other redox initiator component solution (ascorbic acid) was fed into the flask as one shot 1 minute later.

The particle sizing methods, DLS (Nicomp 370), CHDF 2000 and TEM imaging, were used and the particle sizes are compared with each other. The molecular weight was measured by GPC. The viscosity was measured by the Brookfield viscometer and glass transition temperature was measured by DSC. The characterization methods are described in Chapter 2.

Table 3.3: Recipes Used for Batch Redox-initiated Isothermal Emulsion Polymerizations: Effect of Varying the Surfactant (SLS) Concentration (25 ºC)

Reaction	**S1**	**S2**	**S3**	**S4**	**S5**
BMA (g)	10				
DI water (g)	90				
SLS (g) *	0.45 (17.3 mM)	0.30 (11.6 mM)	0.20 (7.7 mM)	0.15 (5.8 mM)	0.10 (3.8 mM)
$FeSO_4$ (g) *	0.002 (0.08 mM)				
NaCl (g) *	0.04 (7.6 mM)				
AA (g) *	0.02 (1.3 mM)				
H_2O_2 (g) *	0.02 (2.0 mM)				

*Molar concentrations based on water

Table 3.4: Recipes Used for Batch Isothermal Emulsion Polymerizations: Effect of Varying the Redox Initiator Concentration (25 ºC)

Reaction	I1	I2	I3	I4
BMA (g)	10			
DI water (g)	90			
SLS (g) *	0.60 (23.1 mM)			
$FeSO_4$ (g) *	0.002 (0.08 mM)			
NaCl (g) *	0.04 (7.6 mM)			
AA (g) *	0.005 (0.3 mM)	0.01 (0.6 mM)	0.02 (1.3 mM)	0.04 (2.6 mM)
H_2O_2 (g) *	0.005 (0.5 mM)	0.01 (1.0 mM)	0.02 (2.0 mM)	0.04 (3.9 mM)

*Molar concentrations based on water

3.3 Results and Discussions

3.3.1 Influence of Electrolyte

The initial redox-initiated emulsion polymerization results are shown in Table 3.5. Recipes A1 and A2 were carried out with monomer (BMA), surfactant (SLS) and redox initiator components (H_2O_2, AA and $FeSO_4$). A3 was carried out with the same ingredients, but with NaCl added as extra electrolyte. The reactions can achieve high conversion (around 95%). The high radical flux generated from redox initiator

decomposition resulted in the formation of latex particles with much smaller diameter and lower molecular weights compared to the thermal-initiated emulsion polymerization. In emulsion polymerization, higher redox initiator concentration and higher concentration of surfactant can result in the formation of smaller latex particles and higher particle number [14]. The surfactant concentration of recipe A2 was increased to achieve similar particle size as A1 at lower redox initiator concentration, in order that the two latexes can have similar particle numbers. However, the viscosity of A2 latex is more than 600 times higher than A1, and A2 formed a gel-like latex. The particle sizes (measured by DLS; Nicomp 370) of the latexes produced in reactions A1 and A2 were very similar (~50 nm) as well as their molecular weights (weight average: ~1,000,000). After adding a small amount of electrolyte (HCl, NaCl, or NaOH) to latex A2, the viscosity dramatically dropped. Thus, the high viscosity is not caused by the latex particle size, but is associated with the electrical double layer of the latex particles. Adding electrolyte can decrease the effective particle volume and viscosity.

Table 3.5: Result of 'Adiabatic' Batch Emulsion Polymerizations of BMA

Sample	A1	A2	A3
Solids Content	23.5%	24.3%	23.1%
Conversion	96.0%	95.4%	94.3%
Coagulum	3.2%	-	0.4%
D_n (nm) *	21.7	26.5	39.9
D_v (nm) *	27.6	39.6	53.6
D_i (nm) *	54.8	58.3	70.7
PDI (D_i / D_n)	2.52	2.20	1.77
Viscosity (10 rpm) (cp)	22	14,200	14
M_n (g·mol^{-1})	279,700	391,700	282,900
M_w (g·mol^{-1})	937,000	1,183,000	817,600
PDI (M_w/ M_n)	3.35	3.02	2.89

*Particle sizing based on DLS

To maintain the size of the latex particles dispersed in the aqueous phase and prevent aggregation, repulsive forces are needed to keep the particles separated. Electrostatic and steric forces are the two types of repulsive forces usually considered in emulsion polymer systems. Since only anionic surfactant (SLS) was used in this research, steric forces were not considered in this work. Electrostatic forces are generated by the charge groups, which include the ionic end groups of the decomposed initiator and anionic surfactant, on the latex particle surface. The layer of

surface charges and the counterions resulting from the surface charges is called the electrical double layer. The electrostatic force can be estimated using the DLVO theory (Derjaguin and Landau [15], Verwey and Overbeek [16]). This force depends on the particle surface potential, which is determined by the surface charge density and electrolyte concentration. Therefore, the electrostatic force is sensitive to the variation of the electrolyte concentration, which can significantly influence the thickness of the electrical double layer. The characteristic thickness of the electrical double layer can be calculated by 1/κ, which can be determined from the Debye-Huckel equation [17] as shown in Eq. (3-3) and (3-4).

$$\frac{1}{\kappa}=\left[\frac{\varepsilon\varepsilon_0 k_b T}{2z^2 e^2 n_\infty}\right]^{1/2} \tag{3-3}$$

$$n_\infty = 1000 \cdot N_A \cdot M \tag{3-4}$$

where z is the valency and M is the molarity (mole/liter). For pure water at T = 298 K, the parameters are as following: the dielectric constant in the solution and in the vacuum, ε = 78.5 and $\varepsilon_0 = 8.85\times10^{-12}$ C^2/Nm^2; the charge of a proton, $e = 1.602\times10^{-19}$ C; the Boltzmann constant, $k_b = 1.381\times10^{-23}$ J/K; n_∞ is the bulk ionic number concentration; and Avogadro's number, $N_a = 6.022\times10^{23}$ mol^{-1}. When symmetrical electrolyte is used, the Debye-Huckel equation can be simplified as Eq. (3-5)

$$\frac{1}{\kappa}=\frac{3.04}{z\sqrt{M}}\times10^{-1} \tag{3-5}$$

where the unit of 1/ κ is in nanometers. The thickness of the electrical double layer (1/κ) at different electrolyte concentrations (NaCl) is shown in Figure 3.1. Ascorbic acid is a weak electrolyte and can result in higher double layer thickness (1/κ).

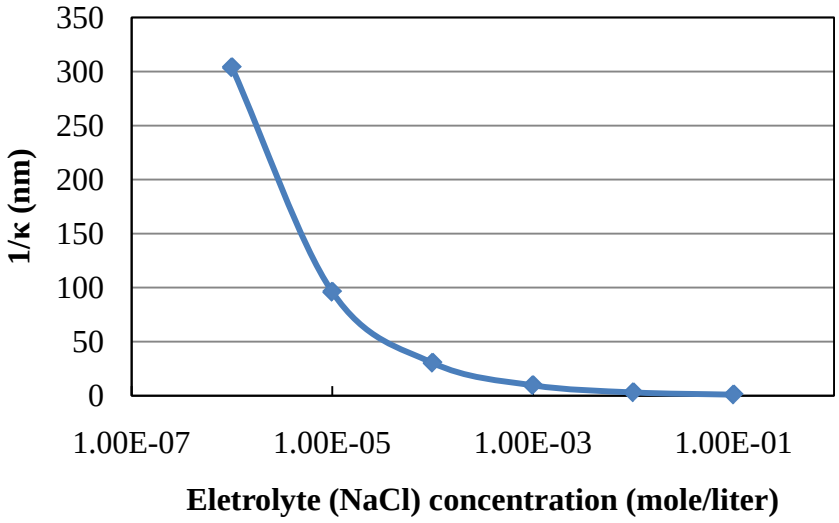

Figure 3.1: *Calculated thickness of the electrical double layer (1/κ) at different electrolyte concentrations (NaCl).*

When the electrolyte is present at a very low concentration, the electrical double layer will be extended, which results in an increase in the hydrodynamic size of the latex particles. This results in an increased particle hydrodynamic volume as well as increased viscosity. Adding a certain amount of electrolyte will help compress the double layer, which can lower the viscosity, as shown in latex A3 (Table 3.5). However, adding too much electrolyte can easily destroy the stability of the latex by compressing the double layer too much. The latex forms irreversible coagulum when too much electrolyte is added. A latex with high viscosity would be hard to stir and lead to poor mass transfer of the monomer, which would lead to a slower polymerization rate and a lower conversion. By adding a certain amount of electrolyte (~ 7 mM NaCl) in this case, which is a similar electrolyte concentration as that used in

KPS-initiated system, the viscosity of the latex can be controlled at a low value to improve mixing. All of the later experiments had NaCl added.

3.3.2 Semi-batch Adiabatic Redox-initiated Emulsion Polymerization

The semi-batch adiabatic redox-initiated emulsion polymerizations were initially studied with a home-made adiabatic reactor, a metal thermos with a wide opening (as shown in Figure 3.2), through which different types of impellers can be inserted into the reactor. A half-moon impeller, a Rushton impeller and a pitched-blade impeller (as shown in Figure 3.3), were used separately at 175 rpm to study the influence of mixing efficiency on conversion. The results of the adiabatic processes are shown in Tables 3.6 and 3.7.

The heat utilization ratio is calculated by using the heat absorbed by the system, which is calculated from the increased temperature of the system, divided by the theoretical polymerization heat, as calculated from the molar heat of polymerization of BMA, as shown in Eq. (3-6).

$$\mathrm{HUC} = \frac{\Delta T \cdot M_{\mathrm{BMA}} \cdot \left(C_{\mathrm{w}} \cdot m_{\mathrm{w}} + C_{\mathrm{m}} \cdot m_{\mathrm{BMA}}(1-x) + C_{\mathrm{p}} \cdot m_{\mathrm{BMA}} \cdot x\right)}{\Delta H_{\mathrm{p}} \cdot m_{\mathrm{BMA}} \cdot x} \qquad (3\text{-}6)$$

where HUC is the heat utilization coefficient; ΔT is the increased reactor temperature; C_{w} is the heat capacity of water (4.2 $\mathrm{J \cdot g^{-1} \cdot K^{-1}}$); C_{m} is the heat capacity of BMA (1.95 $\mathrm{J \cdot g^{-1} \cdot K^{-1}}$) [18]; C_{p} is the heat capacity of PBMA (1.80 $\mathrm{J \cdot g^{-1} \cdot K^{-1}}$) [19]; ΔH_{p} is the polymerization heat of BMA (60 kJ/mol) at 26.9 ºC [20]; m_{w} is the mass of water (g);

m_{BMA} is the mass of the initial BMA (g); x is the final conversion; M_{BMA} is the molecular weight of BMA (142.2 g/mol). HUC can be used to represent the heat loss of the system. The maximum increase in the reactor temperature at different solids content of PBMA under theoretical adiabatic conditions can also be calculated, which is shown in Figure 3.4.

Table 3.6: Results of Semi-batch Adiabatic Redox-initiated Emulsion Polymerizations with Starting Temperature at 25 ºC

Sample	**E0**	**E1**	**E2**	**E3**
Solids Content	23.12%	18.70%	24.71%	24.62%
Conversion	95.4%	75.6%	96.8%	96.4%
Coagulum	1.8%	-	< 1%	< 1%
HUC*	0.67	0.51	0.61	0.62
D_n (nm) **	53.6	39.5	64.5	68.3
D_v (nm) **	60.7	52.1	75.3	74.4
D_i (nm) **	65.4	61.2	82.2	85.3
PDI	1.22	1.55	1.28	1.25
Impeller	Half-moon	Half-moon	Pitched-blade	Rushton

*HUC: heat utilization coefficient

**Particle sizing based on DLS

Table 3.7: Results of Particle size and Molecular Weight

(Seed and Final Latex)

Sample	D_i (nm) *	M_n (g·mol^{-1})	M_w (g·mol^{-1})	MW PDI
E0	65.4	340,700	717,600	2.11
E2-Seed	57.8	141,900	556,500	3.92
E2	82.2	161,200	560,600	3.48
E3-Seed	59.4	174,700	524,900	3.00
E3	85.3	175,200	609,200	3.48

*Particle sizing based on DLS

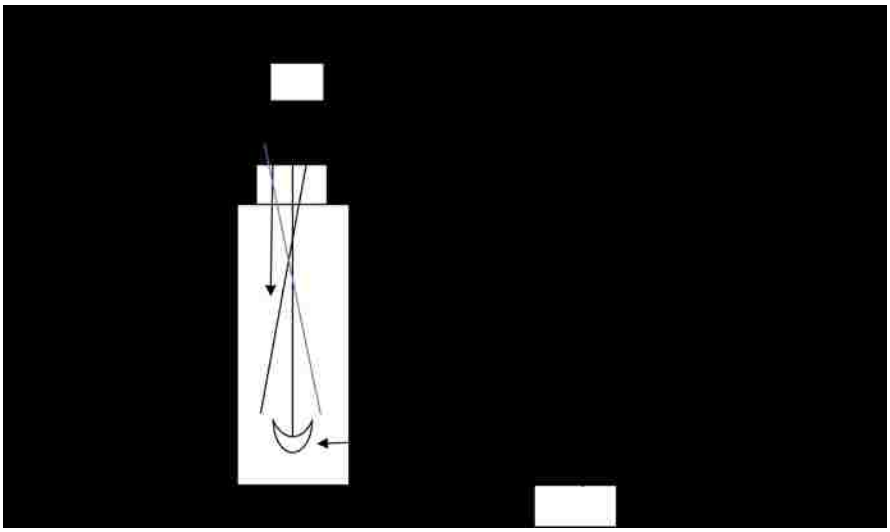

Figure 3.2: *Set-up of the adiabatic reactions with using a metal thermos as the reactor.*

Figure 3.3: *Three different impellers used in semi-batch adiabatic redox-initiated emulsion polymerizations.*

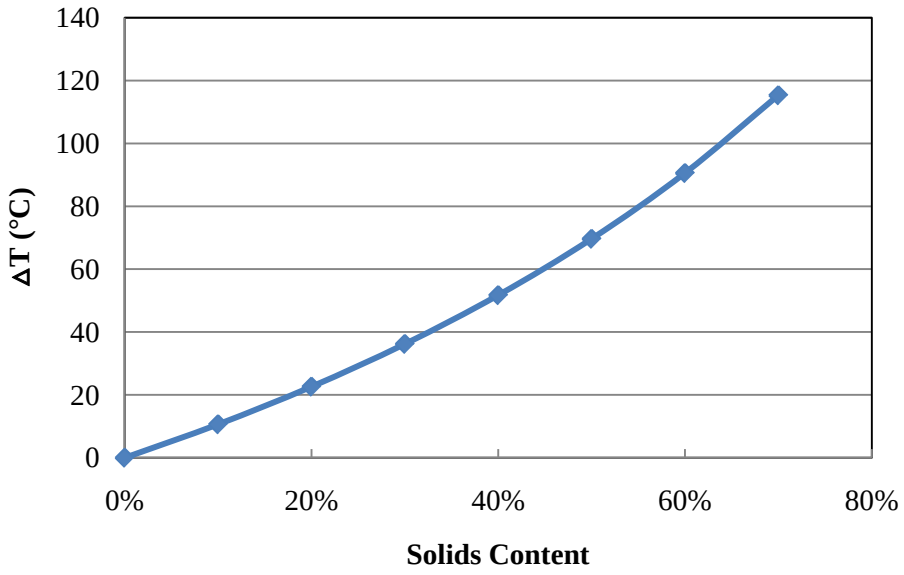

Figure 3.4: *Maximum increase in temperature at different PBMA solids contents under theoretical adiabatic conditions.*

The heat utilization coefficient of this adiabatic system is about 60%, which means there is about 40% heat loss from the reactor. The main heat loss results from the heat capacity of the reactor itself, the impeller and the shaft. Due to the small scale of this reactor, heat loss to the atmosphere is also significant, which is indicated by the reactor temperature decreasing after the reaction was complete. The molecular weights of the latex polymers obtained from reactions E0, E2 and E3 are shown in Table 3.7. In the semi-batch processes (E2 and E3), the molecular weight of the seed is lower than the batch process (E0), which may be influenced by the ratio of the redox initiator concentration to the monomer concentration. In the semi-batch process, there were negligible changes in molecular weight between the seed and final latex.

The reactor temperature profiles for adiabatic polymerizations E0 to E3 are shown in Figure 3.5. The initial temperature is around 25 ºC. In the batch reaction E0, the reactor temperature increased very quickly during the first 40 minutes of polymerization, and then the temperature of the reactor leveled off at high conversions. After the reaction was completed, there was a slight decrease in reactor temperature caused by the heat loss. In the semi-batch process, the temperature initially increased quickly in the seed stages of reactions E1 to E3, indicating a fast reaction rate in the seed stage of around 20 minutes. This time is shorter than E0 because less BMA was used in reactions E1 to E3. The conversion was high after the seed stage, as indicated in Figure 3.6. The increase in temperature was relatively slow during the feed stage, and was controlled by the feeding rate. In reaction E1, the reactor temperature did not increase during the monomer feeding and the fractional

conversion in the feed stage was low, which was caused by the low mixing efficiency of the half-moon impeller. The half-moon impeller has a low mixing efficiency and low shear force. In the batch process (E0), a high concentration of surfactant was present in the emulsion systems and low mixing and shear can keep the emulsion uniform. Therefore, the use of a half-moon impeller can work well in the batch process. Serum replacement using a membrane with a 50 nm pore size was used to obtain the aqueous phase from the seed latex prepared by the semi-batch process to measure the surface tension. The free SLS surfactant concentration after the seed stage was just 0.7 mM, which is not considered sufficient to stablize the monomer droplets introduced during the monomer feed stage. Therefore, in the semi-batch process (E1-E3), better mixing efficiency and additional shear now become important to break up the BMA monomer into small droplets and to disperse BMA droplets uniformly in the continuous phase. The half-moon impeller will not give good mixing or shear which will result in a floating monomer layer on the surface of the dispersion. As a result, the reactor temperature did not increase as monomer was fed into the reactor, and the fractional conversion was low in reaction E1. A pitched-blade impeller (better mixing) was used in reaction E2 and a Rushton impeller (high shear) was used in reaction E3. Both impellers have higher mixing efficiencies and impart greater shear force compared to the half-moon impeller. As a result, E2 and E3 exhibited a continuous increase in the reactor temperature as monomer was feed into the reactor and high fractional conversions was obtained during the feed stage (Figures 3.5 and 3.6). The intensity average particle diameter (D_i) obtained from DLS (Nicomp 370) measurement was used to calculate the particle number. The ratios of the final latex

particle number to the initial seed particle number are 1.04 (E2) and 1.02 (E3), which indicates that the semi-batch process was carried out under monomer-starved feeding conditions without secondary nucleation occurring. Based on the limitations of the semi-batch process carried out in the home-made thermos reactor, the Mettler RC1 reactor was considered as a much better reactor to study the semi-batch emulsion polymerization of BMA under adiabatic conditions.

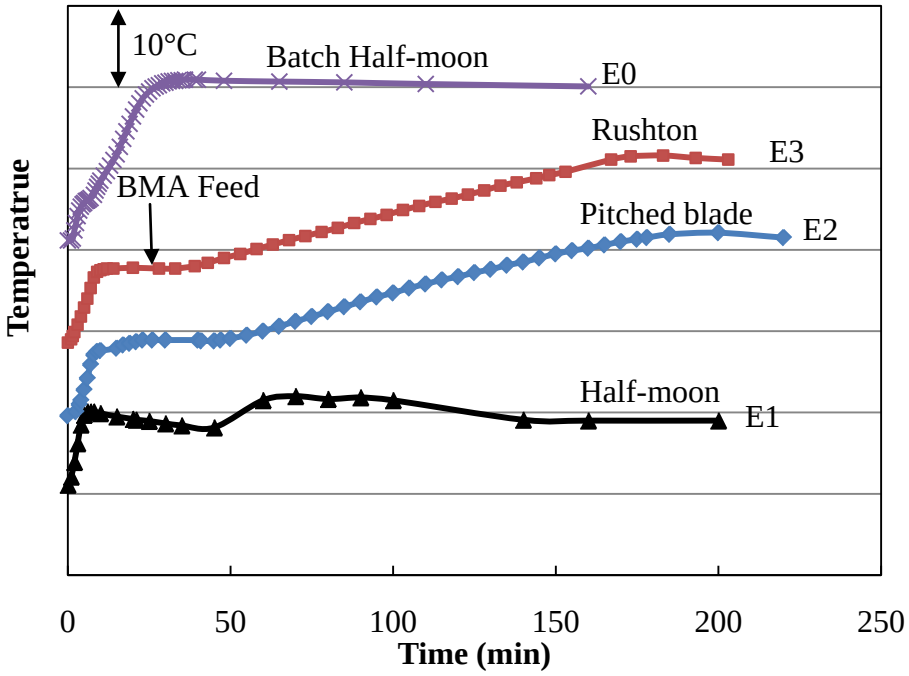

Figure 3.5: *Temperature profiles for the semi-batch adiabatic emulsion polymerizations using different impellers (initial temperature is 25 °C).*

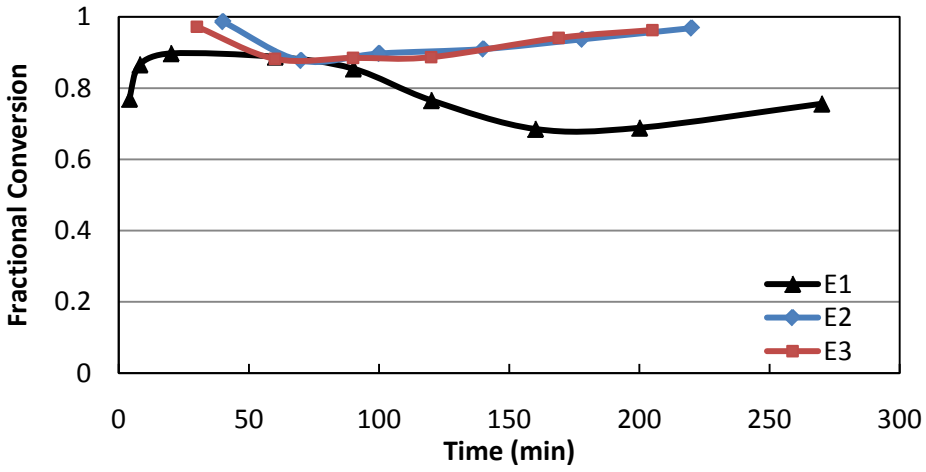

Figure 3.6: *Conversion-time profiles for the semi-batch emulsion polymerizations of BMA using different impellers.*

3.3.3 Batch Redox-initiated Emulsion Polymerization

Batch redox-initiated emulsion polymerizations were carried out at 25 ºC with various SLS and initiator concentrations. Two different particle sizing methods (DLS; Nicomp 370 and CHDF; CHDF 2000) were used to measure the particle size to study the nucleation mechanism. The results are shown in Tables 3.8 and 3.9. The latex particle diameters, measured by DLS and CHDF, were smaller at higher surfactant and initiator concentrations. The particle sizes are also smaller than those obtained from conventional thermal-initiated emulsion polymerization (~100 nm). The smaller particle diameter of the former system results is from the high radical flux from the decomposition of redox initiator. The high radical flux can lead to the formation of a large number of nuclei, not only via micellar nucleation, but also by homogeneous nucleation. The surfactant concentration had a negligible influence on the molecular

weight, as shown in Table 3.8. However, the redox initiator concentration has a significant influence in the molecular weight. When the redox initiator concentration is lower, the radical entering rate per particle is lower, and the molecular weight is higher (shown in Table 3.9).

The particle diameters measured by DLS are smaller, with a broader particle size distribution, compared to the values measured by CHDF. There are significant differences between the two particle sizes obtained from DLS and CHDF analysis, which is caused by the limitations of these instruments. In the DLS (Nicomp 370) method, the average intensity of the signal of the diluted latex sample needs to be around 300 kHz to obtain the most accurate results. The redox-initiated latex samples are translucent, due to their small particle size. To reach the optimal operating conditions of DLS, the latex sample can not be diluted very much, and thus, the solids content of the measured sample is high. In DLS theory, the particle size is calculated based on the results of laser intensity fluctuations and frequency fluctuations caused by the diffusion of the particles. The concentrated sample can result in inaccurate diffusion results, compared with diluted samples. These results indicate that the DLS is not suitable for the particle sizing of redox-initiated latex, when the particle size is smaller than 50 nm.

Table 3.8: Results of Batch Emulsion Polymerizations

with Different SLS Concentrations at 25 ºC *

Sample	**S1**	**S2**	**S3**	**S4**	**S5**
[SLS] (mM)	17.3	11.6	7.7	5.8	3.8
Solids Content	9.81%	9.78%	9.63%	9.49%	9.57%
Conversion	96.2%	96.3%	95.9%	94.9%	96.2%
Particle sizing by DLS					
D_n **(nm)**	9.0	11.1	19.2	20.5	44.5
D_v **(nm)**	12.5	15.4	23.7	28.7	60.1
D_i **(nm)**	19.2	21.3	29.0	39.7	79.4
PDI (D_i **/** D_n**)**	2.13	1.92	1.51	1.94	1.78
Particle sizing by CHDF					
D_n **(nm)**	44.5	49.3	51.6	55.4	61.8
D_v **(nm)**	46.5	52.4	55.0	59.7	70.8
D_w **(nm)**	50.8	58.6	62.0	68.5	99.5
PDI (D_w **/** D_n**)**	1.14	1.19	1.20	1.24	1.61
M_n **(g·mol^{-1})**	199,468	279,725	287,071	176,969	209,491
M_w **(g·mol^{-1})**	582,273	731,361	634,451	698,410	648,549
PDI (M_w**/** M_n**)**	2.92	2.61	2.21	3.95	3.10

*Refer to Table 3.3 for recipe

Table 3.9: Result of Batch Emulsion Polymerizations

with Different Redox Initiator Concentrations at 25ºC *

Sample	**I1**	**I2**	**I3**	**I4**
[H_2O_2] (mM)	0.9	1.8	3.7	7.4
Solids Content	9.90%	10.10%	10.09%	10.17%
Conversion	94.7%	96.9%	96.3%	98.8%
Particle sizing by DLS				
D_n (nm)	8.1	8.0	7.2	6.9
D_v (nm)	12.6	12.4	11.0	9.2
D_i (nm)	19.6	19.3	15.2	13.3
PDI (D_i / D_n)	2.42	2.41	2.11	1.93
Particle sizing by CHDF				
D_n (nm)	46.7	45.9	43.9	44.4
D_v (nm)	48.9	48.2	46.1	46.7
D_w (nm)	53.3	52.9	50.9	48.6
PDI (D_w / D_n)	1.16	1.16	1.15	1.09
M_n (g·mol^{-1})	417,025	430,901	330,096	298,404
M_w (g·mol^{-1})	896,099	911,983	629,581	523,864
PDI (M_w/ M_n)	2.15	2.12	1.91	1.76

*Refer to Table 3.4 for recipe

In the CHDF method, the standards used for calibration of the instrument are 30 nm, 40 nm, 91 nm, 109 nm, 176 nm, 234 nm and 357 nm. However, the capillary

used in the CHDF 2000 is not accurate for the small particles, due to the diameter of the capillary. The 30 and 40 nm latex standards elute from the CHDF at nearly the same time, which result in making inaccurate values in the particle diameter at the low end of the particle size distribution. In the redox-initiated latex samples with 10% solids content, the diameter of many of the samples is between 30 and 50 nm. This indicates the CHDF is also not accurate for those samples. Therefore, TEM imaging was considered to be as the most accurate particle sizing method for redox-initiated latex.

Initially, the latex was directly diluted with deionized water and dried on a copper grid to prepare samples for the TEM imaging analysis. However, few particles can be seen in the TEM image (shown in Figure 3-7 (A)), because of the low glass transition temperature (T_g) of PBMA, determined by DSC to be 36.47 ºC (shown in Figure 3-8). This compares well with the value of 35.2 ºC in the literature [21]. Since the T_g of the latex is low, exposure to the electron beam results in particle deformation and fusion. Therefore, a negative staining technique [1, 22] with phosphotungstic acid was used to obtain sharp images for the particle sizing by forming an electron dense heavy metal shell surrounding the soft latex particles during the drying process. Good TEM images can be obtained with this technique, as shown in Figure 3-7 (B). The particle size distribution is very narrow and accurate particle size can be obtained. Therefore, TEM imaging with negative staining were used for particle sizing in the latter experiments. To further study the kinetics of the redox-initiated emulsion polymerization, the reaction rate during the polymerization is another key factor to

investigate the nucleation mechanism. Therefore, the Mettler RC1 reactor was used in later experiments.

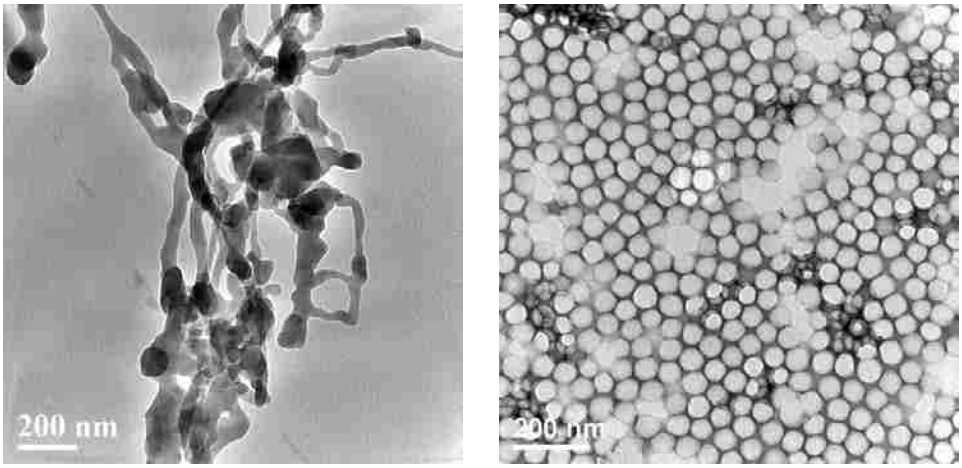

(A) **(B)**

Figure 3.7: *TEM image of PBMA latex particle: (A) normal sample preparation, (B) negative staining with phosphotungstic acid.*

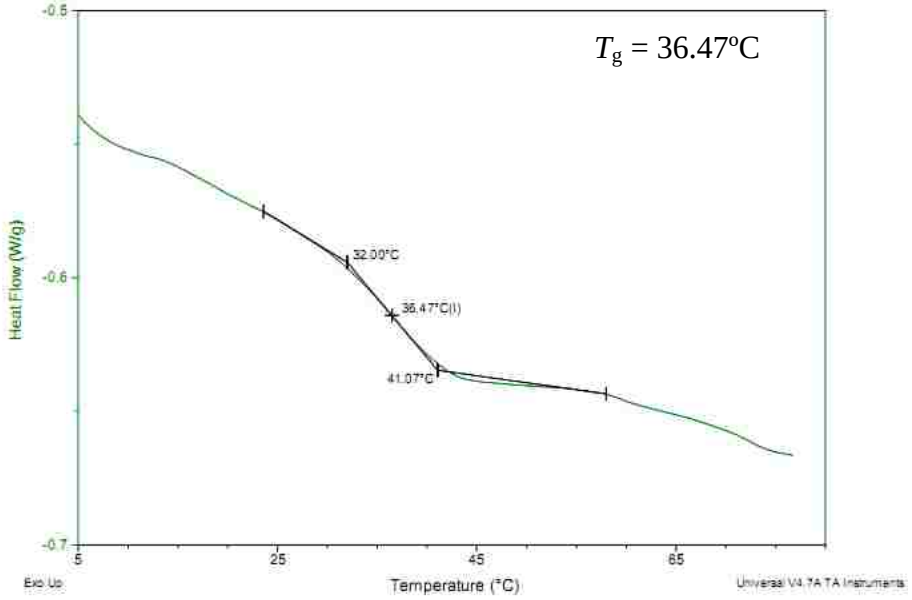

Figure 3.8: *Glass transition temperature of PMBA (T_g =36.47 ºC) with the heating rate of 10 ºC/min.*

3.4 Conclusions

Initial investigations were carried out for screening of the redox-initiated emulsion polymerization recipes. The use of electrolyte is important to control the thickness of the electrical double layer in the redox-initiated system to maintain the low viscosity of the latex. In the semi-batch process, a impeller (pitched-blade or Rushton) with high mixing efficiency is necessary to obtain a consistent polymerization rate during the monomer feed stage. The adiabatic polymerization was carried out in a homemade thermos reactor, where the heat loss is around 40%. The main heat loss is due to the heat capacity of the thermos reactor, impeller, and shaft. Batch redox-initiated emulsion polymerizations were then carried out at different surfactant and initiator concentrations to study the nucleation mechanism. Both DLS and CHDF methods have limitations for particle sizing in this system for low size end and can not give accurate results for particle size for the redox-initiated latex. TEM imaging with negative staining was considered as the only accurate particle sizing method for the redox-initiated latex.

3.5 References

1 Li, M. Ph.D. Dissertation, Lehigh University (2002)

2 Kohut-Svelko, N., Porro, R. Asua, J. M. and Leiza, J. R., *J. Polym. Sci. Polym. Chem.*, **47**, 2917 (2009)

3 Goikoetxea, M., Heijungs, R., Barandiaran M. J. and Asua, J. M., *Macromol. React. Eng*., **2**, 90 (2008)

4 Tsuchida, E. Hatashita, M., Makino, C., Hasegawa, E. and Kimura, N. *Macromolecules*, **25**, 207 (1992)

5 Li, P. and Shan, H., *J. Polym. Mater*., **11**, 223 (1994)

6 Spence, C. P. and Ford, W. T., *J. Polym. Sci. Part A: Polym. Chem.*, **39**, 525 (2001)

7 Wang, C. C., Yu, N. S., Chen, C. Y. and Kuo, J. F., *J. Appl. Polym. Sci*., **60**, 493 (1996)

8 Liu Z., Han, Y., Zhou C., Zhang M., Li W., Zhang H., Liu F., and Liu W., *Ind. Eng. Chem. Res.* **49**, 7152–7158 (2010)

9 Halnan, L. F. , Napper, D. H. and Gilbert, R. G., *J. Chem. Soc*., **80**, 2851-2865 (1984)

10 Qiu, J., Gaynor, S. G. and Matyjaszewski, K., *Macromolecules*, **32**, 2872–2875 (1999)

11 S. Beuermann, M. Buback, T. P. Davis, R. G. Gilbert, R. A. Hutchinson, A. Kajiwara and B. Klumperman, Macromol Chem. Phys., **201**, 1355 (2000)

12 Geurts, J. M., Jacobs, P. E., Muijs, J. G., Steven Van Es J. J. G. and German, A. L., *J. Appl. Polym*. Sci., **61**, 9 (1996)

13 Williams, R. J., Phillips, J. N. and Mysels, K. J., *Trans. Faraday Soc*., **51**, 728 (1955)

14 Smith, W. V. and Ewart, R. H., *J. Chem. Phys*., **16**, 592 (1948)

15 Derjaguin, B. V. and Lykema, L., *Acta Physicochim*, USSR, **14**, 633 (1941)

16 Verwey, E. J. W. and Overbeek, J. Th. G., *Theory of stability of Lyphobic Colloids*, Elsevier, Amsterdam (1948)

17 Li, D., Electrokinetics in Microfluidics, Elsevier, London, p 17 (2004)

18 Lebedev, B. V., Kulagina, T. G. and Smirnova, N. N., *J. Chem. Thermodynamics*, **26**, 941 (1994)

19 Li, Y. C., Wang, C. P. and Liu, X. J., *CALPHAD*, **32**, 217 (2008)

20 (a) Ivin, K. J. in *Polymer handbook*, 2nd ed.; Brandrup, J., Immergut, E. H., McDowell, W. Eds.; John Wiley; New York, p II-421 (1975); (b) Joshi, R. M. *Makromol, Chem*., **66**, 114. (1963); (c) McCurdy, K. G.; Laidler, K. J. *Can. J. Chem*. **42**, 818 (1964)

21 Sitaraman, S. Ph.D. Dissertation, Lehigh University (2002)

22 Chadwick D., *Role of the sarcoplasmic reticulum in smooth muscle*. John Wiley and Sons, p 259–264 (2002)

Chapter 4

KPS-initiated & Redox-initiated Isothermal Batch Emulsion Polymerization of *n*-Butyl Methacrylate

4.1 Introduction

Water-soluble thermal initiator is widely used in emulsion polymerization to produce latex. The reactions are usually carried out at 60 ºC - 90 ºC, due to the high activation energy (125-160 $kJ \cdot mol^{-1}$) of thermal initiators [1]. The radical generation rate is low. A high radical flux initiator, i.e., a redox initiator system has been considered in this study to decrease the particle size of emulsion polymerization. Furthermore, the low activation energy (40-80 $kJ \cdot mol^{-1}$) of redox initiators [1] allows the polymerization to be carried out at room temperature. Hydrogen peroxide (H_2O_2) and ascorbic acid (AA), in conjunction with metal ion (i.e. Fe^{2+}), were used in this study as the redox initiator system, while potassium persulfate (KPS) was used as the thermal initiator in the batch emulsion polymerization of *n*-butyl methacrylate (BMA).

4.1.1 Emulsion Polymerization Process

The emulsion polymerization process, which includes design variables such as reactant type and amounts, reactor type, feed strategy, agitation, and thermal history

(isothermal vs. adiabatic), can be optimized to control the final latex properties, such as particle size, molecular weight, polydispersity of particle size and molecular weight, polymer composition, and particle morphology. In conventional emulsion polymerizations, using hydrophobic monomer, water-soluble thermal initiator, and surfactant concentration above its critical micelle concentration (cmc), the principal site for particle nucleation is within the monomer-swollen micelles. Homogenous nucleation in the aqueous phase dominates nucleation while the surfactant concentration is below the cmc, when no micelles are present, or when hydrophilic monomer is used. The monomer droplets basically act as monomer reservoirs, which supply monomer to the growing latex particles. The monomer droplets are relatively large and the total surface area of monomer droplets for radical capture is relatively small. Therefore, nucleation from monomer droplets is negligible [2].

When the surfactant concentration is above its critical micelle concentration (cmc), monomer-swollen micelles are the main location of particle nucleation. The emulsion polymerization process can be divided into three intervals, which are the particle nucleation stage (Interval I) and particle growth stages (Intervals II and III) [3], which can be divided by the disappearance of monomer droplets. In an emulsion polymers system (as shown in Figure 4.1), a continuous aqueous phase, monomer droplets with surfactant on the surface, micelles, free surfactant and dissolved monomer are all present. When initiator is added, free radicals are generated in the aqueous phase and particles are formed by micellar nucleation, homogenous nucleation and droplet nucleation (negligible). Free surfactant molecules adsorb on the

existing particles and stabilize the growing particles. Both the particle number and polymerization rate increase with time. This stage is termed Interval I in the Smith-Ewart theory (shown in Figure 4.2), which ends when the micelles disappear. During Interval II, the monomer droplets act as reservoirs to provide monomer to the monomer-swollen polymer particles via diffusion through the aqueous phase, while the particle number remains constant. This process maintains the saturation swelling of the growing particles and supports the propagation reaction. Free radicals can initiate polymerization in the aqueous phase when dissolved monomer is present to become oligomers. The oligomers keep growing to a critical length when they can precipitate out and grow [4] for further propagation. The particle number and polymerization rate can be considered to be constant in Interval II (shown in Figure 4.3). The monomer droplets disappear at the end of Interval II, which is usually around 40% conversion.

The kinetics of propagation in emulsion polymerization can be categorized into two systems, zero-one and pseudo-bulk [5, 6]. The zero-one system represents a radical entering a particle, no matter whether it contains a growing chain or not. If the particle contains a growing chain, the entry of a radical results in very rapid termination. If the particle does not contain a growing chain, the entry of a radical results in the formation of a growing chain. In the zero-one system, the steady-state value of the average number of radicals per particle ($\bar{n}$), is around 1/2. In a pseudo-bulk system, radicals move frequently between particles and the system is kinetically equivalent to a bulk system ($\bar{n}$ can take any value).

Interval III starts with the disappearance of monomer droplets, which is shown in Figure 4.4. The reaction continues until the monomer in the monomer-swollen polymer particles is consumed. During this final stage, the particle number also remains constant and the polymerization rate decreases due to the decrease of the monomer concentration in the particles. When the conversion is high, the viscosity of the latex polymer particle increases. The rate of termination becomes limited by diffusion. The polymerization rate may increase again, which is termed the gel effect (Trommsdorff-Norrish effect) [7].

Figure 4.1: *Schematic diagram of emulsion system.*

Figure 4.2: *Schematic diagram of Interval I.*

Figure 4.3: *Schematic diagram of Interval II.*

Figure 4.4: *Schematic diagram of Interval III.*

4.1.2 Nucleation

4.1.2.1 Micellar Nucleation

In the emulsion polymerization carried out with a surfactant above its critical micelle concentration (cmc), initiator radicals are generated in the aqueous phase and

enter the monomer-swollen surfactant micelles, as oligomeric radicals or as single radicals. Polymerization is initiated in the micelles to form monomer-swollen polymer particles, which grow by propagation. Usually only one out of every 100-1000 micelles captures radicals and forms a polymer particle. Other micelles disappear by transport of surfactant from micelles to growing particles. Micellar nucleation ends with the disappearance of micelles, after which the particle number remain constant.

Smith-Ewart theory [8] predicts the relationship between the number of particles, the concentration of initiator, and the concentration of surfactant. At the end of Interval I in the batch emulsion polymerization, the number of particles is predicted to be proportional to the initiator concentration to the power of 0.4, and to the initial surfactant concentration to the power of 0.6, as shown in Eq (4-1). This equation accurately predicts the particle number for emulsion polymerization with styrene and other water insoluble monomers.

$$N_{\mathrm{p}}=K\left(\frac{bR_{\mathrm{i}}}{\mu}\right)^{0.4}\times\left(a_{s}S\right)^{0.6} \tag{4-1}$$

where K is a constant with the value of 0.53 for purely micellar capture, and 0.37 if capture by the new particle is also taken into account [9], bR_{i} is the rate of free radical generation, μ is the rate of particle volume growth, a_s is the stabilized area per surfactant molecule and S is the total number of surfactant molecules in the system.

4.1.2.2 Homogenous Nucleation

In a number of emulsion polymerization systems, aqueous phase radicals can initiate polymerization with monomer first to form oligomers, and then continue to grow until they reach a critical chain length, at which point they precipitate out from the aqueous phase and form particles. The oligomers may also flocculate or coagulate to form new particles. This nucleation process is termed homogenous nucleation. Homogenous nucleation typically occurs for relatively water-soluble monomers and it is the only nucleation mechanism for hydrophobic monomers with no surfactant micelles present.

Fitch and Tsai [10, 11] developed a quantitative theory for homogeneous nucleation, and Ugelstad and Hansen [12, 13] made significant improvements to the Fitch-Tsai theory. Homogeneous nucleation can be presented as Eq (4-2).

$$\left(\frac{\mathrm{d}N}{\mathrm{d}t}\right) = bR_{\mathrm{i}} - R_{\mathrm{c}} - R_{\mathrm{f}} \tag{4-2}$$

where N is the particle number, bR_{i} is the rate of free radical generation, R_{c} is the radicals capture rate by particles, and R_{f} is the coagulative nucleation rate.

4.1.2.3 Droplet Nucleation

Nucleation of monomer droplets is typically not significant in emulsion polymerization. The monomer droplets are large (1-10 μm) and present in much smaller numbers (~10^{13}), compared with the size of micelles (2-20 nm) and number of

micelle (~10^{21}). However, droplet nucleation is important in miniemulsion polymerization.

4.1.3 Initiator

In conventional emulsion polymerizations, the water-soluble thermal initiator is widely used and the free radicals are generated from thermal decomposition of the initiator. Potassium persulfate (KPS) is one of the most well studied thermal initiators in both industry and academia. The KPS radical generation equation is presented in Eq (4-3) and the KPS decomposition rate [14] is presented in Eq (4-4) and (4-5).

$$S_2O_8^{2-} \rightarrow 2\ SO_4^{2-} \bullet \quad (4\text{-}3)$$

$$k_d = 8\times10^{15} \exp\left[-135\text{kJ mol}^{-1}/RT\right] \quad (4\text{-}4)$$

$$t_{1/2} = 0.693/k_d \quad (4\text{-}5)$$

where R is the ideal gas constant (8.314 $J\cdot mol^{-1}\cdot K^{-1}$), and T is the absolute temperature (K). k_d (s^{-1}) is the dissociation rate constant. $t_{1/2}$ is the half life time of KPS.

Besides thermal initiators, redox initiators are also common in emulsion polymerization, and have higher radical generation rates compared to thermal initiator. In the redox initiator system, free radicals are generated from reduction-oxidation reactions. In this work, hydrogen peroxide (H_2O_2) (oxidant) and ascorbic acid (AA) (reductant) are used as the redox initiator system. The mechanism of this redox initiator system is very complicated [15]. Radical generation is simplified as Eq (4-6) and (4-7). The mechanism of the redox reaction involves a one-electron transfer from

the ferrous ion (Fe^{2+}) to hydrogen peroxide with the dissociation of the oxygen-oxygen bond and the generation of one hydroxyl radical and one hydroxyl ion [16] (Eq. 4-6). The reducing agent (AA) is used to regenerate Fe^{2+} from Fe^{3+} in order to maintain the generation of radicals and ascorbic acid becomes dehydroascorbic acid (DHA) [17]. The radical generation rate [18] is presented in Eq (4-8)

$$Fe^{2+} + H_2O_2 \rightarrow Fe^{3+} + OH^- + OH\bullet \quad (4\text{-}6)$$

$$2Fe^{3+} + 2OH^- + AA \rightarrow 2Fe^{2+} + DHA + 2H_2O \quad (4\text{-}7)$$

$$R_r = 5.9\,[H_2O_2]\,[Fe^{2+}]\,N_A \quad (4\text{-}8)$$

where R_r (radicals dm^{-3} sec^{-1}) is the radical generation rate, and N_A is Avogadro's number (6.023×10^{23} mol^{-1}).

4.1.4 Mettler RC1 Reaction Calorimeter

The methods used to investigate the kinetics of emulsion polymerizations involve accurate determination of reaction rates, including non-steady-state conditions. Gravimetric determination of rates cannot provide sufficiently accurate data for this purpose, and calorimetry has usually been employed to obtain rate data with sufficient precision [19]. Therefore, the Mettler RC1 reaction calorimeter was used to carry out the emulsion polymerizations in this study. Experiments were carried out under isothermal conditions and are described in Chapter 4. In the isothermal mode, the desired reaction temperature is set at a constant value in RC1 and the jacket temperature (T_j) changes automatically to maintain the reactor temperature (T_r) at a specific value. By using the RC1, the rate of polymerization can be obtained directly

and continuously from the reaction heat, with the conversion calculated from the integral of the heat of reaction curve. Therefore, a detailed examination of polymerization processes can be obtained for a kinetics study.

During exothermic polymerization, the rate of heat evolution, Q_r ($J \cdot s^{-1}$) is proportional to the rate of polymerization R_p ($mol \cdot dm^{-3} \cdot S^{-1}$), which is according to Eq. (4-9) [20-22]. The monomer conversion x_t, at the time t (s) of the reaction, is obtained using Eq. (4-10)

$$R_p = \frac{Q_r}{\Delta H_p V_w} \tag{4-9}$$

The rate of polymerization is the moles of BMA converted per unit time per unit volume of water in the reactor and V_w (dm^3) is the volume of water in the recipe.

$$x_t = \frac{M_0 \int_0^t Q_r dt}{\Delta H_p m} \tag{4-10}$$

where m (g) is the initial mass of monomer in the recipe, M_0 (g/mol) is the molecular weight of the monomer, ΔH_p ($J \cdot mol^{-1}$) is the molar heat of polymerization, and the integral can be evaluated from the rate of heat evolution measured by the reaction calorimeter.

In this chapter, KPS-initiated and redox-initiated emulsion polymerizations were carried out under isothermal condition at different surfactant concentrations, initiator concentrations, solids contents, and reaction temperatures. The nucleation

mechanism and kinetics of emulsion polymerization under these conditions were studied.

4.2 Experimental

4.2.1 KPS-initiated Emulsion Polymerizations

Recipes used for thermally-initiated emulsion polymerizations under different conditions are shown in Tables 4.1 to 4.4. Table 4.1 shows the variation of different surfactant concentrations, the changes in initiator concentrations is shown in Table 4.2, the variation of solids contents is shown in Table 4.3, and the effect of different reaction temperatures are shown in Table 4.4. The Metter RC1 reactor was equipped with a pitched-blade impeller (as shown in Figure 4.5) with one baffle and the agitation speed was 400 rpm. The KPS-initiated polymerizations were predominantly carried out at 70 ºC, except for the polymerizations carried out at different reaction temperatures (55 ºC and 85 ºC). All components, except KPS solution, were charged into the reactor and then nitrogen was bubbled into the solution for 5 min in order to remove oxygen. After that, the nitrogen inlet and outlet were both shut off and the reactor temperature was increased to the design temperature. KPS was dissolved in 5 g water and was fed into the reactor in one shot in the thermally-initiated process after the reactor contents reached the design temperature. Samples were obtained during the polymerization by sampling from the reactor at different times for particle sizing, conversion and molecular weight. Each sample was ~ 5 g of latex and mixed with ~ 3

g of 1 % hydroquinone solution to stop the further reaction. To eliminate the monomer influence on particle size for samples obtained at low conversion, dialysis membrane tubing (3500 Daltons) was used to clean the latex.

Figure 4.5: *Pitched-blade impeller used in Mettler RC1 reactor.*

Table 4.1: Recipes for Thermally-initiated Emulsion Polymerizations where the Surfactant (SLS) Concentration was Varied, at 70 ºC

Reaction	**T1**	**T2**	**T3**	**T4**	**T5**	**T6**
BMA (g)	125					
DI water (g)	500					
SLS (g) *	0.578 (4.0 mM)	0.866 (6.0 mM)	1.127 (7.8 mM)	1.733 (12.0 mM)	2.890 (20.0 mM)	5.776 (40.0 mM)
KPS (g) *	0.234 (1.7 mM)					
$NaHCO_3$ (g) *	0.234 (5.6 mM)					

* Molar concentrations based on water

Table 4.2: Recipes for Thermally-initiated Emulsion Polymerizations where the Initiator (KPS) Concentration was Varied, at 70 ºC

Reaction	**T7**	**T8**	**T4**	**T9**	**T10**
BMA (g)	125				
DI water (g)	500				
SLS (g) *	1.733 (12.0 mM)				
KPS (g) *	0.058 (0.43 mM)	0.117 (0.86 mM)	0.234 (1.7 mM)	0.468 (3.4 mM)	0.937 (6.8 mM)
$NaHCO_3$ (g) *	0.058 (1.4 mM)	0.117 (2.8 mM)	0.234 (5.6 mM)	0.468 (11.2 mM)	0.937 (22.4 mM)

* Molar concentrations based on water

Table 4.3: Recipes for Thermally-initiated Emulsion Polymerizations where the Solids Content was Varied, at 70 ºC

Reaction	**T11**	**T12**	**T4**	**T13**
BMA (g)	26.3	55.5	125	214.3
DI water (g)	500			
SLS (g) *	1.733 (12.0 mM)			
KPS (g) *	0.234 (1.7 mM)			
$NaHCO_3$ (g) *	0.234 (0.6 mM)			

* Molar concentrations based on water

Table 4.4: Recipes for Thermally-initiated Emulsion Polymerizations where the Reaction Temperature was Varied

Reaction	**T14**	**T4**	**T15**
BMA (g)	125		
DI water (g)	500		
SLS (g) *	1.733 (12.0mM)		
Temperature (°C)	55	70	85
KPS (g) *	0.234 (1.7 mM)		
$NaHCO_3$ (g) *	0.234 (0.6 mM)		

* Molar concentrations based on water

4.2.2 Redox-initiated Emulsion Polymerizations

Recipes used for redox-initiated emulsion polymerizations carried out under different conditions are shown in Tables 4.5 to 4.10. Table 4.5 shows the variation of ferrous sulfate concentration, Table 4.6 shows the variation of surfactant concentration, changes in initiator concentration are shown in Table 4.7, the effect of feeding redox initiator into the reactor at different concentrations is shown in Table 4.8, the variation of solids contents is shown in Table 4.9, and the variation in reaction temperature is shown in Table 4.10. The Metter RC1 reactor was equipped with a pitched-blade impeller with one baffle and the agitation speed was 400 rpm. All

components, except for the redox initiator solutions, were charged into the reactor and then nitrogen was bubbled into the reactor for 5 min in order to remove oxygen. After that, the nitrogen inlet and outlet were both shut off and the reactor temperature was increased to the design temperature. Redox initiators (ascorbic acid and H_2O_2) were dissolved in 5 g water, and fed separately into the reactor as two shots for the redox-initiated process. H_2O_2 solution was fed into the reactor first and ascorbic acid solution was fed one minute later. The redox initiators were also fed into the reactor using a syringe pump with the same feeding rate and time for ascorbic acid and H_2O_2 to study the influence of low radical generation rate. The redox-initiated polymerizations were predominantly carried out at 25 ºC, except for the polymerizations carried out at different reaction temperatures (40 ºC and 55 ºC). Samples were obtained during the polymerization by sampling from the reactor at different times for particle sizing, conversion and molecular weight. Each sample was ~ 5 g of latex and was mixed with ~ 3 g of 1 % hydroquinone solution to stop further reactions. To eliminate the monomer influence on the particle size at low monomer to polymer conversion, dialysis membrane tubing (3500 Daltons) was used to clean the latex.

Table 4.5: Recipes for Redox-initiated Emulsion Polymerizations where the Ferrous ions Concentration was Varied, at 25 ºC

Reaction	**RF0**	**RF1**	**R4**
BMA (g)	125		
DI water (g)	500		
SLS (g) *	1.733 (12 mM)		
$FeSO_4$ (g) *	0	0.0063 (0.04 mM)	0.0125 (0.09 mM)
NaCl (g) *	0.209 (7.2 mM)		
AA (g) *	0.45 (5.1 mM)		
H_2O_2 (30%) (g) *	0.45 (7.9 mM)		

* Molar concentrations based on water

Table 4.6: Recipes for Redox-initiated Emulsion Polymerizations where the Surfactant (SLS) Concentration was Varied, at 25 ºC

Reaction	**R1**	**R2**	**R3**	**R4**	**R5**	**R6**
BMA (g)	125					
DI water (g)	500					
SLS (g) *	0.578 (4.0 mM)	0.866 (6.0 mM)	1.127 (7.8 mM)	1.733 (12.0 mM)	2.890 (20.0 mM)	5.776 (40.0 mM)
$FeSO_4$ (g) *	0.0125 (0.09 mM)					
NaCl (g) *	0.209 (7.2 mM)					
AA (g) *	0.45 (5.1 mM)					
H_2O_2 (30%) (g) *	0.45 (7.9 mM)					

* Molar concentrations based on water

Table 4.7: Recipes for Redox-initiated Emulsion Polymerizations where the Initiator Concentration was Varied, at 25 ºC

Reaction	**R7**	**R8**	**R9**	**R4**	**R10**
BMA (g)	125				
DI water (g)	500				
SLS (g) *	1.733 (12 mM)				
$FeSO_4$ (g) *	0.0125 (0.09 mM)				
NaCl (g) *	0.209 (7.2 mM)				
AA (g) *	0.05 (0.6 mM)	0.11 (1.2 mM)	0.23 (2.5 mM)	0.45 (5.1 mM)	0.90 (10.2 mM)
H_2O_2 (30%) (g) *	0.06 (1.0 mM)	0.11 (2.0 mM)	0.23 (4.0mM)	0.45 (7.9 mM)	0.90 (15.8 mM)

* Molar concentrations based on water

Table 4.8: Recipes for Redox-initiated Emulsion Polymerizations where the Redox Initiators Feeding was Varied, at 25 ºC

Reaction	**R11**	**R12**
BMA (g)	125	
DI water (g)	500	
SLS (g) *	1.733 (12 mM)	
$FeSO_4$ (g) *	0.0125 (0.09 mM)	
NaCl (g) *	0.209 (7.2 mM)	
Ascorbic Acid (g)	0.45 (Feed 1h)	0.09 (Feed 1h)
H_2O_2 (30%) (g)	0.45 (Feed 1h)	0.09 (Feed 1h)

* Molar concentrations based on water

Table 4.9: Recipes for Redox-initiated Emulsion Polymerizations where the Solids Content was Varied, at 25 ºC

Reaction	**R13**	**R14**	**R4**	**R15**
BMA (g)	26.3	55.5	125	214.3
DI water (g)	500			
SLS (g) *	1.733 (12 mM)			
$FeSO_4$ (g) *	0.0125 (0.09 mM)			
NaCl (g) *	0.209 (7.2 mM)			
AA (g) *	0.45 (5.1 mM)			
H_2O_2 (30%) (g) *	0.45 (7.9 mM)			

* Molar concentrations based on water

Table 4.10: Recipes for Redox-initiated Emulsion Polymerizations where the Reaction Temperature was Varied

Reaction	**R4**	**R16**	**R17**
BMA (g)	125		
DI water (g)	500		
SLS (g) *	1.733 (12 mM)		
$FeSO_4$ (g) *	0.0125 (0.09 mM)		
NaCl (g) *	0.209 (7.2 mM)		
Temperature (ºC)	25	40	55
AA (g) *	0.45 (5.1 mM)		
H_2O_2 (30%) (g) *	0.45 (7.9 mM)		

* Molar concentrations based on water

4.2.3 Characterization

The Mettler RC1 reaction calorimeter was used to obtain the continuous reaction rate, conversion, reactor temperature, etc. The final solids content and final conversion were measured gravimetrically. The molecular weight was measured by GPC and TEM images obtained with a negative staining technique were used for particle sizing to obtain accurate particle size. For the TEM images, ~ 1000 particles were counted to obtain the statistical results of the particle size and particle size

distribution for each sample. The viscosity of latex was measured with a Brookfield viscometer with a #1 spindle at 20 rpm. Dialysis membrane tubing (Spectrum Laboratories, Inc., 3500 Daltons) was used to clean the latex. UV spectroscopy (Spetronic Genesys2) was used to detect monomer levels in the aqueous phase. The characterization methods were described in Chapter 2.

4.3 Results and Discussions

To study the reaction rate during the polymerization, a Mettler RC1 reactor calorimeter was used. Accurate reaction rates can be calculated from the reaction heat measured by the Mettler RC1 reactor, indicating the different polymerization stages. The reactions were carried out using thermal initiator (KPS) and redox initiators (H_2O_2 and ascorbic acid) at different surfactant concentrations, initiator concentrations, different solids contents and different reaction temperatures. The results for the thermal-initiated latex are shown in Tables 4.11 and 4.12. The results for the redox-initiated latex are shown in Tables 4.13 and 4.14.

Table 4.11: Results of Thermal-initiated Emulsion Polymerization Reactions

Samples	Solids	Conversion	Coagulum	M_W (g/mol)	M_N (g/mol)	MW PDI
T1	19.86%	99.9%	1.4%	1,013,300	306,100	3.31
T2	19.92%	98.7%	0.3%	1,828,100	817,500	2.24
T3	20.04%	99.6%	0.3%	2,020,400	802,700	2.52
T4	20.19%	99.7%	0.2%	2,234,500	966,300	2.31
T5	20.22%	99.1%	0.1%	2,236,300	944,900	2.37
T6	20.51%	98.8%	0.0%	2,109,800	775,900	2.72
T7	20.12%	97.6%	0.1%	2,447,700	987,700	2.48
T8	20.00%	99.0%	0.2%	2,253,500	966,400	2.33
T9	20.26%	99.6%	0.2%	1,940,700	717,400	2.70
T10	20.33%	99.7%	0.3%	1,602,600	616,100	2.60
T11	5.35%	99.0%	0.0%	2,603,500	1,073,600	2.42
T12	10.12%	97.6%	0.1%	2,572,300	813,500	3.16
T13	30.05%	99.9%	0.5%	2,361,800	1,000,400	2.36
T14	20.16%	99.5%	0.2%	2,580,500	1,216,800	2.12
T15	20.19%	99.7%	0.2%	1,290,500	583,300	2.21

Refer to Tables 4.1 - 4.4 for recipes

Table 4.12: Particle Size Results Based on TEM Imaging from Thermal-initiated Emulsion Polymerization Reactions

Samples	D_w (nm)	D_v (nm)	D_n (nm)	SD (D_n) (nm)	PDI
T1	248.4	246.9	246.2	13.5	1.01
T2	164.4	163.5	163.0	8.7	1.01
T3	119.4	116.8	115.6	12.2	1.03
T4	112.8	111.6	111.0	8.4	1.02
T5	96.4	95.1	94.4	8.3	1.02
T6	78.1	76.2	75.1	9.4	1.04
T7	144.6	142.5	141.5	12.4	1.02
T8	125.8	124.4	123.7	9.9	1.02
T9	104.5	103.1	102.4	8.4	1.02
T10	101.2	98.4	96.9	12.0	1.04
T11	67.6	66.1	65.4	7.2	1.03
T12	90.1	88.2	87.1	9.8	1.03
T13	134.7	133.7	133.2	8.3	1.01
T14	154.5	150.4	148.3	14.1	1.04
T15	90.2	89.4	88.9	6.3	1.01

Refer to Tables 4.1 - 4.4 for recipes

Table 4.13: Results of Redox-initiated Emulsion Polymerization Reactions

Samples	Solids	Conversion	Coagulum	M_W (g/mol)	M_N (g/mol)	MW PDI
RF0	20.11%	99.2%	0.2%	2,913,600	747,300	3.90
RF1	20.17%	99.5%	0.1%	837,400	175,700	4.77
R1	19.80%	99.7%	1.4%	247,300	63,000	3.92
R2	19.96%	99.7%	0.8%	249,200	93,000	2.68
R3	19.94%	99.6%	0.9%	326,000	116,000	2.81
R4	20.24%	99.9%	0.3%	367,100	132,000	2.78
R5	20.43%	99.9%	0.1%	453,000	156,600	2.89
R6	20.38%	97.9%	0.0%	764,600	174,300	4.39
R7	19.38%	99.4%	3.8%	1,281,300	402,400	3.18
R8	19.84%	99.4%	1.6%	695,300	282,200	2.46
R9	20.12%	99.6%	0.4%	513,300	179,300	2.86
R10	20.22%	99.7%	0.3%	290,700	91,500	3.18
R11	20.10%	99.1%	1.7%	2,293,300	430,700	5.32
R12	19.92%	98.7%	0.4%	2,774,600	589,500	4.71
R13	5.34%	98.2%	0.0%	726,000	136,800	5.31
R14	10.33%	99.4%	0.0%	623,100	154,700	4.03
R15	30.02%	99.9%	0.7%	433,900	157,200	2.76
R16	20.13%	99.7%	0.5%	348,000	108,600	3.20
R17	20.05%	99.8%	1.0%	264,800	79,900	3.31

Refer to Tables 4.5 - 4.10 for recipes

Table 4.14: Particle Size Results Based on TEM Imaging from Redox-initiated Emulsion Polymerization Reactions

Samples	D_w (nm)	D_v (nm)	D_n (nm)	SD (D_n) (nm)	PDI
RF0	88.1	87.4	87.0	5.8	1.01
RF1	48.7	47.8	47.3	4.8	1.03
R1	72.1	71.3	70.8	5.5	1.02
R2	61.9	61.2	60.9	4.4	1.02
R3	48.1	47.6	47.4	3.4	1.02
R4	44.0	43.4	43.1	3.6	1.02
R5	39.5	39.1	38.8	3.2	1.02
R6	34.3	33.8	33.6	2.8	1.02
R7	54.2	53.7	53.5	3.4	1.01
R8	50.0	48.8	48.4	4.0	1.03
R9	47.0	46.4	46.1	3.9	1.02
R10	40.8	40.3	40.0	3.3	1.02
R11	62.9	62.4	62.2	3.9	1.01
R12	81.6	81.0	80.7	4.8	1.01
R13	35.6	34.6	34.0	4.3	1.05
R14	38.0	37.0	36.5	4.3	1.04
R15	47.4	46.4	46.0	4.5	1.03
R16	41.3	40.4	40.0	4.2	1.03
R17	44.8	44.3	44.0	3.6	1.02

Refer to Tables 4.5 - 4.10 for recipes

4.3.1 Influence of $FeSO_4$

Ferrous ion concentration is very important in the redox system, which can react with hydrogen peroxide and generate radicals. Therefore, the influence of ferrous ion concentration in redox-initiated systems was studied first. Three different ferrous ion concentrations, a high concentration (R4: 0.09 mM), a low, normal concentration, (RF1: 0.04 mM), and no ferrous ion (RF0: 0 mM), were used in the reactions. Figure 4.6 shows the rate of polymerization (R_p) and the conversion versus reaction time and Figure 4.7 shows the rate of polymerization versus conversion for the reactions carried out with different ferrous ion concentrations. The reaction time started after the ascorbic acid was added. The reaction without ferrous ion has a significant 15 minute induction period, which indicates a very slow radical generation rate. Also, the reaction rate is lower and the reaction time is longer compared with the reactions carried out with ferrous ion present. The reactions with high and low ferrous ion concentrations are fast and have similar reaction curves. The ferrous ion improves the radical generation rate in the redox reaction, resulting in a high radical flux. Smaller particle size and higher particle numbers result from the higher radical flux. The particle size of RF1 (D_w: 48.7 nm) is larger than R4 (D_w: 44.0 nm). This occurs because the radical generation rate can be influenced by the ferrous ion concentration, as shown in Eq (4-6). With higher ferrous concentration, the radical generation rate can be higher, which can result in higher particle number and smaller particle size. The particle size of RF0 (D_w: 88.1 nm) is much larger than RF1 and R4, because the

radical generation rate is much lower without ferrous ion as the catalyst. The particle number of RF0 is 6.79×10^{17} L^{-1} and the particle number of R4 is 5.54×10^{18} L^{-1}, which is about 8 times different. At 40% conversion, the reaction rate of RF0 is 1.47×10^{-3} mol dm^{-3} s^{-1}, and R4 is 11.1×10^{-3} mol dm^{-3} s^{-1}, which is also about 8 times greater. This indicates that the difference in the reaction rates is caused by the difference in particle number. The order of the radical generation rate is R4>RF1>RF0. Therefore, the molecular weight order is R4<RF1<RF0, as shown in Figure 4.8. 0.09 mM ferrous sulfate was used in later reactions to achieve consistent high radical generation rates.

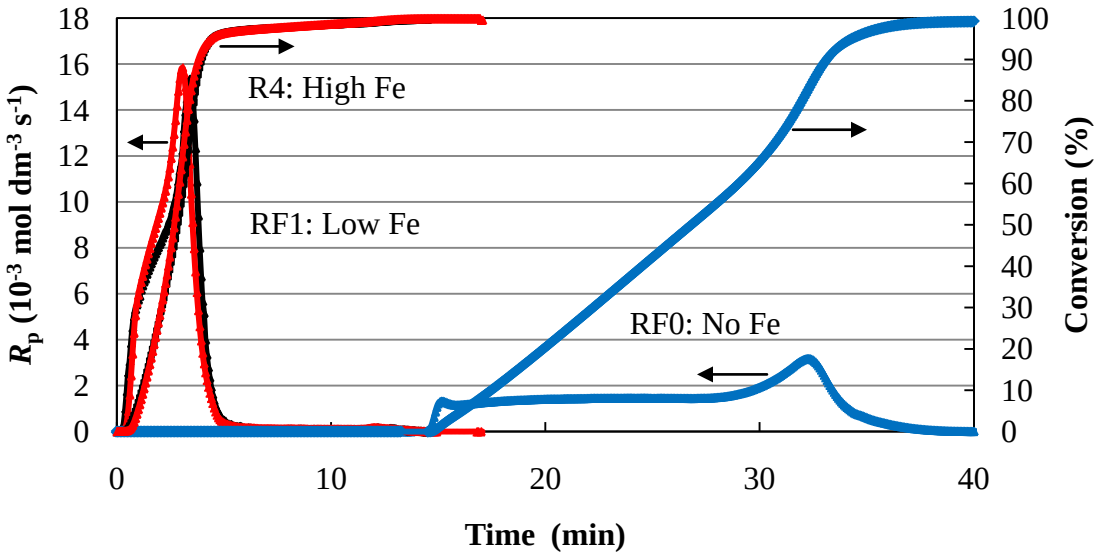

Figure 4.6: *Reaction rates vs. reaction time of redox-initiated emulsion polymerization at different ferrous ion concentrations.*

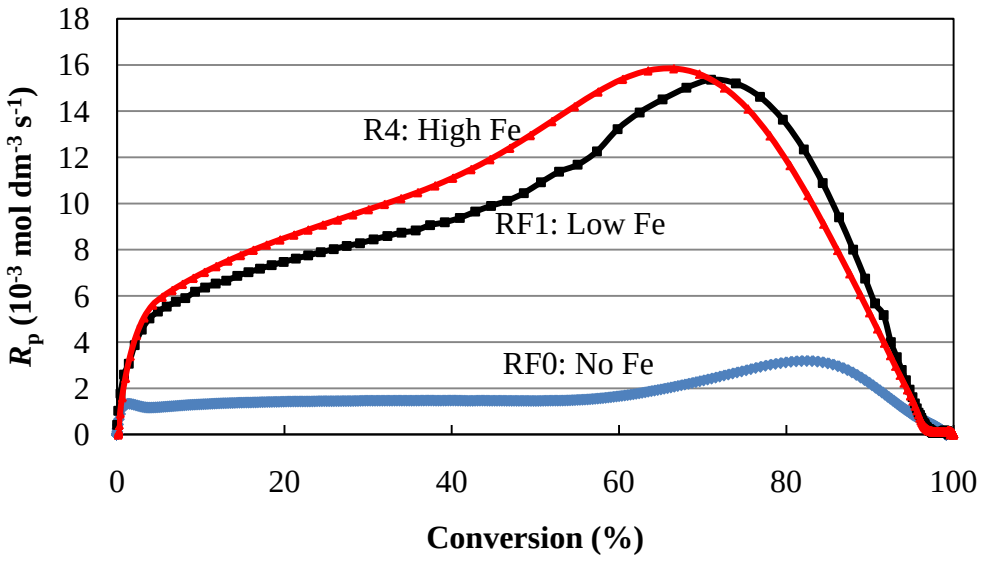

Figure 4.7: *Reaction rates vs. conversion of redox-initiated emulsion polymerization at different ferrous ion concentrations.*

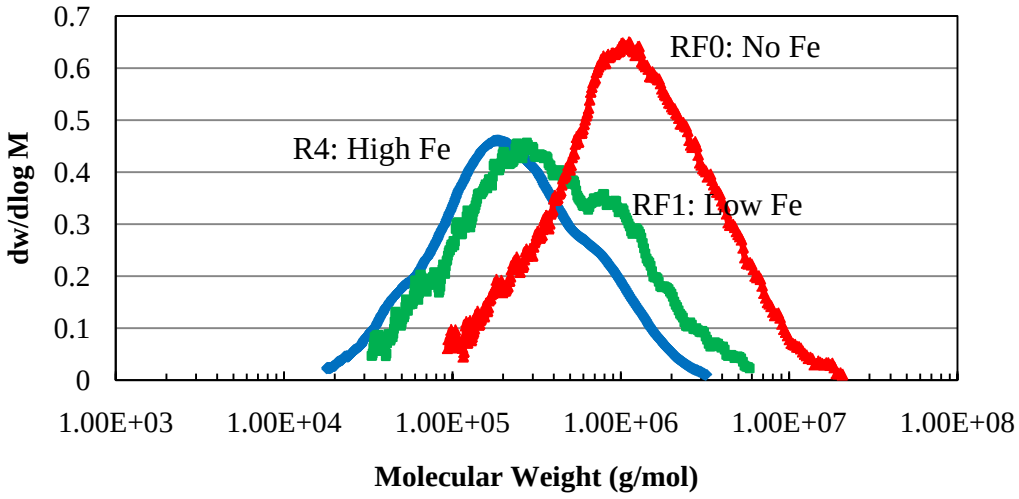

Figure 4.8: *Molecular weight distribution (GPC) of redox-initiated polymer at different ferrous ion concentrations.*

4.3.2 Influence of Surfactant

After studying the influence of the ferrous ion, the influence of surfactant concentration on the kinetics of the emulsion polymerization process was investigated. The reaction rates of KPS-initiated and redox-initiated polymerizations are shown in Figures 4.9 and 4.10. Three Intervals are clearly shown in the KPS-initiated polymerization (Figure 4.9). At the beginning of the reaction, the micellar nucleation process results in a very fast increase in the reaction rate (Interval I). Once the conversion is over 5%, the nucleation process is almost complete and the reaction rate becomes almost constant (Interval II). In some reactions (R4 and R5), there is a slight increase during Interval II, which may be caused by homogenous nucleation [21]. After 40% conversion, the reaction rate decreases, which is caused by the disappearance of the monomer droplets (Interval III). In several experiments (T1, T2 and T3), there is an increase in reaction rate in Interval III, which is caused by the gel effect (around 90% conversion). At high conversion, the concentration of polymer molecules increases, which results in a higher viscosity of the latex. In this case, the termination rate decreases and propagation rate increases, which is termed the gel effect. The gel effect has a smaller influence on smaller particles. The reaction rate is faster at higher surfactant concentrations, which is caused by larger particle numbers resulting from a larger number of micelles. However, in the redox-initiated polymerization, these three intervals are not present to the same extent as in the KPS-initiated process. There is a fast increase in reaction rate at the beginning of the reaction (around 5% conversion) caused by the micellar and homogeneous nucleation processes. However, this is followed by a continuing slower reaction rate increase, until it reaches around 70%

conversion. This increase indicates a significant continuation of homogenous nucleation after the initial micellar nucleation, which also indicates significant secondary nucleation. However, the particle size distribution is narrow, as seen in the TEM image (Figure 4.12). This may occur because the new nuclei formed by homogenous nucleation are not stable at that surfactant concentration. These nuclei aggregate with existing particles or coagulate with each other to form new particles by Brownian collisions and then fuse to form larger particles due to this instability [22]. Due to the smaller particle size of secondary nuclei, the surface area is larger, and the particle growth can be faster compared with larger particles. That can also minimize the particle size difference. A further study of homogenous nucleation will be investigated in Chapter 5. The latex particle size at different times during the reaction were measured to study the emulsion polymerization process as well as the extent of secondary nucleation, which will be discussed later. Finally, there is a fast decrease in the reaction rate until the reaction is complete, which results from the disappearance of the dissolved monomer in the aqueous phase. The reaction rate also increases with increasing surfactant concentration. However, the reaction rate in the redox-initiated polymerization is almost 4 times higher than the KPS-initiated polymerization. This occurs because there are much greater numbers of particles generated in the redox-initiated latex compared to the thermally (KPS)-initiated latex.

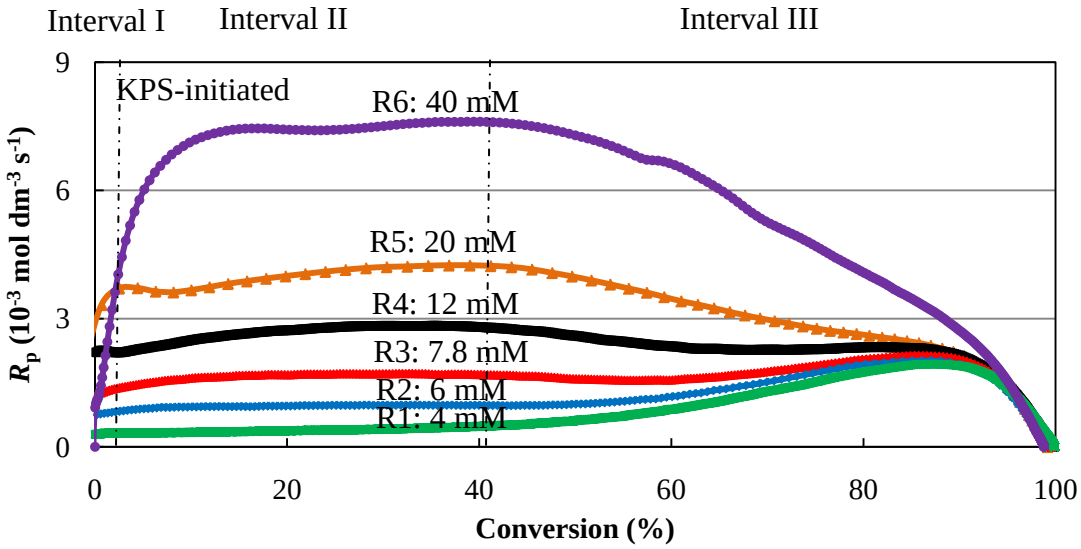

Figure 4.9: *Reaction rates vs. conversion of KPS-initiated emulsion polymerization at different SLS concentrations.*

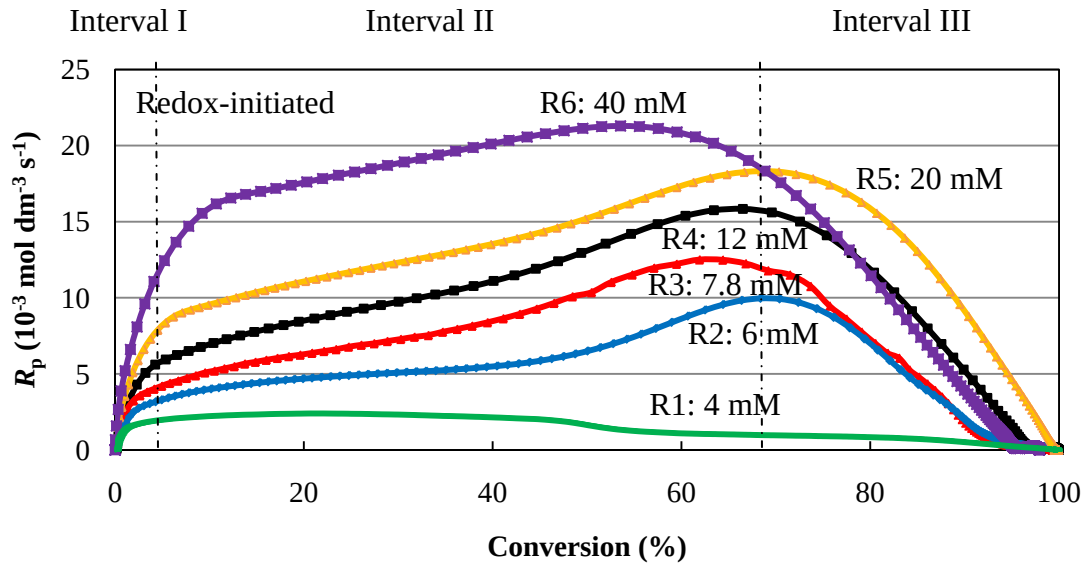

Figure 4.10: *Reaction rates vs. conversion of redox-initiated emulsion polymerization at different SLS concentrations.*

A significant difference in appearance between the KPS-initiated latex and the redox-initiated latex was observed (shown in Figure 4.11). For KPS-initiated latex (T4), the larger particle size (113 nm) results in a white opaque latex, and for redox-initiated latex (R4), the small particle size (44 nm) results in a translucent latex. A negative staining technique (with the addition of phosphotungstic acid aqueous solution) in conjunction with TEM is used to prevent artifacts that arise from the low T_g of PBMA, such as the occurrence of film formation during the sample preparation and imaging steps. In addition, a sharper TEM image can be obtained by this technique. There is a significant difference in particle size between the KPS-initiated and redox-initiated latexes. The particle size distributions are both narrow (shown in Figure 4.12). The KPS-initiated latex and redox-initiated latex (all 20% solids) are shown in Figures 4.13 and 4.14. The KPS-initiated latex is a white opaque latex, and there is no significant difference with any other latexes in their series. However, the appearance of the redox-initiated latex is significantly different at different SLS concentrations. The latex becomes more translucent at high SLS concentrations, which indicates smaller particle size.

Figure 4.11: *Appearance of: (A) KPS-initiated (T4) and (B) redox-initiated (R4) PBMA latexes.*

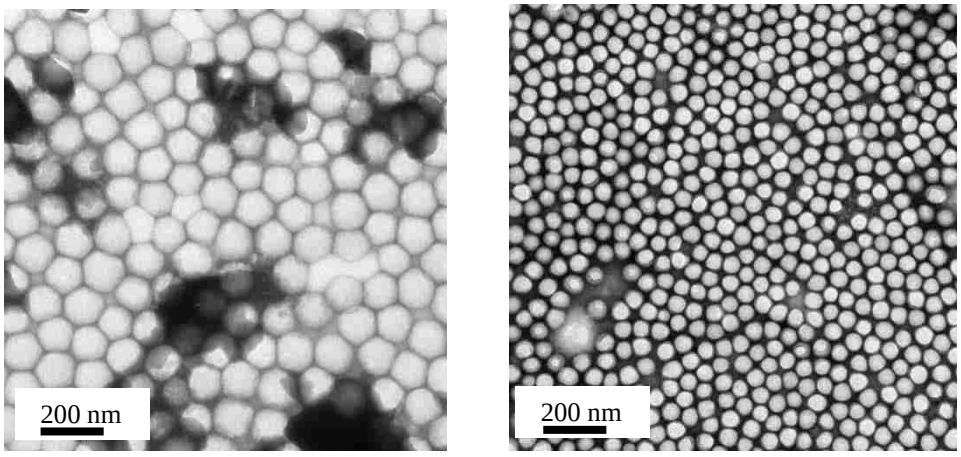

(A) (B)

Figure 4.12: *TEM images of: (A) KPS-initiated (T4) and (B) redox-initiated (R4) PBMA latexes.*

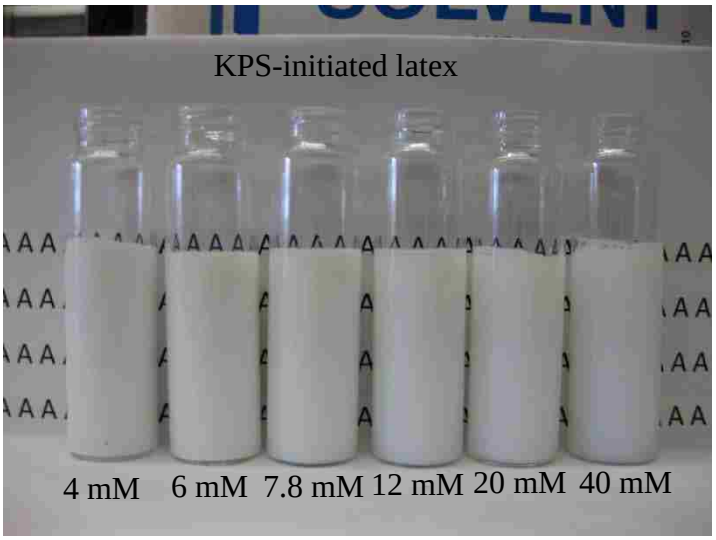

Figure 4.13: *Appearance of KPS-initiated PBMA latexes at different SLS concentrations.*

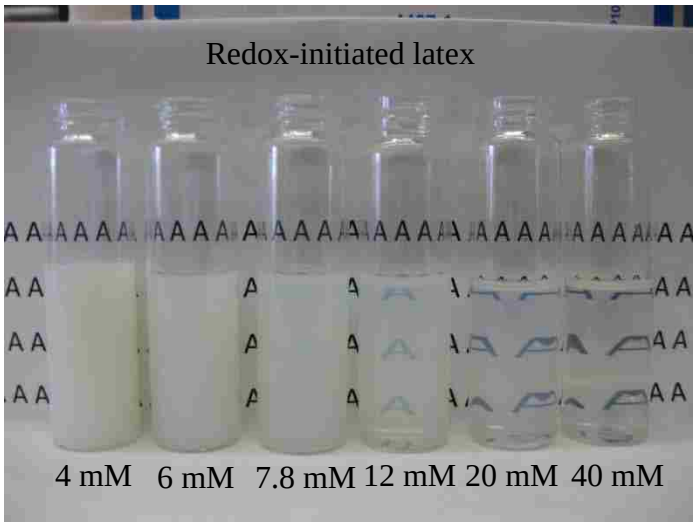

Figure 4.14: *Appearance of redox-initiated PBMA latexes at different SLS concentrations.*

The particle diameter is larger at lower surfactant concentration for both KPS-initiated and redox-initiated latexes, which is shown in Figure 4.15. The particle

number increases with the surfactant concentration, as shown in Figure 4.16. The relationship between particle number and surfactant concentration is $N_p \propto C_{SLS}^{0.81}$ for the KPS-initiated latex, and $N_p \propto C_{SLS}^{0.60}$ for the redox-initiated latex. There is a significant difference in the relationship between KPS-initiated latex and redox-initiated latex. However, both relationships still follow the Smith-Ewart theory. The relationship in redox-initiated latex is more compatible with the Smith-Ewart theory [8] ($N_p \propto C_{SLS}^{0.6}$) than the KPS-initiated latex, which indicates that the micellar nucleation mechanism is operative in both KPS-initiated and redox-initiated polymerization systems. However, there is nearly a 10 times difference in particle number between KPS-initiated latex and redox-initiated latex. The number of micelles is calculated based on the SLS micelle aggregation number at different temperatures [23]. The micelle aggregation number is around 74 at 25 °C and 41 at 70 °C. The particle number and micelle number above the cmc of SLS are shown in Figures 4.17 and 4.18. The particle number is still less than the micelle number for both redox-initiated latex and KPS-initiated latex. In addition, there is significant turning point for the particle number at 7.8 mM (SLS concentration), which is around the cmc of SLS. Therefore, micellar nucleation could be an important nucleation mechanism operating in both KPS-initiated and redox-initiated polymerization systems. The radical flux in the redox-initiated system is much higher than in the KPS-initiated system. This results in more micelles forming latex particles and higher final latex particle number in redox-initiated system. Due to the high radical flux and low BMA water solubility [24] (2.94 mM @ 25 °C) homogeneous nucleation can also contribute to the higher final particle

number. Although there is 10 times difference in the particle number between the redox-initiated polymerization (25 °C) and KPS-initiated polymerization (70 °C), the reaction rate coefficient is ~ 3 times different at different temperatures, so there is ~ 4 times difference in the reaction rate. The molecular weight of KPS-initiated latex and redox-initiated latex are shown in Figure 4.19. The high radical flux not only results in the formation of particles with much smaller particle diameters, but also results in the formation of particles with much lower molecular weight. When the surfactant concentration is higher, the particle number is greater, which results in a lower radical entry rate for each particle. Therefore, the molecular weight increases with increasing surfactant concentration. The molecular weight distribution of KPS-initiated latex as measured by GPC is shown in Figure 4.20 and that of redox-initiated latex is shown in Figure 4.21.

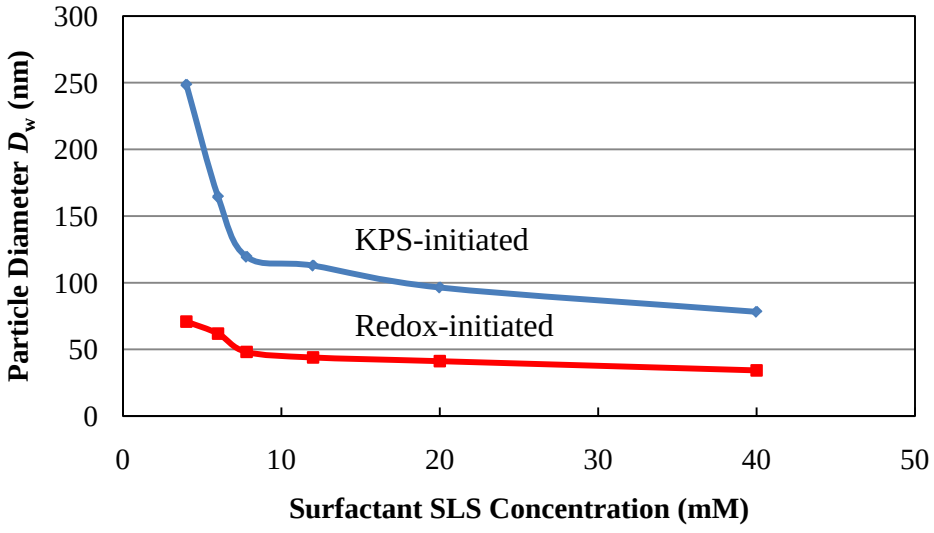

Figure 4.15: *Weight-average particle diameter (D_w) versus surfactant concentration for KPS and redox-initiated latexes.*

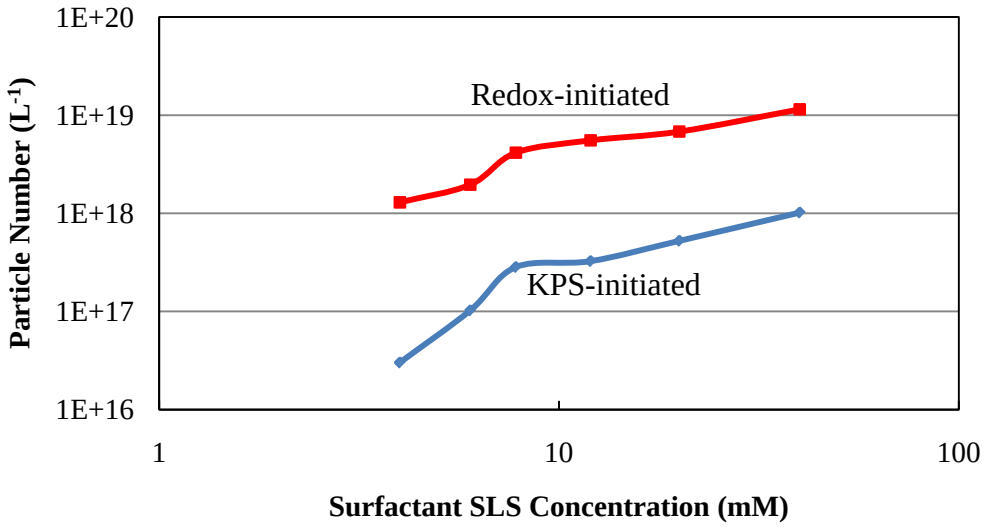

Figure 4.16: *Log-Log plot of particle number versus SLS surfactant concentration for KPS and redox-initiated latexes.*

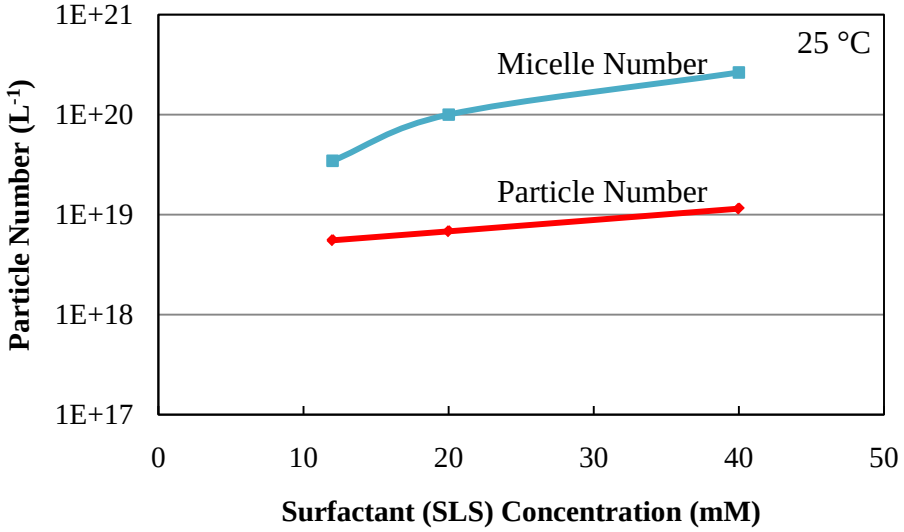

Figure 4.17: *Particle number and micelle number versus surfactant concentration for redox-initiated latexes at 25 °C.*

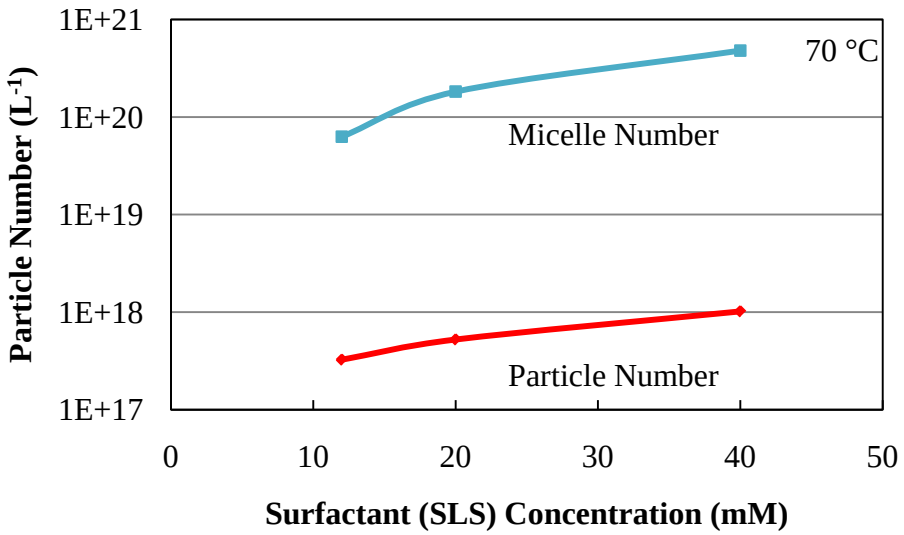

Figure 4.18: *Particle number and micelle number versus surfactant concentration for KPS-initiated latexes at 70 °C.*

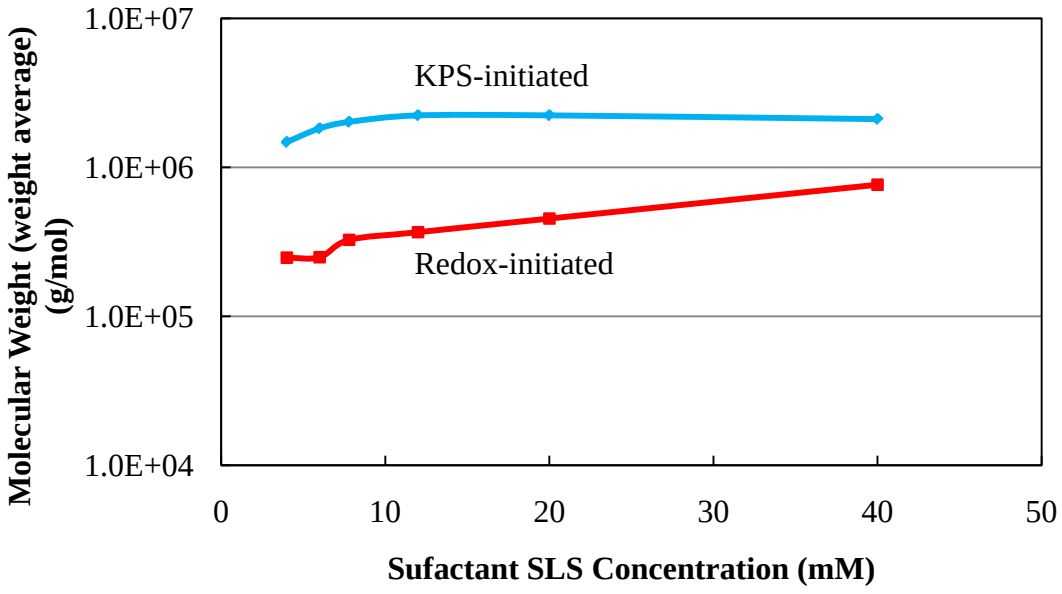

Figure 4.19: *Relationship between molecular weight (weight average) and surfactant concentration.*

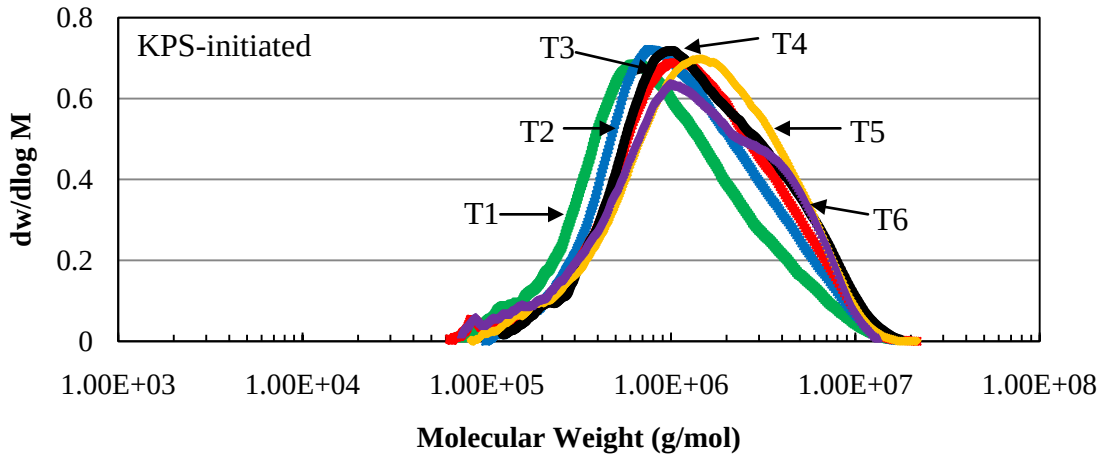

Figure 4.20: *Molecular weight distribution of KPS-initiated polymer as measured by GPC at different SLS concentrations (recipes shown in Table 4.1).*

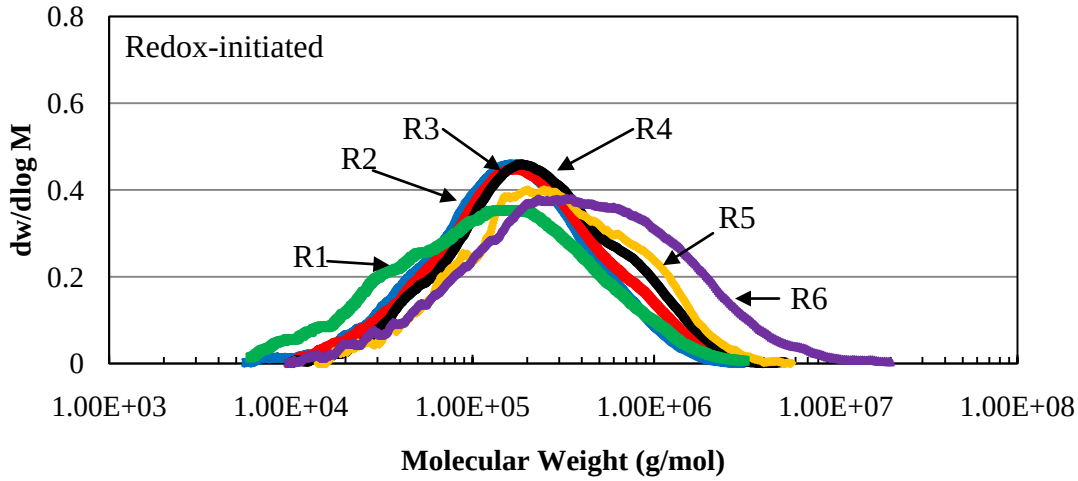

Figure 4.21: *Molecular weight distribution of redox-initiated polymer as measured by GPC at different SLS concentrations (recipes shown in Table 4.6).*

4.3.3 Influence of Initiator

The influence of initiator concentration on the kinetics of emulsion polymerization was studied next. The reaction rates of KPS-initiated and redox-initiated polymerizations are shown in Figures 4.22 and 4.23. The three intervals are clearly shown in the KPS-initiated polymerization, but have different shapes in the redox-initiated polymerization. The reaction rate is higher for polymerizations carried out with higher initiator concentrations, because of the higher particle numbers resulting from the higher radical generation rates. The reaction rate in the redox-initiated polymerization is still much faster than the KPS-initiated polymerization and keeps increasing after the nucleation process is complete (Interval I), which again indicates a significant extent of homogenous nucleation. When the redox initiator concentration is lower, the reaction rate decreases in the nucleation stage with a slower rate of increase in the propagation process (Interval II). A larger particle size and higher molecular weight can also be achieved.

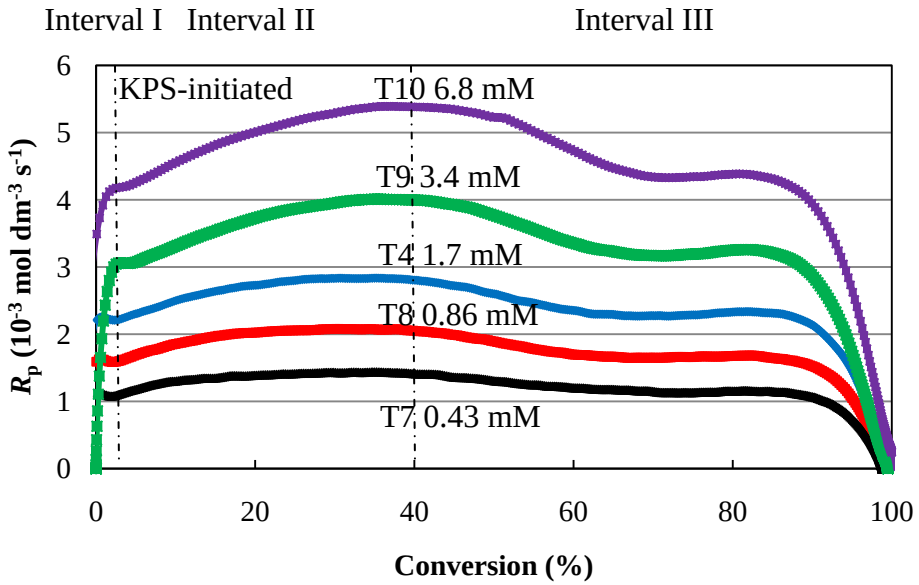

Figure 4.22: *Reaction rates vs. conversion of KPS-initiated emulsion polymerization at different initiator concentrations.*

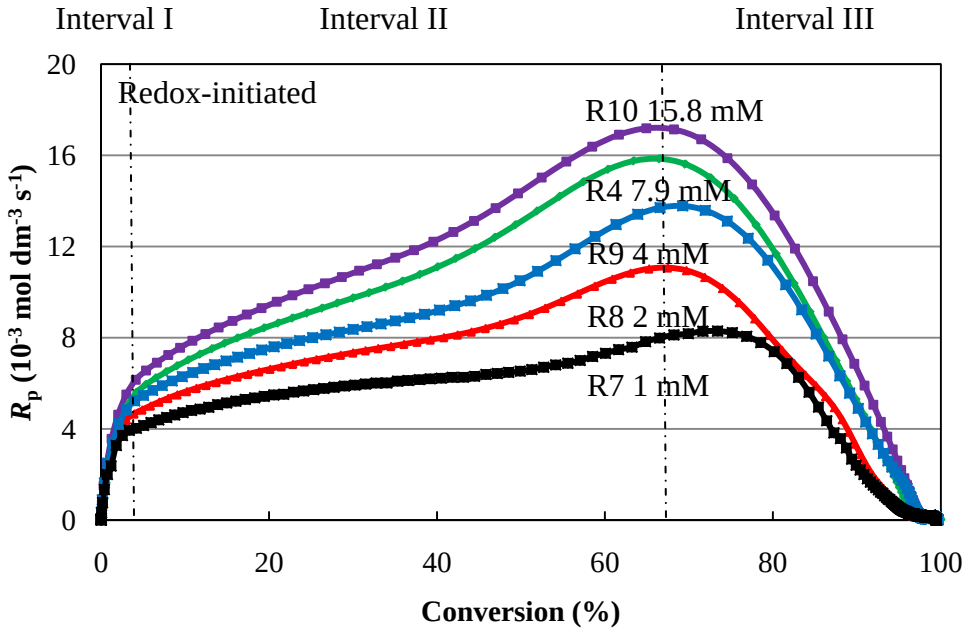

Figure 4.23: *Reaction rates vs. conversion of redox-initiated emulsion polymerization at different initiator (H_2O_2) concentrations.*

In reaction R11, the redox initiators were fed into the reactor separately using a syringe pump (0.45 g ascorbic acid per hour and 0.45 g H_2O_2 (30%) per hour). It was found that there was a lower radical generation rate compared with feeding in the initiator components in one shot. In this case (Figure 4.24), the reaction rate is slower, and the reaction rate then remains almost constant at the beginning of Interval II until it reached 50% conversion, where a rapid increase in reaction rate occurred, which may caused by the gel effect. The reaction rate started decreasing at around 80% conversion. The reaction rate of R11 (redox-initiated system shown in Figure 4.24) at the Interval II plateau is around 4×10^{-3} mol dm^{-3} s^{-1} , which is similar to the reaction rate of T4 (KPS-initiated system shown in Figure 4.22) (around 3×10^{-3} mol dm^{-3} s^{-1}) at the Interval II plateau. However, the rapid increase in reaction rate at around 50% conversion only occurred in the redox-initiated polymerization process. This indicates a significant difference between the redox-initiated and KPS-initiated polymerization process. In the R12 reaction, when the feed rate of redox initiators is lower (0.09 g ascorbic acid per hour and 0.09 g H_2O_2 (30%) per hour), the reaction rate is lower, while the reaction curve is similar to R11.

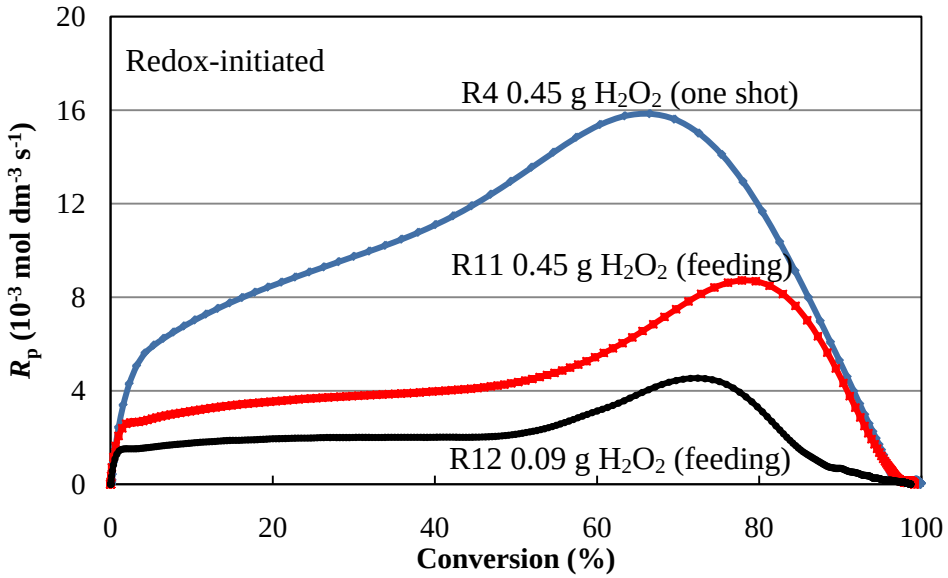

Figure 4.24: *Reaction rates vs. conversion of redox-initiated emulsion polymerization at different initiator concentrations and different feeding of initiator.*

The initiator concentrations are quite different between the KPS-initiated polymerization and redox-initiated polymerization. To compare these two systems in one figure, a relative initiator concentration was first used to study the process. A certain KPS concentration (1.7 mM) was set as the value of 1, and a certain redox component (H_2O_2) concentration (7.9 mM) was set to a value of 1. These conditions were selected since these are the initiator concentrations carried out in other reactions. The particle size is larger at lower initiator concentrations, which is shown in Figure 4.25. The particle number increases with initiator concentration, which is shown in Figure 4.26. The relationship between particle numbers and initiator concentrations is $N_p \propto C_I^{0.40}$ for the KPS-initiated latex and $N_p \propto C_I^{0.28}$ for the redox-initiated latex. The relationship for the KPS-initiated latex is in better agreement with the Smith-

Ewart theory [8] ($N_p \propto C_I^{0.40}$) compared to the redox-initiated latex. The relationships between particle number and concentration of surfactant/initiator indicate that micellar nucleation should be the main nucleation mechanism.

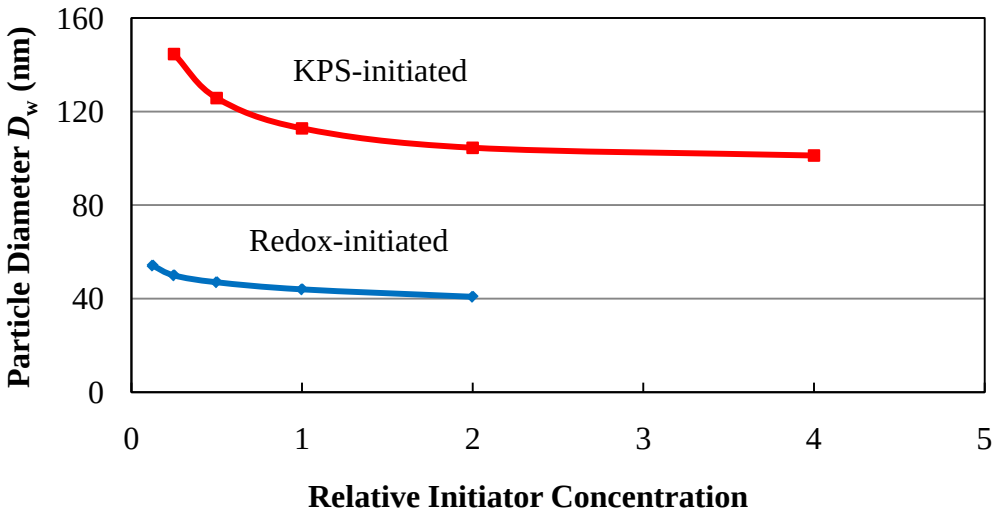

Figure 4.25: *Particle diameter (D_w) versus relative initiator concentration (standardized such that 1.7 mM KPS= 1, and 7.9 mM H_2O_2 = 1).*

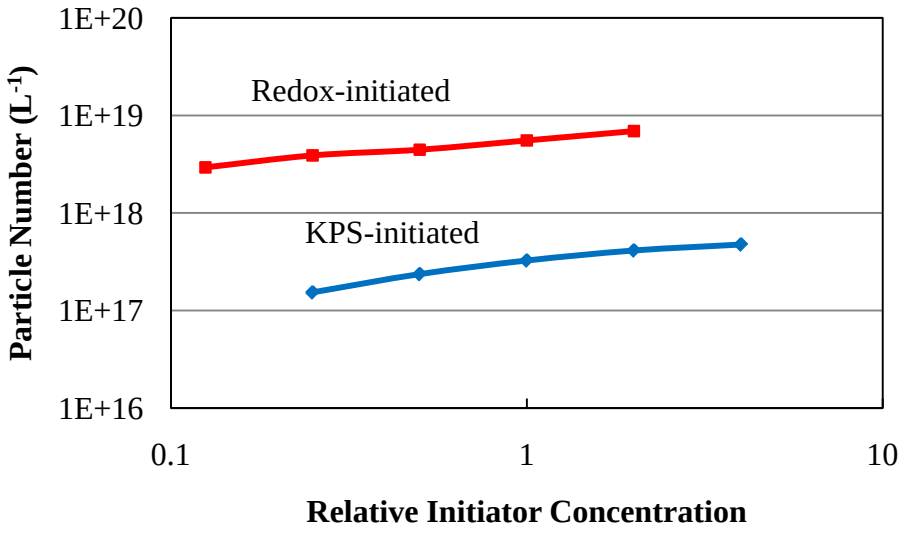

Figure 4.26: *Log-Log plot of particle number versus relative initiator concentration (standardized such that 1.7 mM KPS= 1, and 7.9 mM H_2O_2 = 1).*

Since the radical generation rates of KPS and redox are different, the radical generation rate was used to study each process. The initial initiator concentrations were used to calculate the radical generation rate, which is shown in Figure 4.27. There is ~ 10 times difference in the particle number between the KPS-initiated latex and the redox-initiated latex, and more than 10 times the difference in the radical generation rate. Homogenous nucleation in redox-initiated emulsion polymerization may be induced by this high radical flux. The particle number increases with the radical generation rate, which is shown in Figure 4.28. However, there is no overlap for the two relationships between particle numbers and radical generation rates in KPS-initiated systems and redox-initiated systems. This occurs because the radical generation mechanism for redox initiator is complicated and the radical generation rate

used for redox initiator is not very accurate. The side reactions of redox reaction are further described in Appendix A. The molecular weight of the KPS-initiated latex and the redox-initiated latex are shown in Figure 4.29. The use of redox initiator results in the formation of particles with much lower molecular weights compared to particles prepared using the KPS initiator, due to the high radical flux from the redox initiator. When the initiator concentration is higher, the radical flux is higher. This results in a higher radical entry rate for each particle. Therefore, the molecular weight decreases with increasing initiator concentration. The molecular weight results for KPS-initiated latex measured by GPC are shown in Figure 4.30 and the molecular weight results for the redox-initiated latex are shown in Figures 4.31 and 4.32.

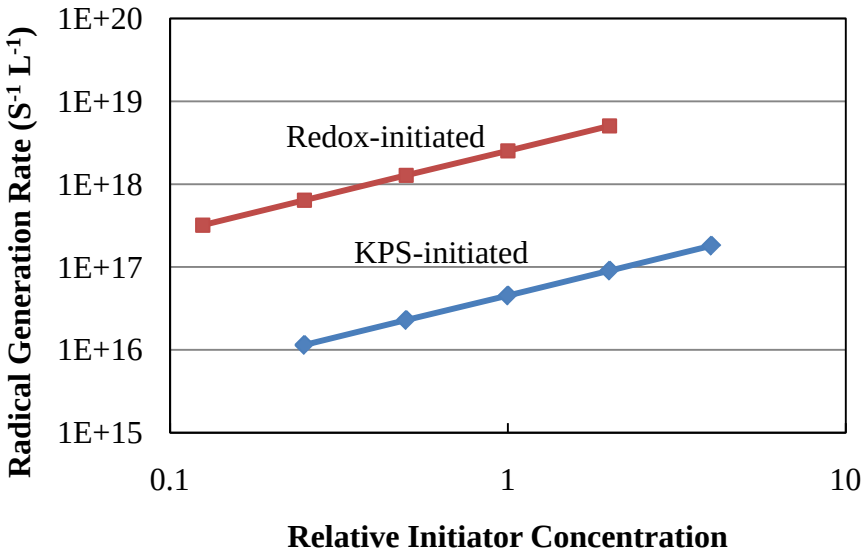

Figure 4.27: *Log-Log plot of radical generation rate versus relative initiator concentration (standardized such that 1.7 mM KPS= 1, and 7.9 mM H_2O_2 = 1).*

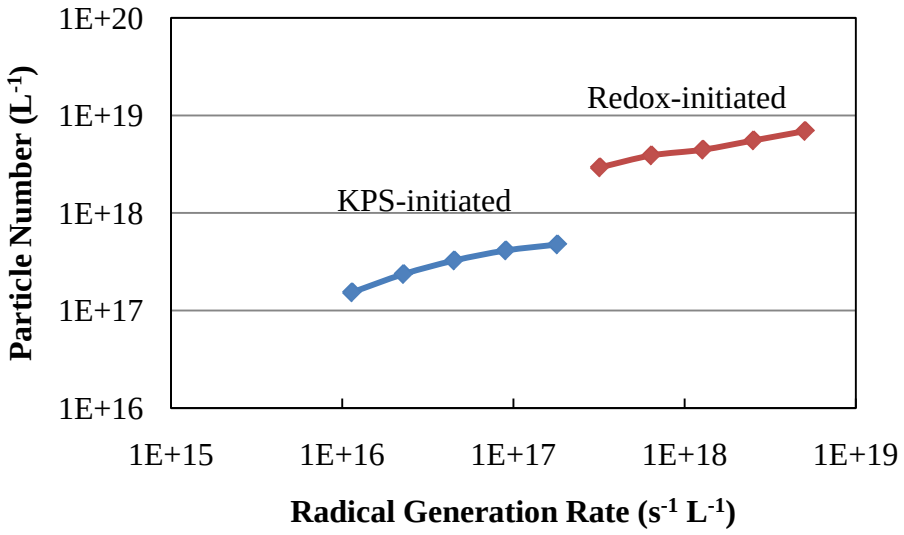

Figure 4.28: *Log-Log plot of particle number versus radical generation rate.*

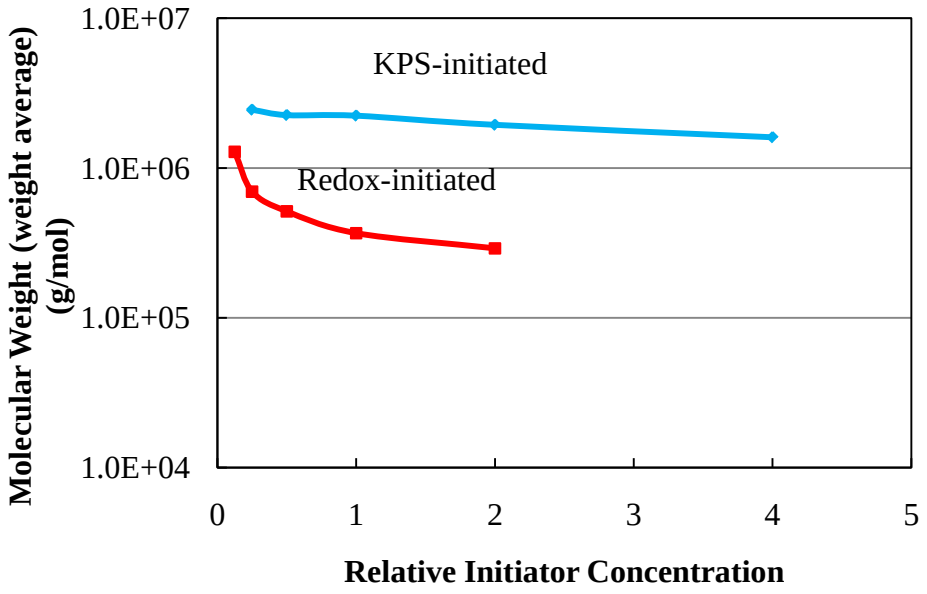

Figure 4.29: *Relationship between molecular weight (weight average) and relative initiator concentration (standardized such that 1.7 mM KPS= 1, and 7.9 mM H_2O_2 = 1).*

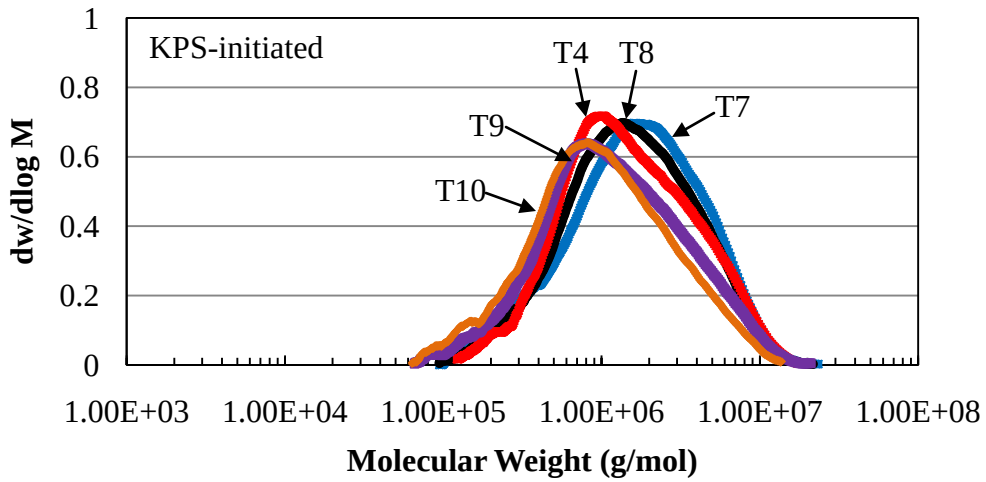

Figure 4.30: *Molecular weight distribution of KPS-initiated polymer measured by GPC at different KPS initiator concentrations (recipes shown in Table 4.2).*

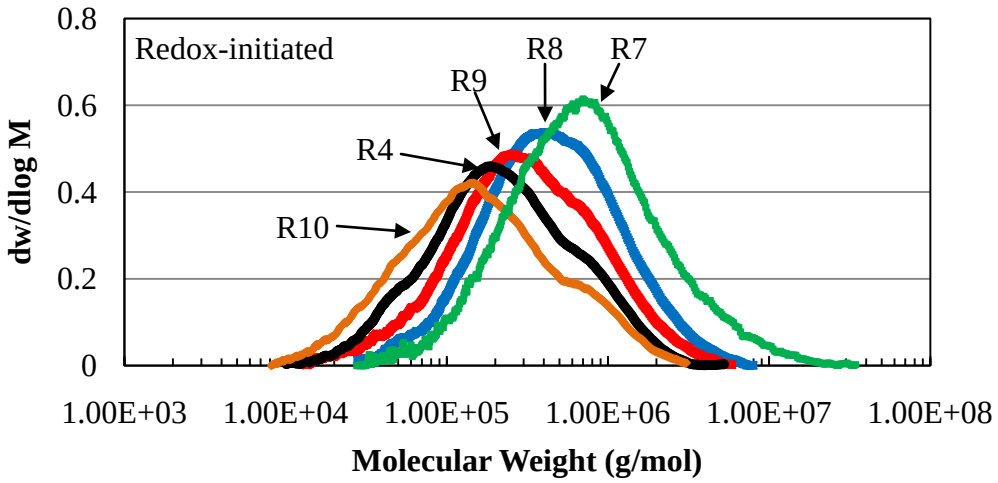

Figure 4.31: *Molecular weight distribution of redox-initiated polymer measured by GPC at different redox initiator concentrations (recipes shown in Table 4.7).*

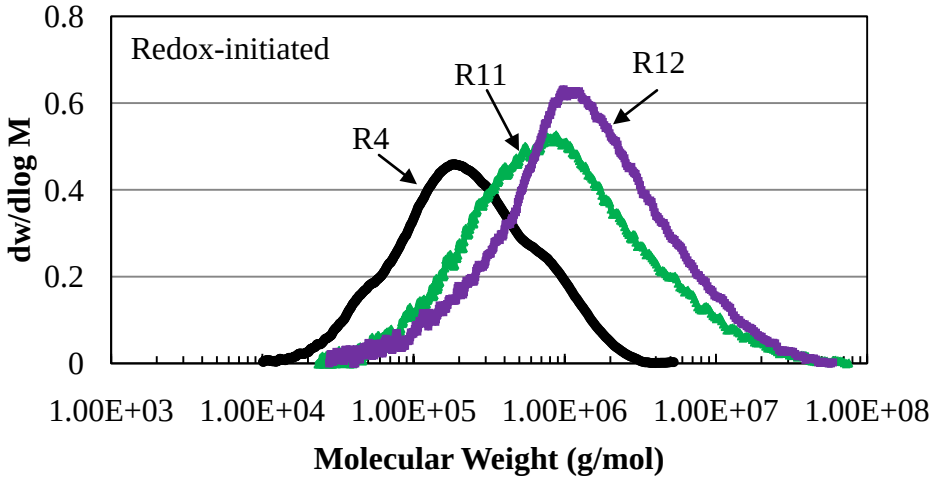

Figure 4.32: *Molecular weight distribution of redox-initiated polymer measured by GPC at different redox initiator concentrations (recipes shown in Tables 4.7 and 4.8).*

4.3.4 Influence of Solids Contents

The influence of solids contents was then studied. The reaction rates of KPS-initiated and redox-initiated polymerizations are shown in Figures 4.33 and 4.34. The three intervals are still clearly shown in the case of KPS-initiated polymerization, but not in the redox-initiated polymerization system. In KPS-initiated polymerization, the reaction rate is almost the same at different solids contents. This occurs because the surfactant concentration is the same, which results in a similar number of micelles. In micellar nucleation, the particle number only depends on the number of micelles. Therefore, similar micelle numbers should result in similar particle numbers, i.e., similar reaction rates. However, the reaction rate in the redox-initiated polymerization increases with increasing solids content, and it is much higher than the KPS-initiated

polymerization. This also indicates the existence of a significant amount of homogenous nucleation. When there is more monomer in the system, there is more homogenous nucleation and it occurs for a longer period. At higher solids content, more monomer in the system results in more homogenous nucleation which in turn results in the formation of greater particle numbers at higher solids content, and subsequently higher reaction rates in the redox-initiated polymerization system. For redox-initiated polymerizations carried out at 30% solids content, there is some fluctuation in the reaction rate after 60% conversion. This occurs because that the redox-initiated latex at 30% solids content has a much higher viscosity compared with other latexes at lower solids contents, as shown in Figure 4.35. Therefore, the mass transfer of radical and monomer may not be enough to maintain the high reaction rate near the end of the polymerization and results in fluctuations in the reaction rate.

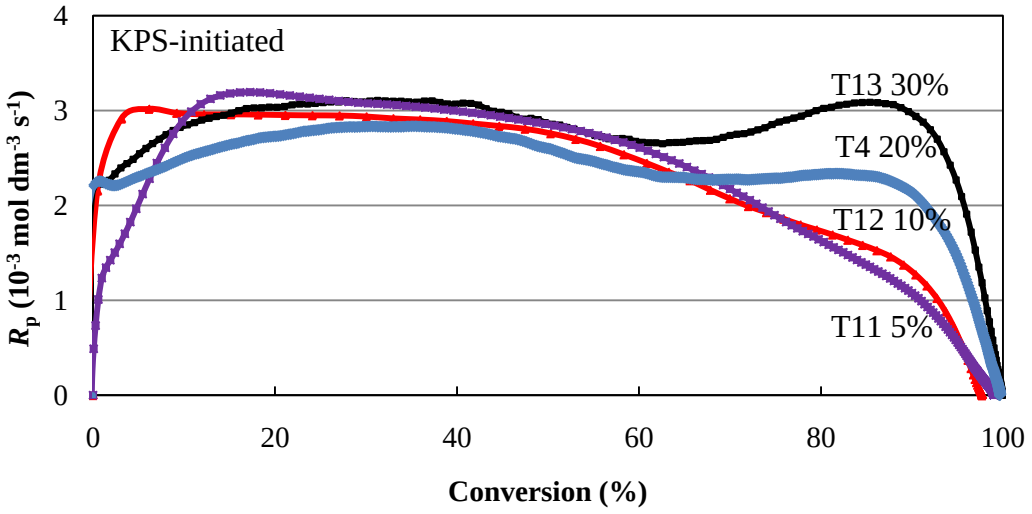

Figure 4.33: *Reaction rates vs. conversion of KPS-initiated emulsion polymerization of BMA at different solids contents.*

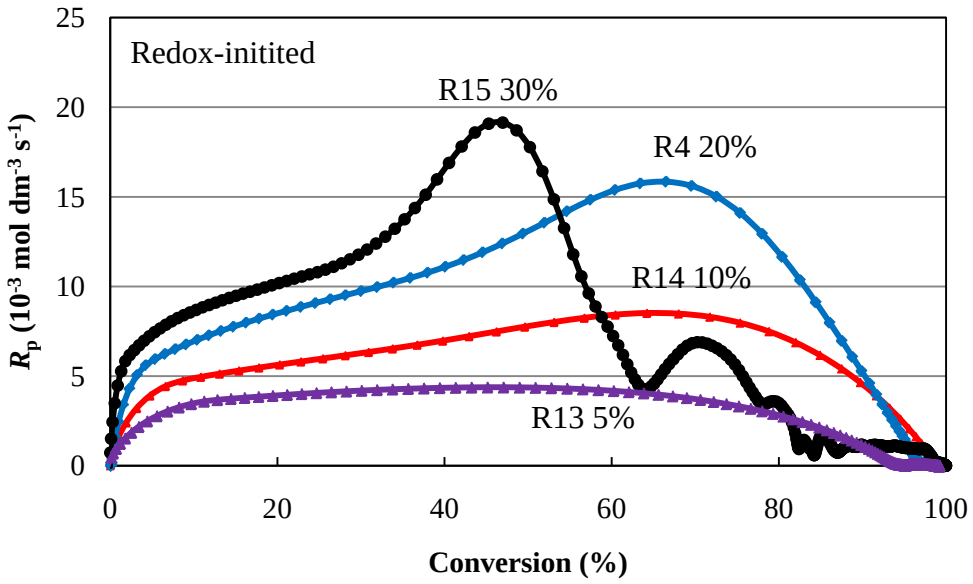

Figure 4.34: *Reaction rates vs. conversion of redox-initiated emulsion polymerization at different solids contents.*

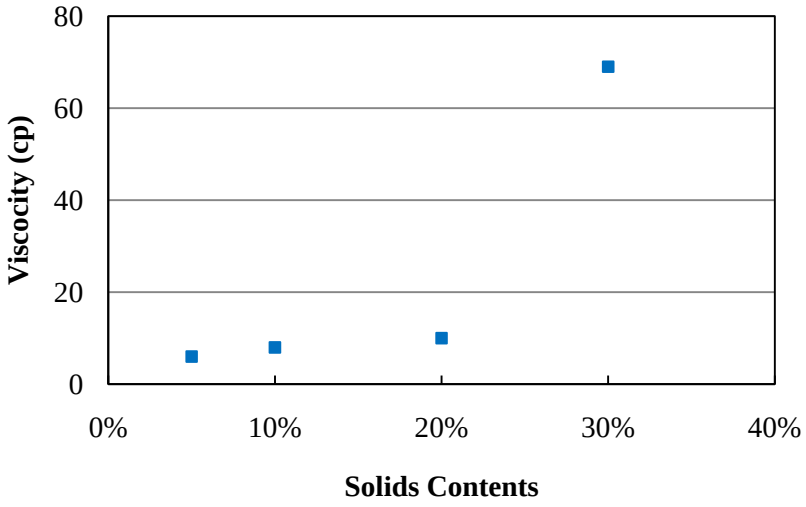

Figure 4.35: *Viscosity of redox-initiated latex at different solids contents.*

The particle diameter is larger for latexes with a higher solids content, which is shown in Figure 4.36. The particle number remains constant for KPS-initiated

polymerizations and increases with the solids content in redox-initiated polymerizations (shown in Figure 4.37). Micellar nucleation is the main nucleation mechanism in KPS-initiated polymerization. The use of the same surfactant concentration will result in a similar number of micelles, which results in a similar particle number. The particle number is independent of solids contents in KPS-initiated polymerization systems. Homogenous nucleation and micellar nucleation are the main nucleation mechanisms in redox-initiated polymerizations. In redox-initiated polymerizations, the particle number increases with solids content, which results in higher reaction rates at higher solids content. The relationship between particle number and solids contents is $N_p \propto \text{Solids}^{-0.03}$ for the KPS-initiated latex and $N_p \propto \text{Solids}^{0.66}$ for the redox-initiated latex. This indicates that homogeneous nucleation plays an important role in the nucleation mechanism in redox-initiated polymerization. The molecular weights of KPS-initiated and redox-initiated latexes are shown in Figure 4.38. The use of redox initiator results in a much higher radical flux compared to the thermal initiator, which make the radicals per latex particle much higher in redox-initiated system, and the molecular weight much lower. The molecular weight distribution of KPS-initiated latex measured by GPC is shown in Figure 4.39, and the molecular weight for redox-initiated latex is shown in Figure 4.40. The molecular weights do not change significantly with different solids contents for the KPS-initiated latex. However, for the redox-initiated latex, the solids contents significantly influence the molecular weight. There is a shoulder in the GPC peak representing the high molecular weight for the latex with 10% solids content (R14),

which becomes a peak for the latex with 5% solids content (R13). That could be the influence of homogeneous nucleation from redox-initiated systems. The molecular weight of latex particles formed by micellar nucleation may be different from the particles produced by homogeneous nucleation, due to the different nucleation mechanisms. The lower solids contents can minimize the extent of homogeneous nucleation process, which may result in a higher molecular weight because of the micellar nucleated particles. The molecular weight at different conversions during polymerization for the latex with 5 % solids content (R13) is shown in Figure 4.41. The peak of the molecular weight distribution shifts to a higher value with higher conversion.

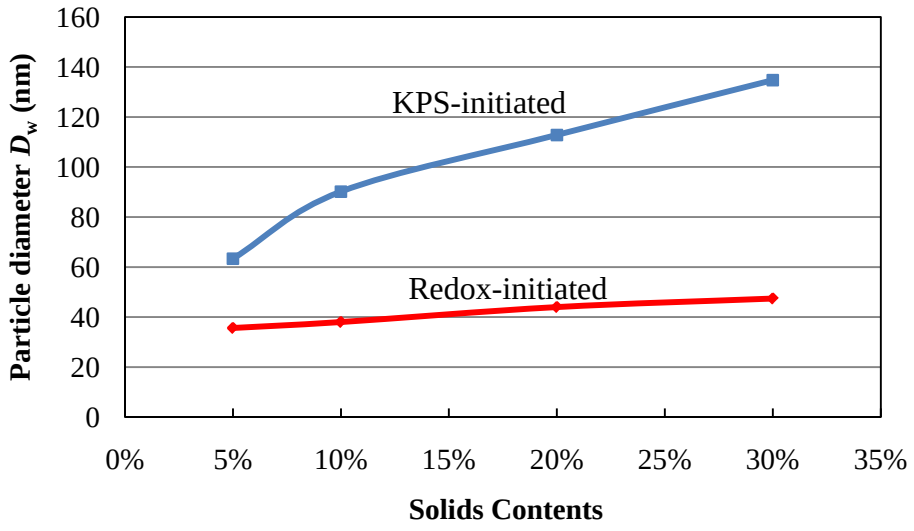

Figure 4.36: *Particle diameter (D_w) versus solids contents for KPS-initiated and redox-initiated latexes.*

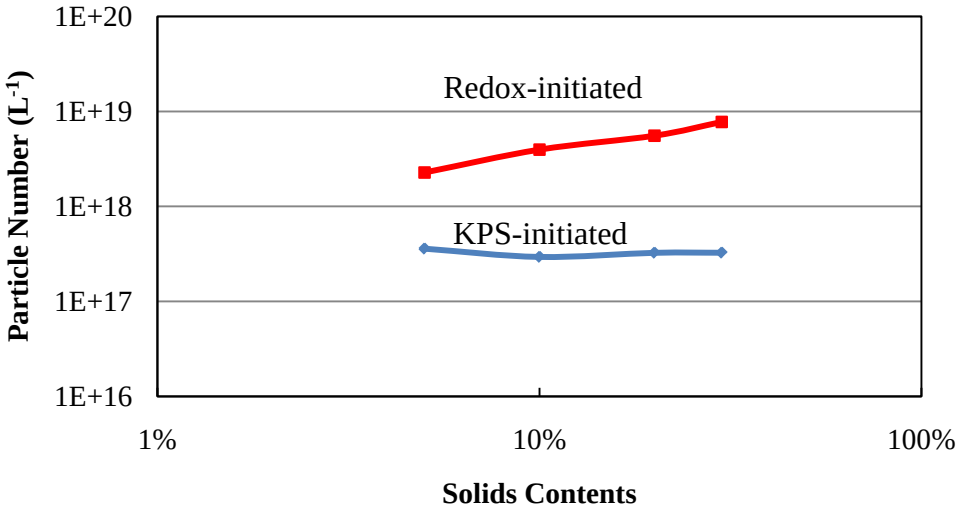

Figure 4.37: *Log-Log plot of particle number versus solids contents for KPS-initiated and redox-initiated latexes.*

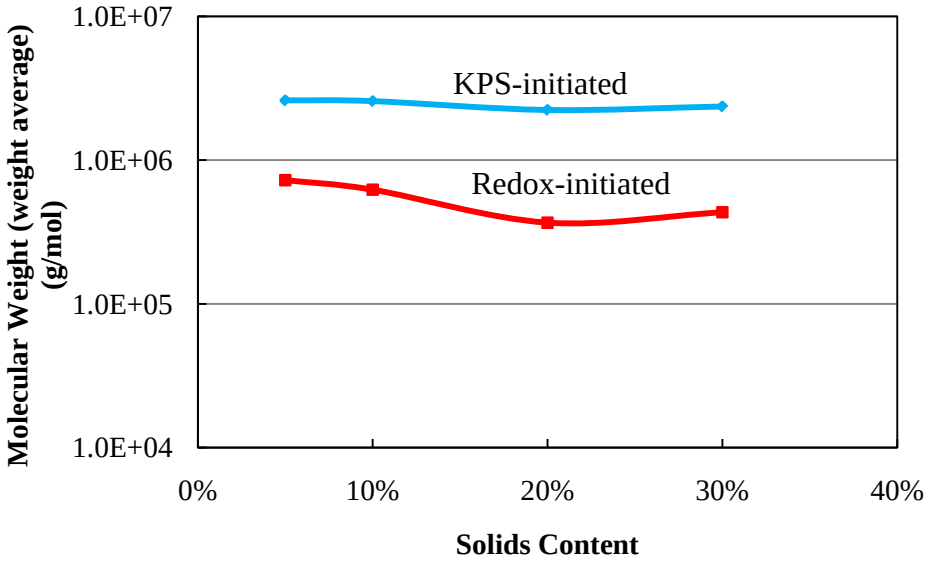

Figure 4.38: *Relation between molecular weight (weight average) and solids contents for KPS-initiated and redox-initiated latexes.*

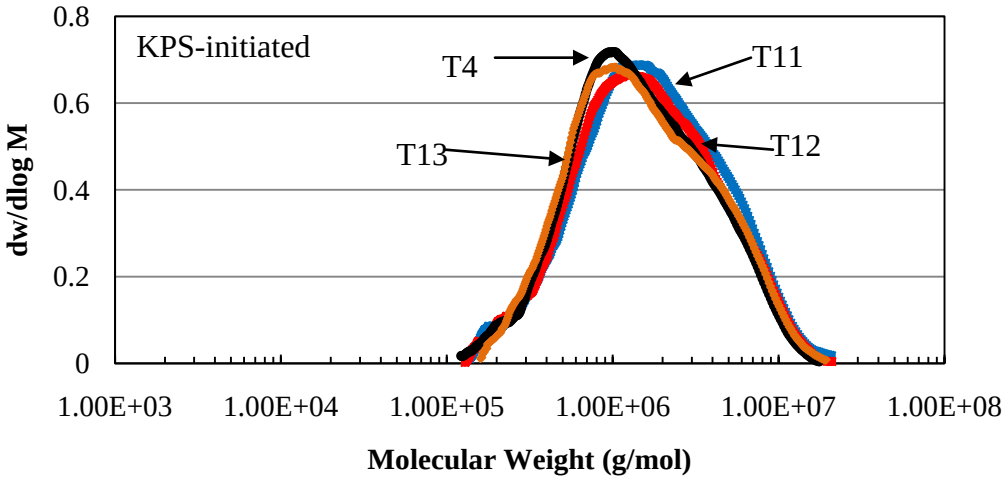

Figure 4.39: *Molecular weight distribution of KPS-initiated polymer measured by GPC at different solids contents (recipes shown in Table 4.3).*

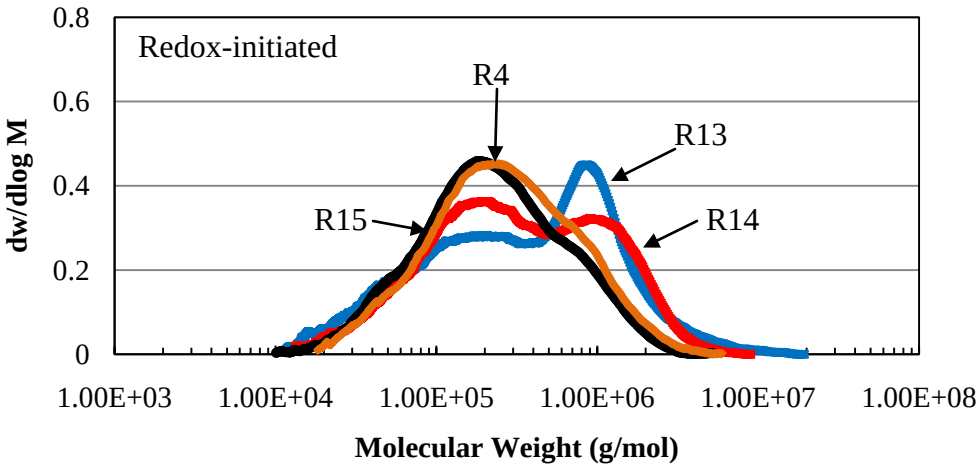

Figure 4.40: *Molecular weight distribution of redox-initiated polymer measured by GPC at different solids contents (recipes shown in Table 4.9).*

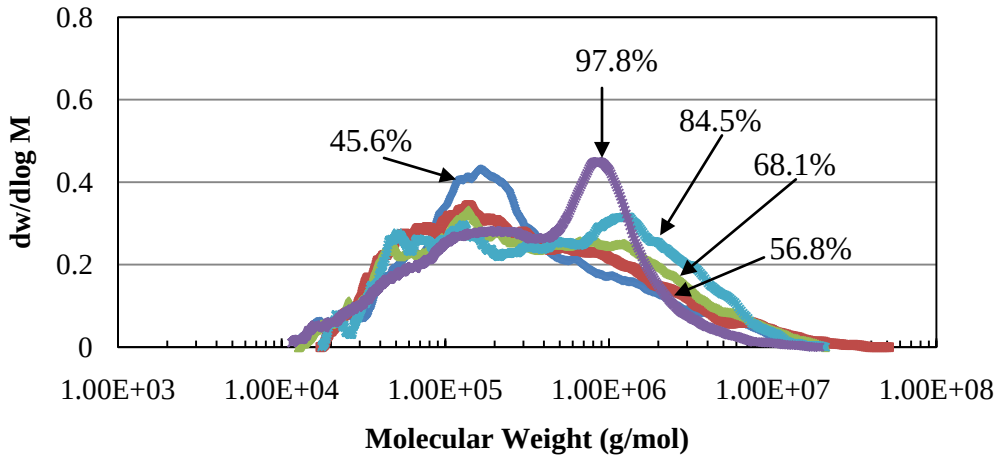

Figure 4.41: *Molecular weight distribution of redox-initiated polymer (5% solids) measured by GPC at different conversion during the polymerization (R13).*

4.3.5 Influence of Reaction Temperature

The influence of reaction temperature was also studied. The reaction rates of KPS-initiated and redox-initiated polymerizations are shown in Figures 4.42 and 4.43. The three Intervals are still clearly shown in the KPS-initiated polymerization, but not in the redox-initiated polymerization process. In both KPS-initiated and redox-initiated polymerizations, the reaction rates increase at higher reaction temperature. This occurs because of the higher reaction rate constant and higher radical generation rate at higher temperature.

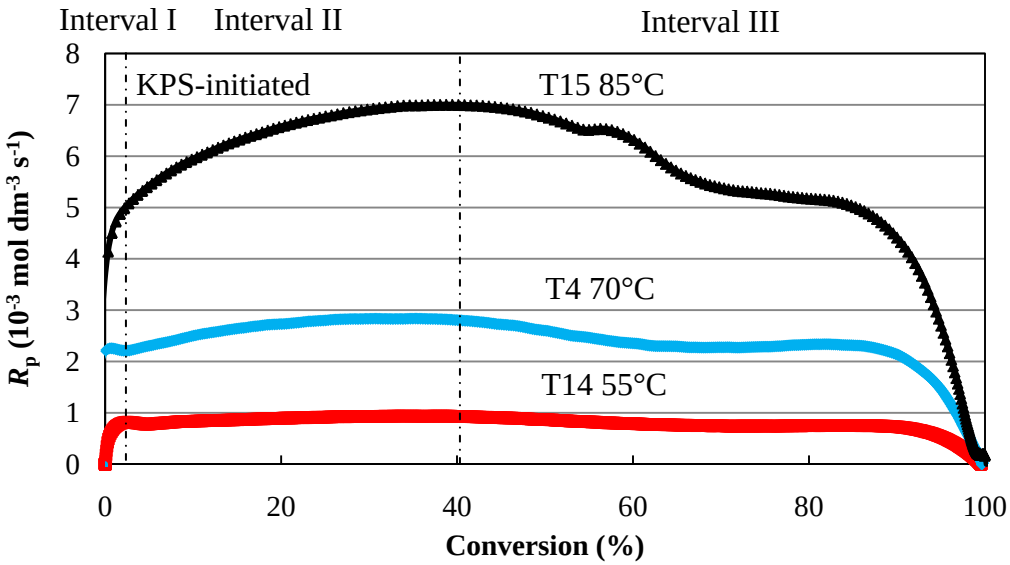

Figure 4.42: *Reaction rates vs. conversion of KPS-initiated emulsion polymerization at different reaction temperatures.*

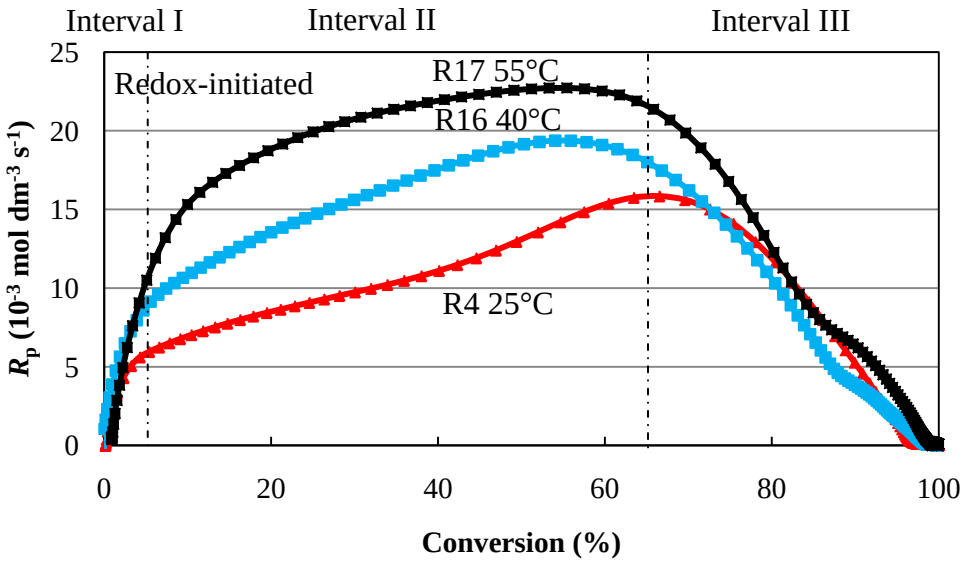

Figure 4.43: *Reaction rates vs. conversion of redox-initiated emulsion polymerization at different reaction temperatures.*

The particle size becomes smaller in the KPS-initiated process and is not significantly influenced in the redox-initiated process at higher temperatures, which is shown in Figure 4.44. In the KPS-initiated process, the radical generation rate is higher when the temperature is higher. Higher radical flux results in higher particle numbers in KPS-initiated system. However, in the redox-initiated process, the particle size is not significant influenced by reaction temperature. In the redox-initiated systems, the radicals are generated by the reduction-oxidation reaction, which may be not greatly influenced by the temperature as in the case of thermal initiators. The particles formed in the redox-initiated process are not as stable as in the KPS-initiated process due to the higher particle number at the same surfactant concentration, especially during the secondary nucleation process. Therefore, higher reaction temperatures can lead to instability of particles in the redox-initiated process which decreases the particle number, and increases the particle size. The use of redox initiator results in a much lower molecular weight compared to thermal initiator, which is caused by the high radical flux, which is shown in Figure 4.45. The molecular weight is lower at higher reaction temperature in the redox-initiated process. However, this trend is not significant in the KPS-initiated process. This occurs because the molecular weight can be influenced by the radical generation rate, the reaction rate constant and the particle number. The combination of those three factors influences the molecular weight. The molecular weight distribution of KPS-initiated latex measured by GPC is shown in Figure 4.46 and the molecular weight result for redox-initiated latex is shown in Figure 4.47.

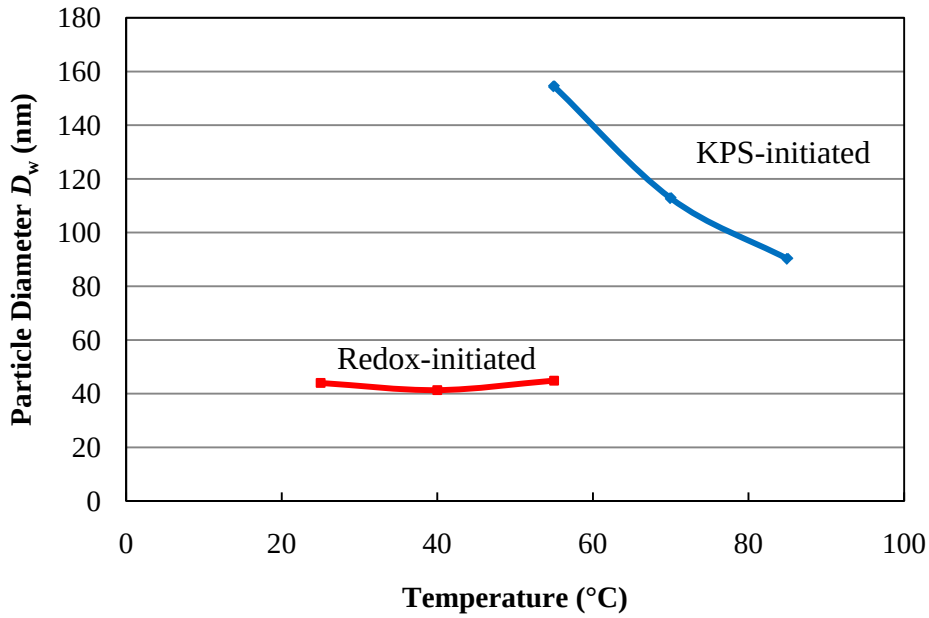

Figure 4.44: *Particle diameter (D_w) versus reaction temperatures for KPS-initiated and redox-initiated latexes.*

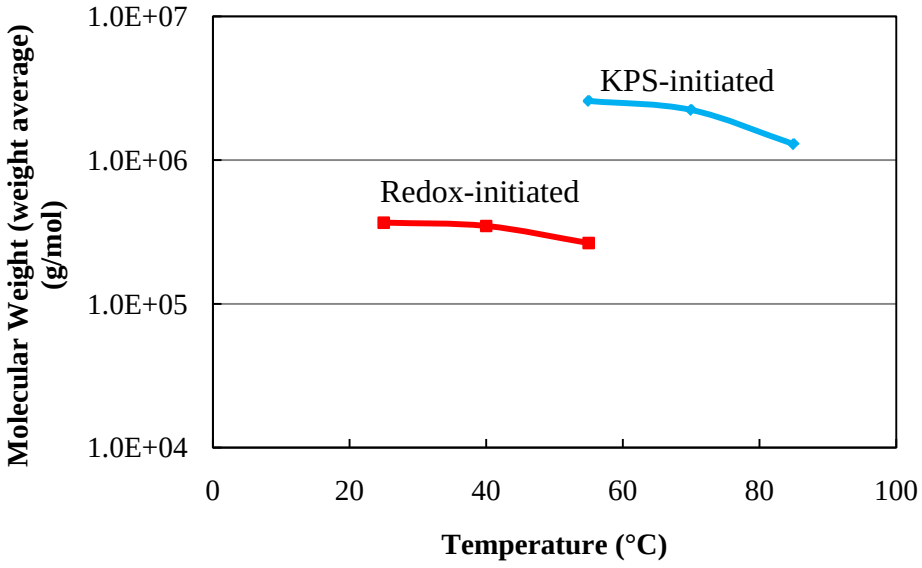

Figure 4.45: *Relation between molecular weight (weight average) and reaction temperatures for KPS-initiated and redox-initiated latexes.*

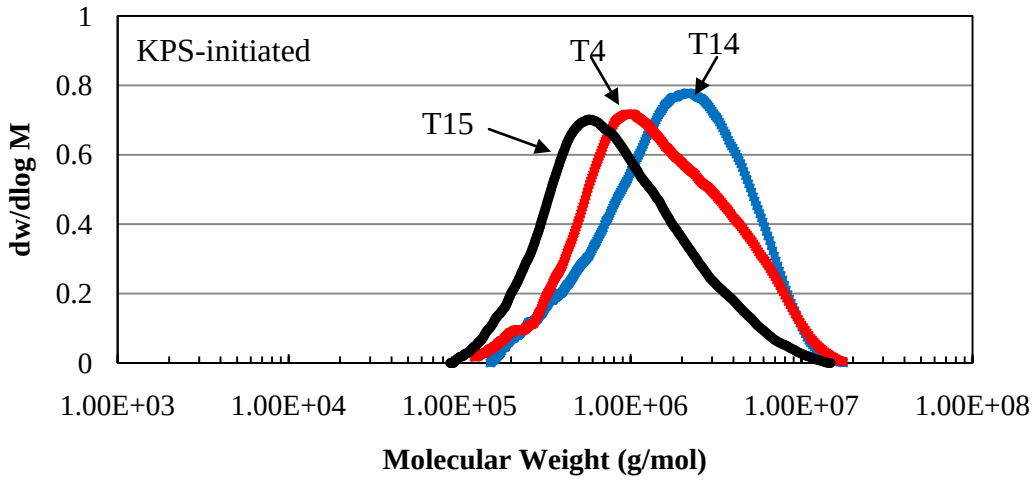

Figure 4.46: *Molecular weight distribution of KPS-initiated polymer measured by GPC at different reaction temperatures (recipes shown in Table 4.4).*

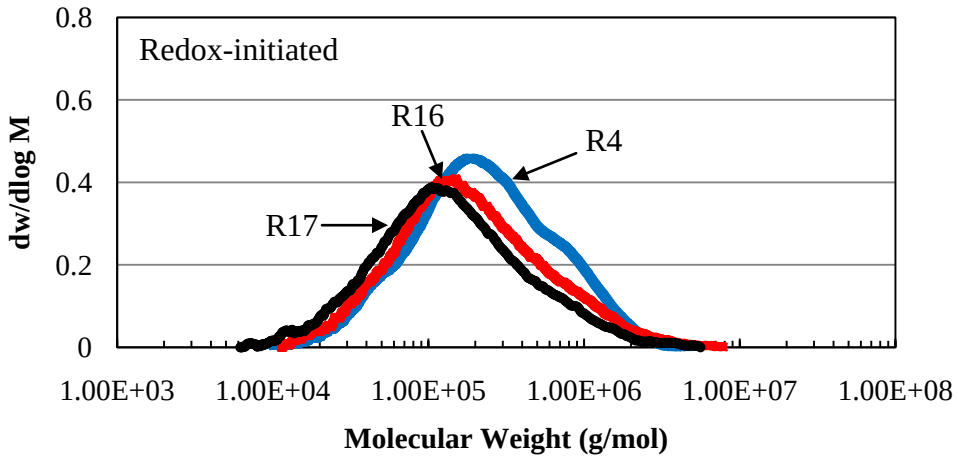

Figure 4.47: *Molecular weight distribution of redox-initiated polymer measured by GPC at different reaction temperatures (recipes shown in Table 4.10).*

4.3.6 Kinetics during Emulsion Polymerization

From the previous study, the relationships between particle number and surfactant concentration/ initiator concentration indicate that micellar nucleation is the main nucleation mechanism for redox-initiated and KPS-initiated polymerizations. However, the relationship between the particle number and solids content, and the continuous increase in the reaction rate during the polymerization in the redox-initiated process indicate significant homogenous nucleation occurs. Samples were obtained during the polymerization by sampling from the reactor at different times for redox-initiated (R4) and KPS-initiated (T4) polymerizations (as shown in Tables 4.1 and 4.6). Each sample was ~ 5 g of latex and mixed with ~ 3 g of 1 % hydroquinone solution to stop the further reaction. The particle size was measured from TEM images (shown in Figures 4.48 and 4.51), where around 1000 particles are counted for each sample. The particle size distributions are shown in Figures 4.49 and 4.52. To eliminate the monomer influence on the particle size at low conversion, dialysis membrane tubing (3500 Daltons) was used to clean the latex. 10 ml of diluted latex sample was put in the dialysis membrane tube, and the tube was put into 1 liter beaker with DI water with magnetic stirring. The cleaning process took five days with changing DI water in the beaker every day. UV spectroscopy was used to detect the monomer level in the aqueous phase to make sure no residual monomer remained in the cleaned latex. From the TEM images, the particle size distribution is broad at lower conversions in redox-initiated polymerization, whereas the particle size distribution is narrower in the KPS-initiated polymerizations. This occurs because

homogeneous nucleation in the redox-initiated latex broadens the particle size distribution. During the polymerization, the particle size increases slightly in the redox-initiated system, and increases significantly in the KPS-initiated system. The particle numbers and reaction rates versus conversion are shown in Figures 4.50 and 4.53. In the redox-initiated system, the number of particles keeps increasing during the polymerization, whereas the particle numbers remain constant in the KPS-initiated polymerization process. The increase in particle number during the polymerization indicates that secondary nucleation occurred in the redox-initiated process. Secondary homogenous nucleation generated smaller particles during the redox-initiated polymerization, which is shown in the TEM images at low conversion (Figure 4.48). The aqueous phase of the first latex sample (~ 20 % conversion) was obtained using a serum replacement cell for both the redox-initiated and the KPS-initiated polymerizations. Surface tension was measured by the Du Nuoy ring method and the surfactant concentration was calculated. In the redox-initiated system, the SLS concentration is 1.4 mM at 28.3% conversion. In the KPS-initiated system, the SLS concentration is 2.3 mM at 17.8% conversion. The SLS concentration at that point was lower than critical micelle concentration and micellar nucleation could not occur. Any newly formed particles can only form via homogenous nucleation. Therefore, homogeneous nucleation was confirmed to be an important nucleation mechanism in the redox-initiated process. The molecular weight of polymer obtained from redox-initiated and KPS-initiated polymerization is shown in Figure 4.54. The molecular weight of the redox-initiated latex is lower than the KPS-initiated latex, and they remain almost constant during the polymerization.

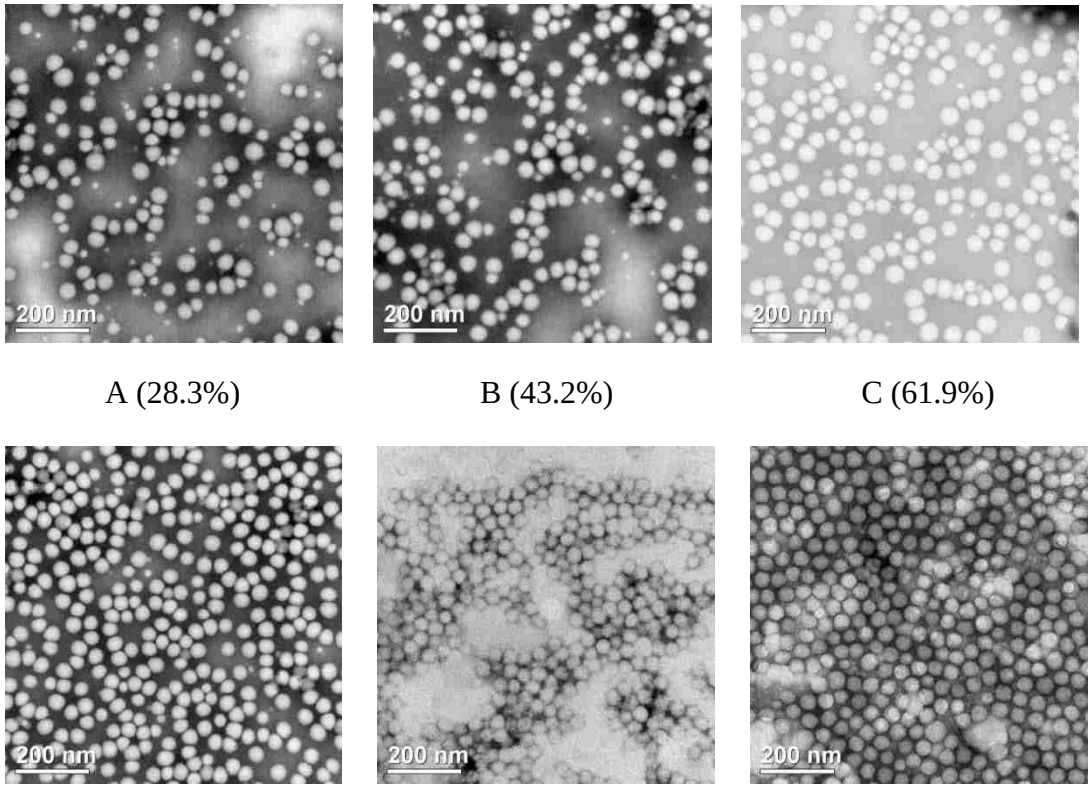

A (28.3%) B (43.2%) C (61.9%)

D (70.8%) E (83.6%) F (99.6%)

Figure 4.48: *TEM images of latex particles obtained during the redox-initiated polymerization process at different conversions (R4).*

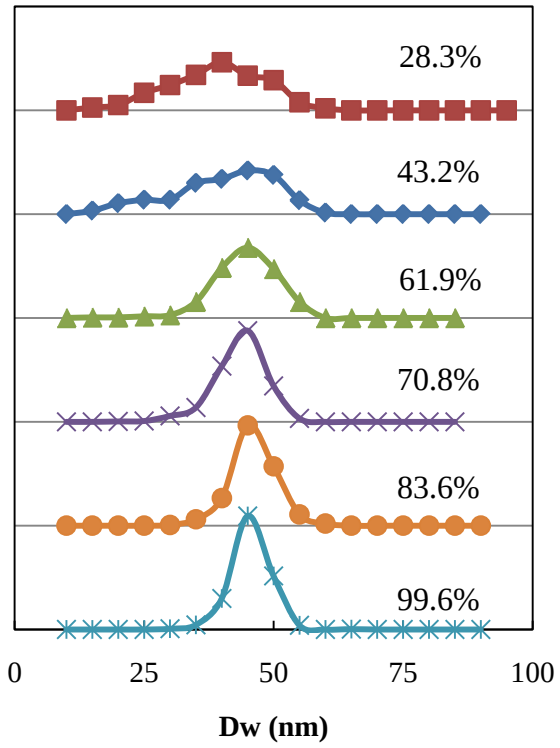

Figure 4.49: *Latex particle size distribution for samples obtained during the redox-initiated polymerization process at different conversions based on TEM imaging.*

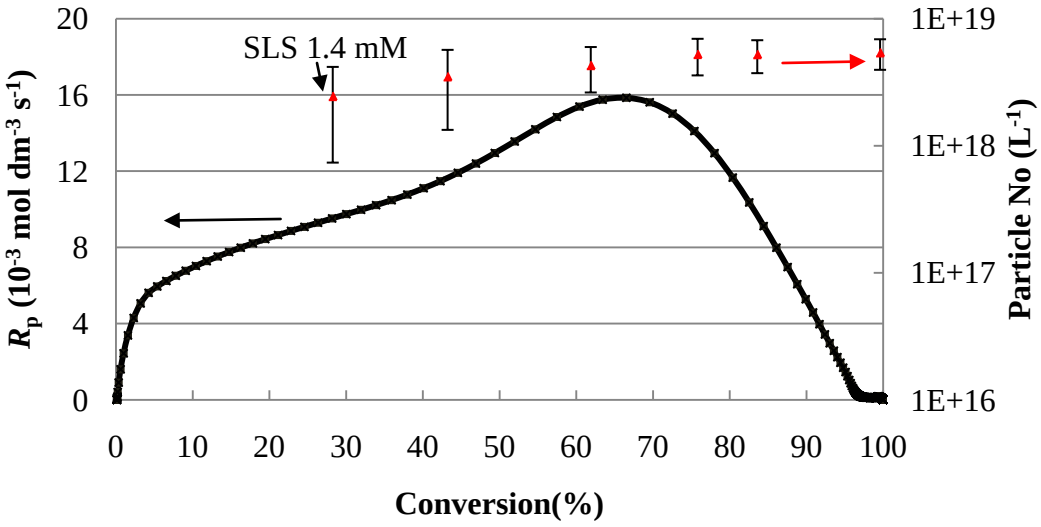

Figure 4.50: *Latex particle number and reaction rates vs. conversion for redox-initiated emulsion polymerization (R4, recipe shown in Table 4.6).*

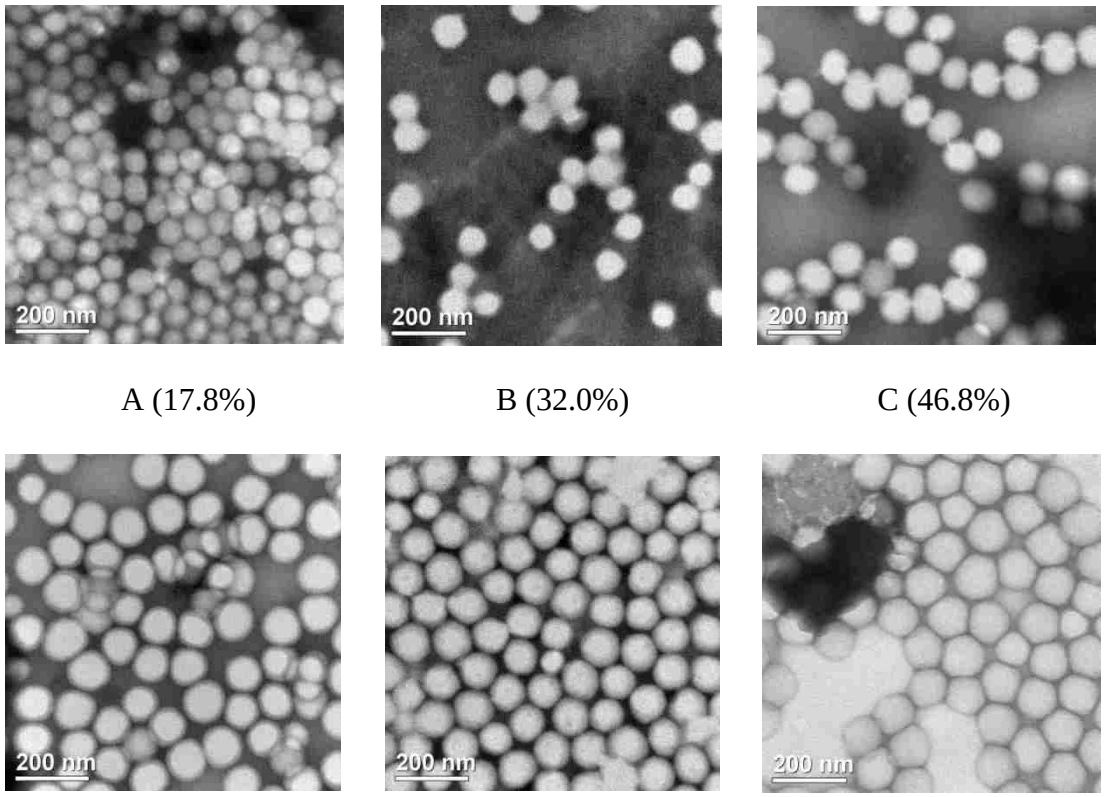

Figure 4.51: *TEM images of latex particles obtained during the KPS-initiated polymerization process at different conversions (T4).*

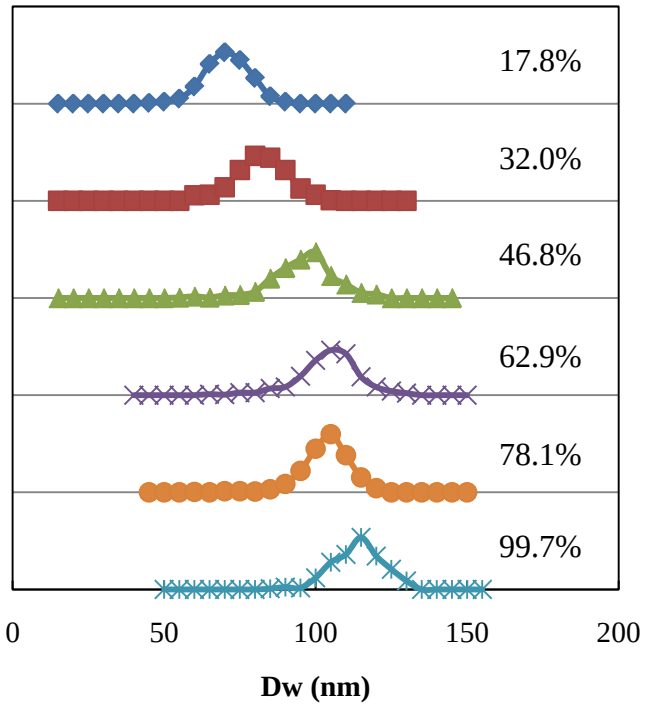

Figure 4.52: *Latex particle size distribution for samples obtained during the KPS-initiated polymerization process at different conversions based on TEM imaging.*

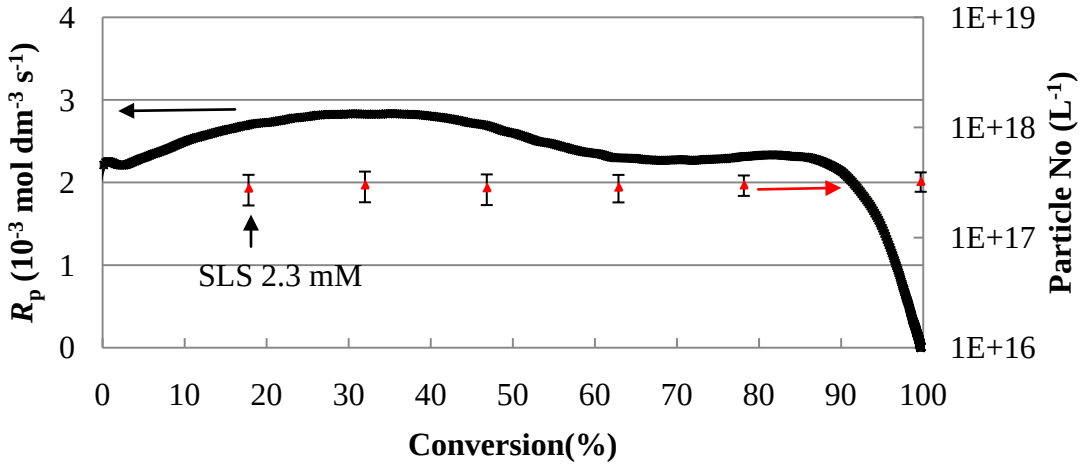

Figure 4.53: *Latex particle number and reaction rates vs. conversion for KPS-initiated emulsion polymerization (T4, recipe shown in Table 4.1).*

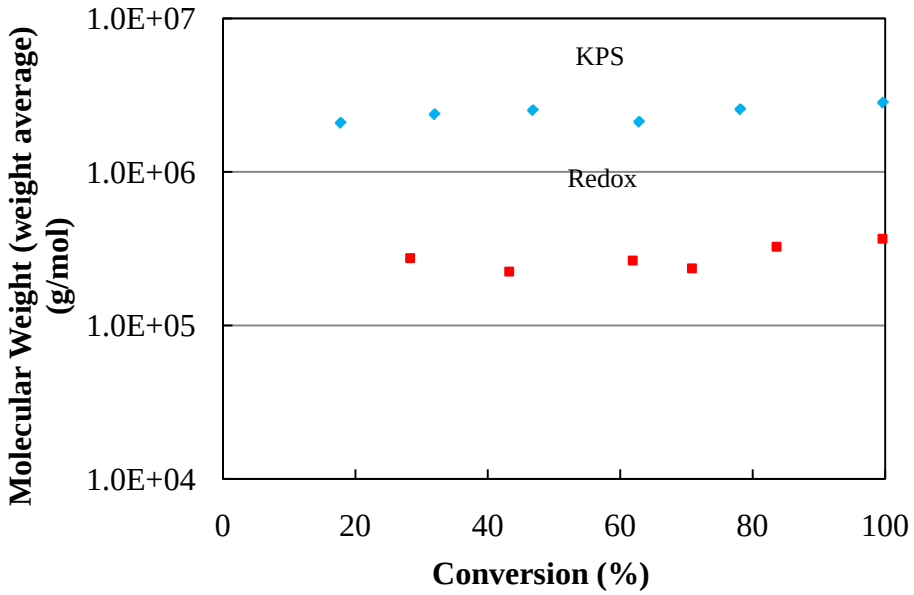

Figure 4.54: *Molecular weight (weight average) versus conversion for KPS-initiated and redox-initiated latexes.*

4.4 Conclusions

Redox initiator was used with ferrous sulfate catalyst in emulsion polymerization to study the difference in the kinetics of emulsion polymeriztaion, compared to the use of KPS initiator. The presence of ferrous ion is important to maintain a high radical generation rate. The high radical flux generated from the redox initiator can result in the formation of relatively small latex particles with low molecular weights compared to the latex particles formed from the KPS-initiated process. A significant difference in the reaction rate between the redox-initiated and KPS-initiated system was observed, which is caused by the different particle numbers.

From the particle number dependence on surfactant and initiator concentrations, results show that redox-initiated systems and KPS-initiated systems both follow the Smith-Ewart theory, although there are significant differences between those two systems. However, the particle number increases with increasing solids contents in redox-initiated systems, whereas the particle number is almost independent of solids contents in KPS-initiated systems. As a result, the relationships between particle number and surfactant/initiator concentration and solids contents and reaction rate differences for the redox-initiated and KPS-initiated systems reflect the different nucleation mechanisms. Micellar nucleation plays an important role in the KPS-initiated systems and both micellar and homogenous nucleations are very important in the redox-initiated process. The increase of particle numbers and reaction rate in the redox-initiated system during the polymerization confirmed that homogenous nucleation occurred in the redox-initiated system. Different reaction temperatures can also influence the emulsion polymerization significantly. The particle size decreases in the KPS-initiated process at higher reaction temperature, and is not significantly influenced in the redox-initiated process. With high particle number, aggregation may influence the particle size at a higher reaction temperature during the redox-initiated process.

4.5 References

1 Sarac, A. S., *Prog. Polym. Sci*., **24**, 1149 (1999)

2 Harkins, W. D. *J. Am. Chem. Soc*., **69**, 1428 (1947)

3 El-Aasser, M. S., Sudol, E. D., in *Emulsion Polymerization and Emulsion Polymers*, Lovell, P. A. and El-Aasser, M. S. Ed., John Wiley and Son, Chichester, p38-41 (1997)

4 Lamb, D. J., Fellows, C. M. and Gilbert, R. G., *Polymer*, **46**, 7874 (2005)

5 Hawkett, B. S., Napper, D. H. and Gilbert, R.G., *J. Chem. Soc. Faraday Trans 1*, **76**, 1323 (1980)

6 Ballard, M. J., Gilbert, R. G. and Napper, D. H., *J. Polym. Sci., Polym. Lett. Ed*, **19**, 533 (1981)

7 van der Hoff, B. M. E., *J. Polym. Sci*., **33**, 487 (1958)

8 Smith, W. V. and Ewart, R. H., *J. Chem. Phys.*, **16**, 592 (1948)

9 Gerrens, H., *Fortsch. Hochpolym. Forsch*., **1**, 234 (1959)

10 Fitch, R.M. and Tsai, Ch. H., Homogeneous nucleation of polymer colloids, In *Polymer colloids*, Fitch, R.M., Plenum press, New York, p 73-102 (1971)

11 Fitch, R. M., *Br. Polym. J*. **5**, 467-483, (1973)

12 Hansen, F. K. and Ugelstad, J., *J. Polym. Sci., Polym. Chem. Ed*., **16**, 1953 (1978)

13 Hansen, F. K. and Ugelstad, J., *J. Polym. Sci., Polym. Chem. Ed*., **17**, 3033 (1979)

14 Gilbert, R. G. *Emulsion polymerization: A Mechanistic Approach*, Academic Press: London, (1995)

15 Deutsch, J. C., *Anal. Biochem*., **255**, 1(1998)

16 Jellinek, H. G., *Pure Appl. Chem*., **4**, 419 (1962)

17 Deutsch, J. C., *Anal. Biochem.*, **255**, 1 (1998)

18 Baxendale, J. H., Evans, M. G. and Park, G. S., *Trans. Faraday Soc*., **42**, 155 (1946)

19 Varela de la Rosa, L., Sudol, E. D., El-Aasser, M. S. and Klein, A. *J. Polym. Sci*., **34**, 461 (1996)

21 Varela de la Rosa, L. Ph.D. Dissertation, Lehigh University (1996)

22 Barrett, K. E. J., Thomas, H. R. *Br. Polym, J*., **2** , 45-48 (1970)

23 Malliaris, A., Moigne, J., Sturm, J. and Zana, R., *J. Phys. Chem*., **89**, 2709 (1985)

24 Geurts, J. M., Jacobs, P. E., Muijs, J. G., Steven Van Es, J. J. G. and German, A. L., *J. Appl. Polym. Sci.,* **61**, 9 (1996)

Chapter 5

Theoretical Calculation of Homogeneous Nucleation during Emulsion Polymerization

5.1 Introduction

In conventional emulsion polymerization, micellar nucleation is the principal particle nucleation mechanism when hydrophobic monomer is used and the surfactant concentration is above the critical micelle concentration (cmc), as described in Chapter 4. When the surfactant concentration is below the cmc, or more hydrophilic monomer is used, homogenous nucleation in the aqueous phase can significantly influence the nucleation process.

In the homogeneous nucleation theory [1], aqueous phase radicals polymerize to first form oligomers, and then continue to grow until they reach a critical chain length, and then precipitate and form particles. The oligomers may also flocculate or coagulate to form new particles. Priest [2] first studied the polymerization of vinyl acetate and concluded that aqueous phase nucleation is important in systems with high water solubility monomer. Primary particle formation occurs throughout the reaction process. In 1968, Roe [3] developed the Smith-Ewart theory [4] from homogeneous

nucleation theory. Homogenous nucleation is the only mechanism which is applicable to hydrophobic monomer when no surfactant micelles are present.

Fitch and Tsai [5, 6] developed a quantitative theory for homogeneous nucleation. By using the collision theory for radical capture, the rate of radical capture is a function of radical production, particle number, particle size, and diffusion distance between radical and particles. Primary particles may coagulate with each other because of their small size and lower surface charge. As particles coagulate, the surface to volume ratio decreases, which causes an increase in the surface potential. When the particles are sufficiently large, coagulation ceases due to insufficient kinetic energy needed to overcome the particle surface repulsion. Homogeneous nucleation can be presented mathematically as Eq (5-1).

$$\left(\frac{\mathrm{d}N}{\mathrm{d}t}\right)=bR_{\mathrm{i}}-R_{\mathrm{c}}-R_{\mathrm{f}} \tag{5-1}$$

where N is the particle number, bR_{i} is the rate of free radical generation, R_{c} is the radical capture rate by particles, and R_{f} is the particle coagulation rate.

By assuming that radical capture is by electrostatic interactions between particles and oligomeric radicals, and it is irreversible. The rate for capture of oligomeric radicals by particles, R_{c}, is given as: Eq (5-2) and (5-3),

$$R_{\mathrm{c}}=k_{\mathrm{c}}[\mathrm{M}\cdot]N \tag{5-2}$$

$$k_{\mathrm{c}}=\frac{4\pi D_{\mathrm{w}}r_{\mathrm{p}}}{W'} \tag{5-3}$$

where k_c is the rate constant for capture of oligomeric radicals by particles, [M•] is the oligmeric radical concentration in water, D_w represents the diffusion coefficient for particles in water, r_p is the radius of the particles, and W' is the Fuchs stability factor for a charged radical colliding with a particle, which is 1 for styrene [7], and which is considered to be the same value for BMA.

The diffusion coefficient (D_w) can be calculated from the Stokes-Einstein equation in Eq (5-4).

$$D_w = \frac{k_B T}{3\pi d\mu} \tag{5-4}$$

where k_B is the Boltzmann constant (1.38×10^{-23} $m^2\cdot kg\cdot s^{-2}\cdot k^{-1}$), T is the absolute temperature, d is the diameter of the latex particle, and μ is the viscosity. Eq (5-2) can be converted into Eq (5-5).

$$R_c = \frac{2k_B T}{3\mu}[M\cdot]N \tag{5-5}$$

In particle coagulation, a precursor particle is unstable, which is caused by its small size and low surface charge. Due to the small size and hydrophilic nature of the precursor particle, the precursors have low swelling capacities and high radical desorption rates. Therefore, the propagation rate is low, and the precursor particles tend to coagulate with other precursors or mature latex particles [8]. The value of the particle coagulation rate (R_f) is calculated from the DLVO theory [9, 10], which is shown in Eq (5-6) and (5-7).

$$R_f = \left(\frac{4\pi D_{pq} r_{pq}}{W_{pq}}\right)N^2 \tag{5-6}$$

where D_{pq} represents the mutual diffusion coefficient [11, 12] for particles of size p and q, r_{pq} is the collision radius (the sum of the radii of p and q particles), W_{pq} is the Fuchs stability factor for particles of size p and q, and N is the particle number.

$$D_{pq}=\frac{k_B T}{3\pi\mu}\left(\frac{1}{d_p}+\frac{1}{d_q}\right) \tag{5-7}$$

The Fuchs stability factor (W_{pq}) can be estimated using the results of a blender test (described in Chapter 7) through Eq (5-8), which is based on von Smoluchowski's theory [13].

$$W=\frac{-4\phi\gamma t}{\pi \ln(1-c)} \tag{5-8}$$

where ϕ is the volume fraction of particles, γ is the shear rate, and c is the fraction of particles coagulated at time t. The shear rate γ can be calculated from Eq (5-9)

$$\gamma=K_s N_r \tag{5-9}$$

where K_s is the Metzner-Otto constant, and N_r is the rotation speed (rev/s).

Ugelstad and Hansen [11, 12] made significant improvements to the Fitch-Tsai theory. They proposed that free radicals react with dissolved monomer in the aqueous phase to form oligomers. Monomer units can be added to the oligomer until it reaches a critical chain length, at which phase separation occurs and primary particles are formed by precipitation. During the growth from monomer to a primary particle, each oligomer can: (i) terminate with other radicals, (ii) precipitate if the length exceeds the critical chain length, or (iii) be captured by the particle. The rate of appearance of primary particles, i.e., the nucleation rate, is equal to the rate of oligomers with the

critical chain length formed, and can be presented as Eq (5-10). In Eq (5-10), coagulative nucleation was not considered.

$$\left(\frac{\mathrm{d}N}{\mathrm{d}t}\right)=k_{\mathrm{p}}[\mathrm{M}]_{\mathrm{w}}[\mathrm{M}\cdot]_{(j-1)\mathrm{w}} \tag{5-10}$$

where N is the particle number, k_{p} is the propagation rate constant ($dm^3 \cdot mol^{-1} \cdot s^{-1}$), [M] is the monomer concentration in water (mole/L), [M•] is the oligmeric radical concentration in water (mole/L) and j is the critical chain length. The radicals (R•) are formed by initiator decomposition and disappearance of radicals by propagation, termination and capture, which is shown in Eq (5-11). In this situation, it is assumed that the oligomeric radicals are at a steady state and termination of primary radicals is negligible. The formation rate of primary particles can be simplified, and is given in Eq (5-12).

$$\left(\frac{\mathrm{d}[\mathrm{R}\cdot]}{\mathrm{d}t}\right)=bR_{\mathrm{i}}-k_{\mathrm{p}}[\mathrm{R}\cdot]_{\mathrm{w}}[\mathrm{M}]_{\mathrm{w}}-k_{\mathrm{t}}[\mathrm{R}\cdot]_{\mathrm{w}}[\mathrm{M}\cdot]_{\mathrm{w}}-k_{\mathrm{c}}[\mathrm{R}\cdot]_{\mathrm{w}}N \tag{5-11}$$

$$\left(\frac{\mathrm{d}N}{\mathrm{d}t}\right)=bR_{\mathrm{i}}\left(1+\frac{k_{\mathrm{t}}[\mathrm{M}\cdot]_{\mathrm{w}}}{k_{\mathrm{p}}[\mathrm{M}]_{\mathrm{w}}}+\frac{k_{\mathrm{c}}N}{\mathrm{k_p}[\mathrm{M}]_{\mathrm{w}}}\right)^{1-j} \tag{5-12}$$

where N is the particle number, bR_{i} is the rate of free radical generation ($L^{-1} \cdot s^{-1}$), k_{t} is the radical termination rate constant in water ($dm^3 \cdot mol^{-1} \cdot s^{-1}$), k_{p} is the propagation rate constant ($dm^3 \cdot mol^{-1} \cdot s^{-1}$), k_{c} is the average capture rate constant ($dm^3 \cdot s^{-1}$), [M] is the monomer concentration in water (mole/L), [M•] is the oligmer radical concentration in water (mole/L), and j is the critical chain length, which is 5 for styrene [7] and is considered to be the same value for BMA.

During emulsion polymerization, the number of new particles formed by homogenous nucleation can be calculated based on the theories and equations shown above. However, the difficulty is that the Fuchs stability factor, *W*, is a function of time. In this chapter, an effort has been made to calculate the Fuchs stability factor for latex particles during the polymerization as well as the oligmeric radical concentration in water. The radical generation rates, capture rates and coagulation rates were calculated based on the real data obtained from the KPS-initiated and redox-initiated emulsion polymerization systems during the polymerization processes.

5.2 Experimental

Recipes used for thermally-initiated emulsion polymerizations under different conditions are shown in Table 5.1. The Metter RC1 reactor was equipped with a pitched-blade impeller and the agitation speed was 400 rpm. Isothermal conditions were applied by selecting the Tr mode in the Mettler RC1, where the jacket temperature was varied to maintain the reactor temperature at a constant value.

Table 5.1: Recipes for KPS-initiated and Redox-initiated Batch Emulsion Polymerizations

Reactions	T4	R4
BMA (g)	125	
DI water (g)	500	
SLS (g) *	1.733 (12.0mM)	
Temperature (ºC)	70	25
KPS (g) *	0.234 (1.7 mM)	-
$NaHCO_3$ (g) *	0.234(0.6 mM)	-
$FeSO_4$ (g) *	-	0.0125 (0.09 mM)
NaCl (g) *	-	0.209 (7.2 mM)
Ascorbic Acid (g) *	-	0.45 (5.1 mM)
H_2O_2 (30%) (g) *	-	0.45 (7.9 mM)

*Based on water

The Mettler RC1 reaction calorimeter was used to obtain the continuous reaction rate, conversion, and reactor temperature. The final solids content and conversion were measured gravimetrically. TEM imaging with negative staining technique was used for particle sizing to obtain accurate particle size. For the TEM images, ~ 1000 particles were counted to obtain the statistical results of the particle size and particle size distribution for each sample. Dialysis was used to clean the latex. UV spectroscopy (Spetronic Genesys2) was used to detect residual monomer level in the aqueous phase. The characterization methods are described in Chapter 2.

5.3 Results and Discussions

To study homogenous nucleation during emulsion polymerization, the particle sizes during the polymerization were obtained by sampling from the reactor at different times during the polymerization. Each sample is ~ 5 g of latex and is mixed with 3 g of 1 % hydroquinone solution to stop any further reactions. The latexes were cleaned using dialysis membrane tubing to remove the residual monomer and eliminate the effect of residual monomer on the latex particles. The results are shown in Table 5.2.

The radical generation rates for redox initiator and KPS initiator were first calculated. The radical generation rate (25 °C) from redox initiator [14] is presented in Eq (5-13) and the radical generation rate (70 °C) from KPS [15] is presented in Eq (5-14)

$$R_{redox}=5.9\ [H_2O_2]\ [Fe^{2+}]\ N_A \quad (5\text{-}13)$$

$$R_{KPS}=4.41\times10^{-5}\ [KPS]\ N_A \quad (5\text{-}14)$$

where R (radicals l^{-1} sec^{-1}) is the radical generation rate, and N_A is Avogadro's number (6.022×10^{23} mol^{-1}). The different radical generation rates at different initiator concentrations are shown in Figures 5.1 and 5.2. The use of higher initiator concentrations results in a higher radical generation rate. The redox initiator generates a much higher radical flux and a faster decomposition rate, compared with the KPS initiator. In reaction R4, the hydrogen peroxide (H_2O_2) concentration is 7.9 mM, and in reaction T4, the KPS concentration is 1.7 mM. The total reaction time is ~ 5 minutes for redox-initiated system (R4), and is ~ 20 minutes for KPS-initiated system

(T4). Figure 5.1 (the redox-initiated system) indicates that the radical generation rate during the polymerization process can be considered as a linear relationship with time, $R_{redox} = -1.21\times10^{15} \times t + 2.53 \times 10^{18}$ (R^2=0.999). According to Figure 5.2 (KPS-initiated system), the radical generation rate during the polymerization process can be considered as a constant value, $R_{KPS} = 4.6\times10^{16}$ $L^{-1}\cdot s^{-1}$.

Table 5.2: Results of Latex Particle Size during Emulsion Polymerizations

Samples	**Conversion**	D_w **(nm)**	D_v **(nm)**	D_n **(nm)**	**SD (D_n) (nm)**	**PDI (D_w/D_n)**	N_p **(L^{-1})**
HT1	17.8 %	67.3	65.8	65.0	7.4	1.04	2.84×10^{17}
HT2	32.0 %	80.0	78.2	77.4	8.6	1.03	3.04×10^{17}
HT3	46.8 %	92.7	90.6	89.5	10.3	1.03	2.86×10^{17}
HT4	62.9 %	101.3	99.5	98.6	10.1	1.03	2.90×10^{17}
HT5	78.1 %	106.6	104.5	104.9	8.0	1.02	3.03×10^{17}
T4	99.7%	112.8	111.6	111.0	8.3	1.02	3.19×10^{17}
HR1	28.3 %	41.0	37.4	34.8	9.3	1.18	2.46×10^{18}
HR2	43.2 %	42.5	38.3	36.1	9.8	1.18	3.51×10^{18}
HR3	61.9 %	41.6	40.3	39.2	6.3	1.06	4.31×10^{18}
HR4	75.8 %	41.6	40.3	40.1	4.9	1.04	5.26×10^{18}
HR5	83.6 %	42.8	41.7	41.3	4.2	1.04	5.25×10^{18}
R4	99.9 %	44.0	43.4	43.1	3.6	1.02	5.40×10^{18}

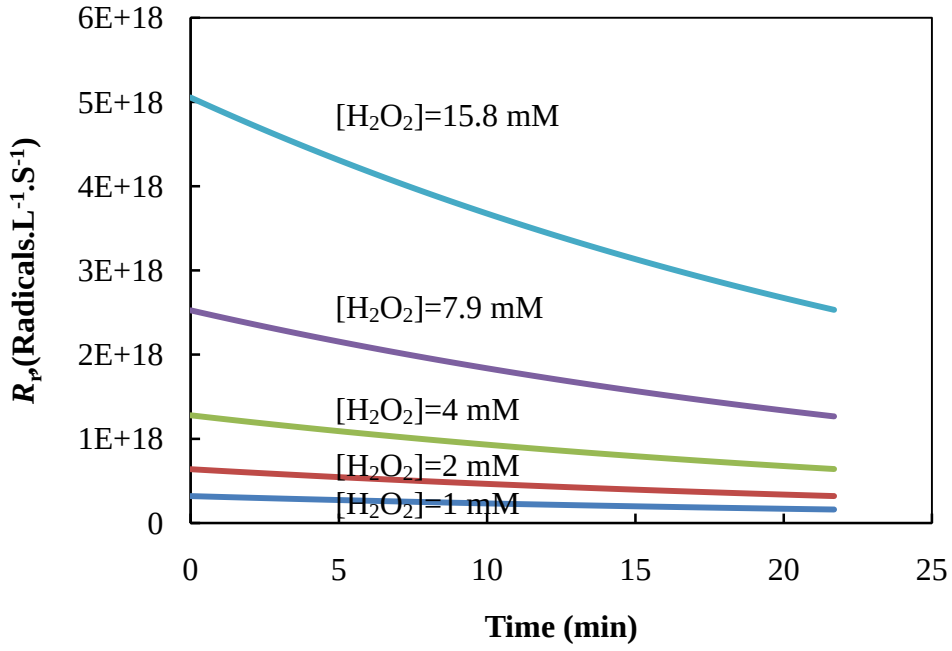

Figure 5.1: *Radical generation rates at different redox initiator concentrations.*

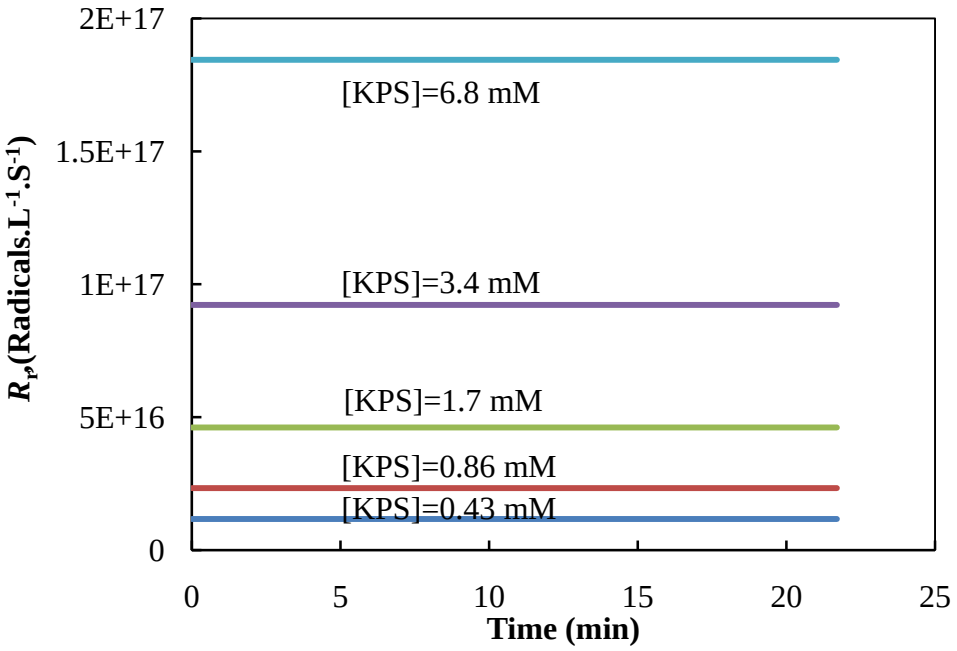

Figure 5.2: *Radical generation rates at different KPS initiator concentrations.*

5.3.1 Theoretical Calculation of Homogenous Nucleation (Fitch-Tsai Theory)

The Fuchs stability factor, *W*, as well as the oligmeric radical concentration in the aqueous phase were investigated to study the homogeneous nucleation process during emulsion polymerization. The radical generation rates, capture rates and coagulation rates, as well as homogeneous nucleation rates were calculated.

The Fitch and Tsai theory, Eq (5-1), was first used to study homogenous nucleation. In the KPS-initiated system, the particle number is a constant value (3×10^{17} L^{-1}). Therefore, it is assumed that no secondary nucleation occurred during the polymerization. The latex viscosity for the KPS-initiated system is μ =0.01 Pa·s, and the viscosity is assumed to be constant during the polymerization. The reaction temperature is considered to be constant as well during the reaction (T=343.15 K). The micellar nucleation time is assumed to be very short and is not considered in this process. The surfactant concentration is below its cmc after micellar nucleation. The radical generation rate during the polymerization process, R_{KPS}, is 4.6×10^{16} $L^{-1}\cdot s^{-1}$ based on Eq (5-14). Therefore, Eq (5-1) can be converted to Eq (5-15).

$$bR_i = R_c = k_c N[\mathrm{M}\cdot] = \frac{2k_b TN[\mathrm{M}\cdot]}{3\mu} \tag{5-15}$$

where k_B is the Boltzmann constant (1.38×10^{-23} $m^2\cdot kg\cdot s^{-2}\cdot k^{-1}$). The oligomeric radical concentration can be calculated, where [M·] is 4.86×10^{14} ($L^{-1}\cdot s^{-1}$).

In the redox-initiated system, the particle number increased during the polymerization, which indicates the presence of homogenous nucleation. During the polymerization, the particle number increased up to 70% conversion, and then remained constant. For convenience, the relationship between particle number (N_p) and conversion (x) is assumed as a linear relationship, $N_p = 6 \times 10^{18}\, x + 0.9\times10^{18}$ (L^{-1}), when the reaction is below 70% conversion. After 70% conversion, the particle number is considered to be a constant value, 5.25×10^{18} (L^{-1}). The reaction temperature is constant during the reaction, and T=298.15 K. The oligomeric radical concentration in the redox-initiated system is assumed to be the same value as in the KPS-initiated system ([M·] = 4.86×10^{14} $L^{-1}\cdot s^{-1}$). In the redox-initiated system, the radical generation rate is $R_{redox} = -1.21\times10^{15}\, t + 2.53 \times 10^{18}$ ($L^{-1}\cdot s^{-1}$), where t is the reaction time (s). The redox-initiated latex viscosity is μ =0.01 Pa·s, and the viscosity is assumed to be constant during the polymerization. For particle coagulation calculation, it is assumed that the primary nuclei diameters are 5 nm and existing latex particles is 40 nm during the polymerization. Therefore, the mutual diffusion coefficient (D_{pq}) for particles of size p and q is 9.83×10^{14} ($m^2\cdot s^{-1}$), and the collision radius (r_{pq}) is 22.5 (nm). The homogenous nucleation rate is given in Eq (5-16), and can be calculated using Eq (5-17).

$$\left(\frac{dN}{dt}\right) = bR_i - R_c - R_f = bR_i - \frac{2k_b TN[R\cdot]}{3\mu} - \left(\frac{4\pi D_{pq} r_{pq}}{W_{pq}}\right) N^2 \qquad (5\text{-}16)$$

$$\left(\frac{dN}{dt}\right) = (-10^{15} \times t + 3\times10^{18}) - 0.1333\times N - \left(\frac{2.78\times10^{-15}}{W_{pq}}\right) N^2 \qquad (5\text{-}17)$$

Based on the above relationship between the particle number and reaction time, the Fuchs stability factor for particles of size p and q (W_{pq}) can be calculated from the experimental data, and the results are shown in Figure 5.3. Before 70% conversion (less than 200 seconds), $W_{pq}= 586.0 \times e^{0.0234t}$ ($R^2=0.987$), and after 70% conversion, $W_{pq}= 55.8 \times t+ 35528$ ($R^2=0.985$). This shows that the latex particles are really unstable at the beginning of the reaction and the stability increases during the polymerization. Based on the Fitch-Tsai theory and the assumptions above, the theoretical calculated results for radical generation rates, radical capture rates, radical coagulation rates, and particle numbers during the redox-initiated batch emulsion polymerization are shown in Figure 5.4. The radical generation rates decrease during the polymerization, due to the decrease in the redox initiator concentration. The radical capture rates increase with increasing particle number during the emulsion polymerization, and remain constant when no new particles are formed. The radical coagulation rates decrease during the polymerization, due to the increasing stability of the latex particles. The particle numbers increase during the polymerization, which is the combination result of radical generation rates, radical capture rates, and radical coagulation rates. The particle numbers remain constant after ~200 seconds, where the conversion is ~ 70 %. At that point, no new particles are formed, due to insufficient monomer in the aqueous phase.

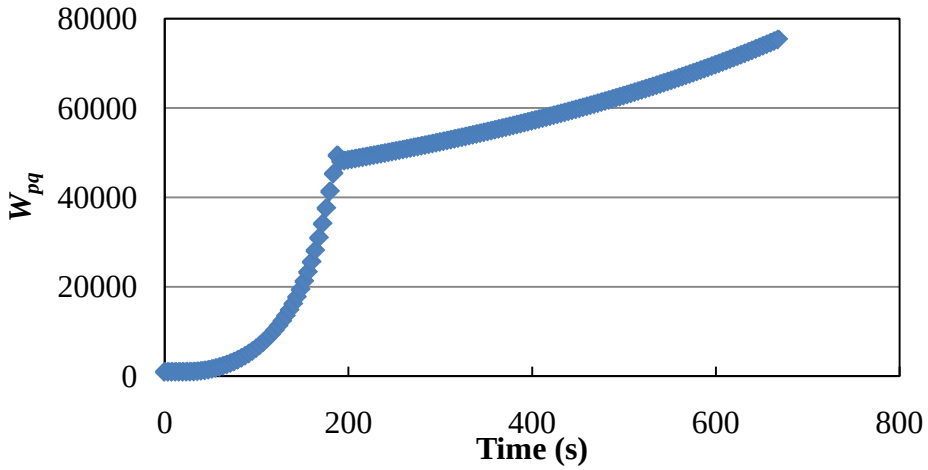

Figure 5.3: *Fuchs stability factor, for particles of size p and q (W_{pq}) during the redox-initiated batch emulsion polymerization of BMA.*

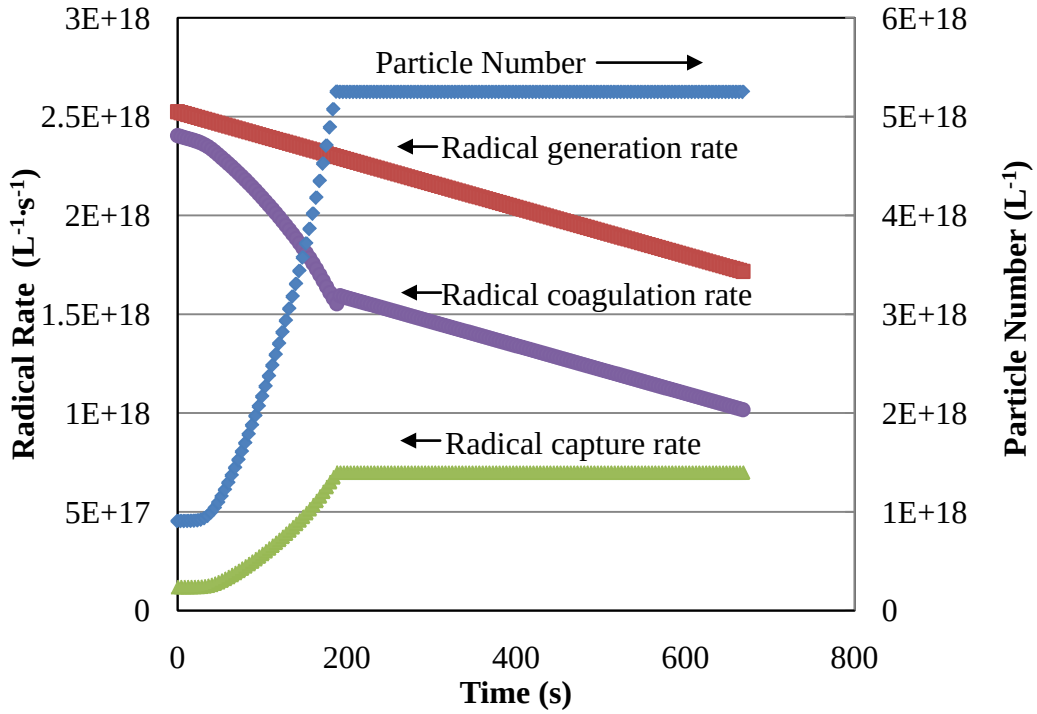

Figure 5.4: *Theoretical calculated results for radical generation rates, radical capture rates, radical coagulation rates, and particle numbers during the redox-initiated batch emulsion polymerization of BMA.*

For the final redox-initiated latex (R4, 20 % solids content), a blender test was used to test the mechanical stability. The Metzner-Otto constant (K_s), is a dimensionless number; for the A310 fluid-foil impeller the constant is 3.4 and is 5.4 for the 45° pitch-bladed turbine [17, 18]. The blender impeller has a similar shape to the A310 impeller and pitch-bladed turbine, which is shown in Figure 5.5. Therefore, the Metzner-Otto constant (K_s) of the blender impeller is considered to have a value of 5. The rotation speed (Nr) is 133.3 (rev/s), so the shear rate (γ) of the blender is 666.7 (s^{-1}), which is calculated from Eq (5-9). The total time for the blender test is 300 (s) and the fraction of latex particles that were coagulated for the redox-initiated latex is 0.277. Therefore, the Fuchs stability factor (W) can be calculated as 157110 for the final redox-initiated latex, which is much higher than the Fuchs stability factor obtained during the polymerization. This is reasonable, because the latex particles are swollen with monomer during the polymerization, which greatly decreases the Fuchs stability factor.

(A) **(B)** **(C)**

Figure 5.5: *Impellers: (A) blender impeller, (B) A310 impeller, and (C) pitch-bladed turbine*.

5.3.2 Theoretical Calculation of Homogenous Nucleation (Ugelstad-Hansen Theory)

The Ugelstad and Hansen theory, Eq (5-12), was then used to study homogenous nucleation. In the KPS-initiated system, the particle number is considered to be constant (3×10^{17} L^{-1}). The KPS-initiated latex viscosity is μ =0.01 Pa·s, and the viscosity is assumed to be constant during the polymerization. The reaction temperature is constant during the reaction as well, at T=343.15 K. At 70 °C, the BMA water solubility [19] is 3.2×10^{-3} mol/L, the BMA propagation rate constant [20] is 1241.6 $dm^3 \cdot mol^{-1} \cdot s^{-1}$, and the BMA radical termination rate constant [21] is 2.688×10^7 $dm^3 \cdot mol^{-1} \cdot s^{-1}$. The oligomeric radical concentration was taken as [M·], i.e. 4.86×10^{14} $L^{-1} \cdot s^{-1}$. The radical generation rate during the polymerization process is considered to be constant, R_{KPS} =4.6×10^{16} $L^{-1} \cdot s^{-1}$. Therefore, Eq (5-12) can be simplified as Eq (5-18).

$$\left(\frac{dN}{dt}\right)=4.6\times10^{16}\left(1+5.5\times10^{-3}+23.8\right)^{-4}=1.2\times10^{11}\ L^{-1}\cdot s^{-1} \qquad (5\text{-}18)$$

The calculated result for the particle nucleation rate is a large number. However, compared with the total particle number (3×10^{17} L^{-1}), the homogenous nucleation rate is negligible for the KPS-initiated emulsion polymerization. The constant particle number during polymerization provides evidence for negligible homogenous nucleation during the KPS-initiated emulsion polymerization.

In the redox-initiated system, homogenous nucleation is significant. During the emulsion polymerization, the particle number increased before 70% conversion, and then remained constant after 70% conversion. Therefore, the relationship between particle number (N_p) and conversion (x) is assumed to be linear, $N_p = 6 \times 10^{18}\ x + 0.9\times10^{18}$ (L^{-1}), when the reaction is below 70% conversion. After 70% conversion, the particle number is considered to be a constant value, 5.25×10^{18} (L^{-1}). The reaction temperature is constant during the reaction, at 298.15 K. At 25 °C, the water solubility of BMA [19] is 2.9×10^{-3} mol/L, the propagation rate constant of BMA [20] is 369.7 $dm^3\cdot mol^{-1}\cdot s^{-1}$, and the BMA radical termination rate constant [21] is 1.557×10^7 $dm^3\cdot mol^{-1}\cdot s^{-1}$. The oligomeric radical concentration in the redox-initiated system is assumed to be the same value as in the KPS-initiated system, and [R·] is 4.86×10^{14} ($L^{-1}\cdot s^{-1}$). In the redox-initiated system, the radical generation rate is $R_{redox} = -1.21\times10^{15}\ t + 2.53 \times 10^{18}$ ($L^{-1}\cdot s^{-1}$), where t is the reaction time (s). The redox-initiated latex viscosity is μ =0.01 Pa·s, and the viscosity is assumed to be constant during the polymerization. It is assumed that the primary nuclei diameter is 5 nm, and the existing latex particles are 40 nm during the polymerization. Therefore, the mutual diffusion coefficient (D_{pq}) for particles of size p and q is 9.83×10^{14} ($m^2\cdot s^{-1}$), and the collision radius (r_{pq}) is 22.5 (nm). The homogenous nucleation rate is given in Eq (5-19) and can be calculated using Eq (5-20).

$$\left(\frac{\mathrm{d}N}{\mathrm{d}t}\right)=bR_{\mathrm{i}}\left(1+\frac{k_{\mathrm{t}}[\mathrm{R}\cdot]}{k_{\mathrm{p}}[\mathrm{M}]_{\mathrm{w}}}+\frac{2k_{\mathrm{B}}TN}{3\mu k_{\mathrm{p}}[\mathrm{M}]_{\mathrm{w}}}\right)^{-4} \tag{5-19}$$

$$\left(\frac{\mathrm{d}N}{\mathrm{d}t}\right)=bR_{\mathrm{i}}\left(1+1.17\times10^{-2}+2.56\times10^{-16}N\right)^{-4} \tag{5-20}$$

Based on the relationship, $N_p = 6 \times 10^{18}\, x + 0.9\times10^{18}$ (L^{-1}), the particle number is 0.9×10^{18} (L^{-1}), at the beginning of the reaction. In this case, the homogenous nucleation rate at the beginning of the reaction is only about 8.54×10^{8} (L^{-1}), which is negligible compared to the particle number, 0.9×10^{18} (L^{-1}). The homogenous nucleation rate decreased at higher conversion, due to higher particle number and lower radical generation rate. The reason for this low homogenous nucleation rate is that the rate constant for capture of oligomeric radicals by particles, k_c, is very high, as shown in Eq (5-3).

$$k_c = \frac{4\pi D_w r_p}{W'} \tag{5-3}$$

In Eq (5-3), the value of *W'*, which is the Fuchs stability factor for a radical colliding with a particle, is considered to be a value of 1 in the system for the calculation. The real value of *W'* may be much higher than 1, which can make k_c much smaller. Therefore, the homogenous nucleation rate can be significant during the polymerization.

5.4 Conclusions

During emulsion polymerization, there is a negligible amount of homogenous nucleation in the KPS-initiated system and a significant extent of homogenous nucleation in the redox-initiated system. The new particles formed by homogenous nucleation can be calculated based on the Fitch-Tsai theory and the Ugelstad-Hansen

theory. In this chapter, the radical generation rates, capture rates and coagulation rates were calculated based on real data obtained from the KPS-initiated and redox-initiated emulsion polymerization systems during the polymerization processes. The Fuchs stability factor for latex particles during the polymerization and the oligmeric radical concentrations in water were calculated and agree with the Fitch-Tsai theory. However, the theoretical calculation results based on the Ugelstad-Hansen theory are not compatible for redox-initiated system.

5.5 References

1 Fitch, R.M., In *Polymer colloids: a comprehensive introduction*, Academic press, San Diego, p 13-20 (1997)

2 Priest, W. J., Phys. Chem. J., 56, 1077 (1952)

3 Roe, C. P., Ind, Eng. Chem., 60, 20 (1968)

4 Smith, W. V. and Ewart, R. H., *J. Chem. Phys.*, **16**, 592 (1948)

5 Fitch, R.M. and Tsai, Ch. H., Homogeneous nucleation of polymer colloids, In *Polymer colloids*, Fitch, R.M., Plenum press, New York, p 73-102 (1971)

6 Fitch, R. M. Br. Polym. J. **5**, 467-483, (1973)

7 Hansen, F. K., In *Polymer Latexes* (Daniels, E. S., Sudol, S. D. and El-Aasser, M. S. eds), ACS Symposium Series 492, p13, American Chemical Society, Washington, DC. (1992)

8 Napper, D. H. and Gilbert, R. G., *Makromol. Chem., Macromol. Symp*., **10/11**, 503 (1987)

9 Derjaguin, B. V. and Lykema, L., Acta Physicochim, USSR, **14**, 633 (1941)

10 Verwey, E. J. W. and Overbeek, J. Th. G., *Theory of stability of Lyphobic Colloids*, Elsevier, Amsterdam (1948)

11 Hansen, F. K. and Ugelstad, J., J. Polym. Sci., Polym. Chem. Ed., 16, 1953 (1978)

12 Hansen, F. K. and Ugelstad, J., J. Polym. Sci., Polym. Chem. Ed., 17, 3033 (1979)

13 von Smoluchowski, M., *Z. Physik. Chem*., **92**, 155 (1917)

14 Baxendale, J. H., Evans, M. G. and Park, G. S., *Trans. Faraday Soc*., **42**, 155 (1946)

15 Gilbert, R. G. *Emulsion polymerization: A Mechanistic Approach*, Academic Press: London, (1995)

16 (a) Korus, R. and O'Driscoll K. F., in *Polymer handbook*, 2nd ed.; Brandrup, J., Immergut, E. H., McDowell, W. Eds.; John Wiley; New York, p II-48 (1975); (b) Yokota, K., Kani, M. and Ishii, Y., *J. Polym. Sci*., **6**, 1325 (1968)

17 Weetman, R. J., Oldshue, J. Y. *Power, flow and shear characteristics of mixing impellers*. Proceedings of the 6th European Conference on Mixing, May 24–26, Pavia, Italy (1988)

18 Wu, J., Graham, L. J. and Mehidi, N. N., *AIChE Journal*, 52, 2323 (2006)

19 Geurts, J. M., Jacobs, P. E., Muijs, J. G., Steven Van Es J. J. G. and German, A. L., *J. Appl. Polym*. Sci., **61**, 9 (1996)

20 S. Beuermann, M. Buback, T. P. Davis, R. G. Gilbert, R. A. Hutchinson, A. Kajiwara and B. Klumperman, Macromol Chem. Phys., **201**, 1355 (2000)

21 Barth, J., Buback, M., Hesse, P. and Sergeeva, T., *Macromolecules*, **42**, 481 (2009)

Chapter 6

Miniemulsion Polymerization of *n*-Butyl Methacrylate with KPS and Redox Initiators

6.1 Introduction

In Chapters 4 and 5, the nucleation mechanisms in emulsion polymerization were described. Micellar nucleation is the main mechanism for KPS-initiated emulsion polymerization. Due to the high radical flux of redox initiator, both micellar nucleation and homogenous nucleation play important roles in redox-initiated emulsion polymerization systems. Due to the large monomer droplet size in the emulsion system, droplet nucleation was not considered to be a significant nucleation mechanism for both KPS- and redox-initiated emulsion polymerizations. However, droplet nucleation is the main nucleation mechanism in miniemulsion polymerization. Therefore, the influence of high radical flux on droplet nucleation is described in this chapter.

In emulsion polymerization, particle nucleation takes place either by micellar or homogeneous nucleation. Radicals can enter the monomer droplets, but droplet nucleation is generally not significant due to the small surface area of the monomer droplets.

In miniemulsion polymerization [1], the system begins with relatively stable submicron (50 nm -500 nm) monomer droplets. A miniemulsion is usually prepared by applying high shear forces (sonification). The droplets are stabilized against degradation by using the combination of a surfactant and a co-stablizer (hexadecane). The co-stabilizer, which has low water solubility and high solubility in monomer [2] with a low moleculaer weight [3], can significantly retard Ostwald ripening, and thus keep the monomer droplets stable. No micelles are present in the miniemulsion system, since the surfactants have been adsorbed on the monomer-water interfacial area. Nucleation by entry of free radicals into the pre-existing monomer droplets is the main nucleation mechanism in miniemulsion polymerization [4-9]. Monomer mass transfer is not involved in an ideal miniemulsion polymerization. This unique droplet nucleation mechanism of miniemulsion polymerization could contribute to the preparation of hybrid or encapsulated latex particles, which are hydrophobic.

In this chapter, KPS-initiated and redox-initiated miniemulsion polymerizations were carried out to study the influence of the high radical flux on droplet nucleation.

6.2 Experimental

Recipes used for KPS-initiated emulsion polymerization and miniemulsion polymerization under isothermal conditions at 70 ºC are shown in Table 6.1. Recipes

used for redox-initiated emulsion polymerization and miniemulsion polymerization under isothermal conditions at 25 ºC are shown in Table 6.2. The Metter RC1 reactor was equipped with a pitched-blade impeller with one baffle and the agitation speed was 400 rpm. Hexadecane was mixed with BMA monomer with a magnetic stirrer first. The mixture was then subjected to 5 minutes of mixing to allow fully dissolution of hexadecane. The SLS aqueous solution was then added all at once to the oil phase with continuous stirring. The emulsion (630 g) was then sonicated using a Branson Sonifier (model 450) at a duty cycle of 50% and a power output of 5 for 10 minutes in an ice bath. 0.234 g KPS was dissolved in 5 g water and was fed into the reactor in one shot for the KPS-initiated system after the reactor contents reached the designed temperature. The two components of the redox initiators (ascorbic acid and H_2O_2) were separately dissolved in 5 g water each and fed into the reactor in one shot for the redox-initiated process. H_2O_2 solution was fed into the reactor first and ascorbic acid solution was fed one minute later.

Table 6.1: Recipes for Thermally-initiated Emulsion Polymerization and Miniemulsion Polymerization at 70ºC

Reaction	**MK**	**T4**
Polymerization	miniemulsion	emulsion
BMA (g)	125.0	
DI water (g)	500.0	
SLS (g) *	1.733 (12.0 mM)	
Hexadecane (g)	4.0	n/a
KPS (g) *	0.234 (1.7 mM)	
$NaHCO_3$ (g) *	0.234 (0.6 mM)	

*Based on water

Table 6.2: Recipes for Redox-initiated Emulsion Polymerizations and Miniemulsion Polymerization at 25 ºC

Reaction	**MR**	**R4**
Polymerization	miniemulsion	emulsion
BMA (g)	125.0	
DI water (g)	500.0	
SLS (g) *	1.733 (12 mM)	
$FeSO_4$ (g) *	0.0125 (0.09 mM)	
NaCl (g) *	0.209 (7.2 mM)	
Hexadecane (g)	4.0	n/a
AA (g) *	0.45 (5.1 mM)	
H_2O_2 (30%) (g) *	0.45 (7.9 mM)	

*Based on water

The Mettler RC1 reaction calorimeter was used to obtain the continuous reaction rate, conversion, reactor temperature, etc. The final solids contents and conversions were measured by the gravimetric method. The molecular weight was measured by GPC, and the TEM imaging with a negative staining technique were used for accurate particle sizing. The characterization methods are described in Chapter 2.

6.3 Results and Discussions

To study the reaction rate during the polymerization, a Mettler RC1 reactor calorimeter was used. Time-dependent reaction rates indicating the different polymerization stages can be calculated from the reaction heat measured by the Mettler RC1 reaction calorimeter. The reactions were carried out using thermal initiator (KPS) and redox initiator (H_2O_2 and ascorbic acid) for emulsion polymerization and miniemulsion polymerization. The results are shown in Table 6.3.

Table 6.3: Results of Emulsion and Miniemulsion Polymerization Reactions

Sample	T4	MK	R4	MR
Solids	20.19%	20.07%	20.24%	20.04%
Conversion	99.7%	99.5%	99.6%	99.4%
Coagulation	0.2%	0.1%	0.3%	0.1%
M_N (g/mol)	966,300	418,300	132,000	56,800
M_W (g/mol)	2,234,500	1,438,600	367,100	163,500
MW PDI	2.31	3.44	2.78	2.88
D_n (nm)	111.0	167.3	43.1	101.9
D_v (nm)	111.6	167.9	43.4	102.5
D_w (nm)	112.8	169.0	44.0	103.9
PDI (D_w/D_n)	1.02	1.01	1.02	1.02
N_p (L^{-1})	3.25×10^{17}	9.56×10^{16}	5.54×10^{18}	4.19×10^{17}

In the KPS-initiated emulsion polymerization, micellar nucleation is the main nucleation mechanism. However, in miniemulsion polymerization, droplet nucleation is the main nucleation mechanism. Figure 6.1 shows the rate of polymerization (R_p) and conversion versus reaction time and Figure 6.2 shows the rate of polymerization versus conversion for the KPS-initiated emulsion polymerization (T4) and miniemulsion polymerization (MK). The reaction time started immediately after the KPS solution was added. Three Intervals are clearly shown in the KPS-initiated emulsion polymerization (Figure 6.1). At the beginning of the reaction, the micellar nucleation process results in a very fast increase in the reaction rate (Interval I). After Interval I, there is a slightly increase in reaction rate in Interval II. However, the particle number is constant during the KPS-initiated emulsion polymerization (Chapter 4). Therefore, there is no more nucleation, and the particle number becomes constant (Interval II). After 40% conversion, the reaction rate decreases with the disappearance of the monomer droplets (Interval III). In the miniemulsion polymerization, there is also a fast increase in reaction rate during the nucleation and a constant rate during polymer propagation. However, the monomer supply is from the nucleated monomer droplet itself. Therefore, monomer transfer through the aqueous phase is limited and the disappearance of dissolved monomer should not influence the reaction rate. In miniemulsions, the reaction rate decrease in Interval III is due to insufficient monomer supply in the polymer particles. The reaction rate increases up to around 90% conversion, which is caused by the gel effect. The gel effect has a smaller influence in emulsion polymerization, due to the smaller particles. In emulsion polymerization, the

reaction rate is higher compared with miniemulsion polymerization, which is caused by the smaller particle size, and the reaction time is shorter.

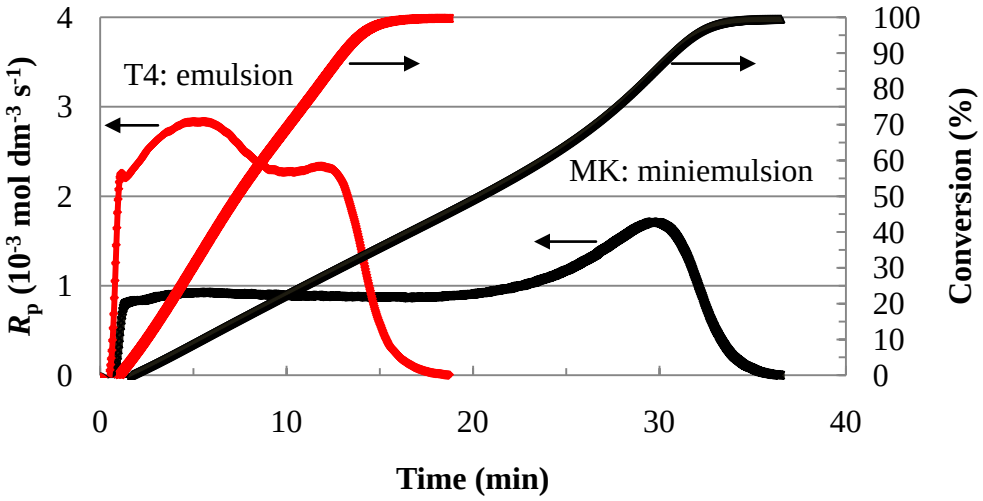

Figure 6.1: *Reaction rates and conversion vs. reaction time for KPS-initiated emulsion polymerization and miniemulsion polymerization at 70 ºC.*

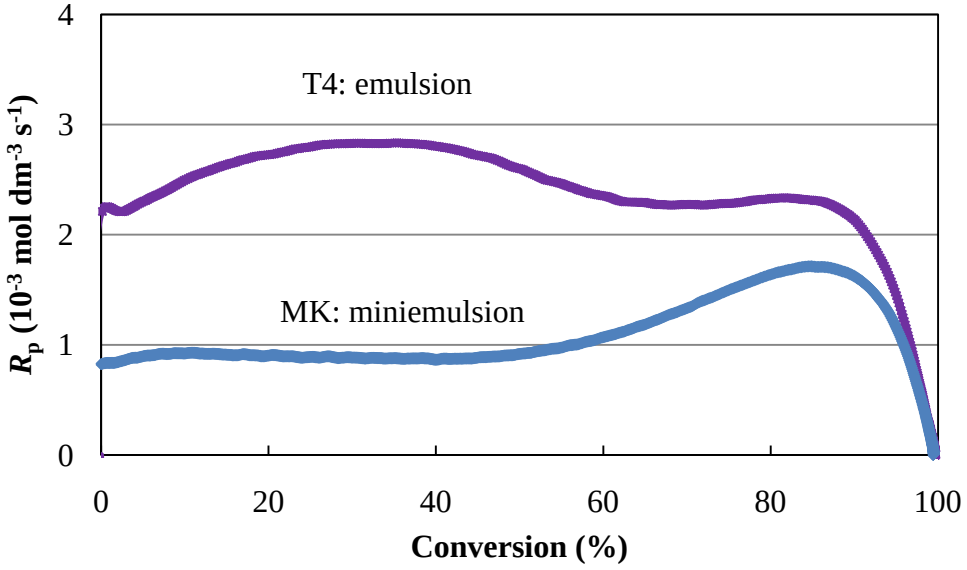

Figure 6.2: *Reaction rates vs. conversion of KPS-initiated emulsion polymerization and miniemulsion polymerization at 70 ºC.*

In redox-initiated emulsion polymerization, micellar nucleation and homogenous nucleation both play important roles, which is caused by the high radical flux (described in Chapter 4) from redox initiator. In miniemulsion polymerization, the influence of high radical flux on the droplet nucleation was studied. Figure 6.3 shows the rate of polymerization (R_p) and conversion versus reaction time and Figure 6.4 shows the rate of polymerization versus conversion for the redox-initiated emulsion polymerization (R4) and miniemulsion polymerization (MR). The reaction time started after the ascorbic acid solution was added. The shapes of three Intervals are different from the KPS-initiated polymerization (see Figure 6.1). At the beginning of the reaction, the micellar nucleation process results in a very fast increase in the reaction rate (Interval I). After Interval I, there is continuous homogenous nucleation and the reaction rate increases (Interval II). After 70% conversion, the reaction rate decreases (Interval III). In the miniemulsion polymerization, the intervals are similar in the KPS-initiated and redox-initiated systems. For the redox-initiated miniemulsion polymerization, there is no reaction rate increase during Interval II, indicating negligible homogenous nucleation. High radical flux can result in homogenous nucleation in emulsion polymerization. However, in miniemulsion polymerization, the monomer is primarily located in the monomer droplets, and monomer droplets do not serve as reservoirs to provide monomer to the growing polymer particles. Therefore, monomer transfer through the aqueous phase is limited, which limits homogenous nucleation. In miniemulsion polymerization, the reaction rate is constant during Interval II, which also indicates that homogenous nucleation is negligible in miniemulsion polymerization. In redox-initiated miniemulsion polymerization, the

reaction rate is lower compared with redox-initiated emulsion polymerization. This is because that the particle number in the miniemulsion system (4.19×10^{17} L^{-1}) is lower than in the emulsion system (5.54×10^{18} L^{-1}). Higher radical flux in the redox-initiated miniemulsion system can result in higher efficiency of monomer droplet nucleation compared with the KPS-initiated system. Therefore, the particle number in the redox-initiated miniemulsion system (4.19×10^{17} L^{-1}) is much higher than in the KPS-initiated miniemulsion system (9.59×10^{16} L^{-1}). In addition, the reaction temperature in the KPS-initiated miniemulsion system (70 ºC) is higher than the redox-initiated system (25 ºC). The instability of droplets at higher temperature can result in larger monomer droplets for the KPS-initiated miniemulsion polymerization. Therefore, the combination of the higher droplet nucleation efficiency and smaller droplet size at low temperature results in the higher particle numbers in the redox-initiated miniemulsion process.

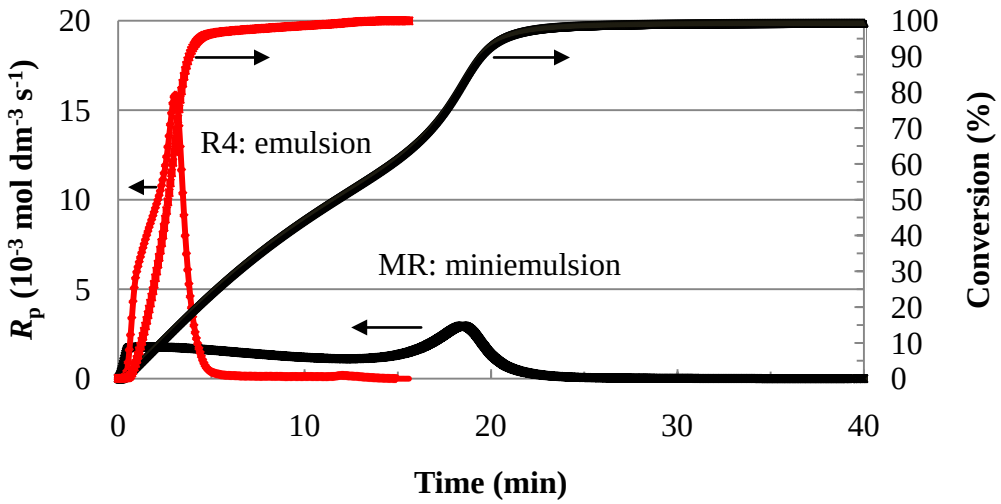

Figure 6.3: *Reaction rates and conversion vs. reaction time for redox-initiated emulsion polymerization and miniemulsion polymerization at 25 ºC.*

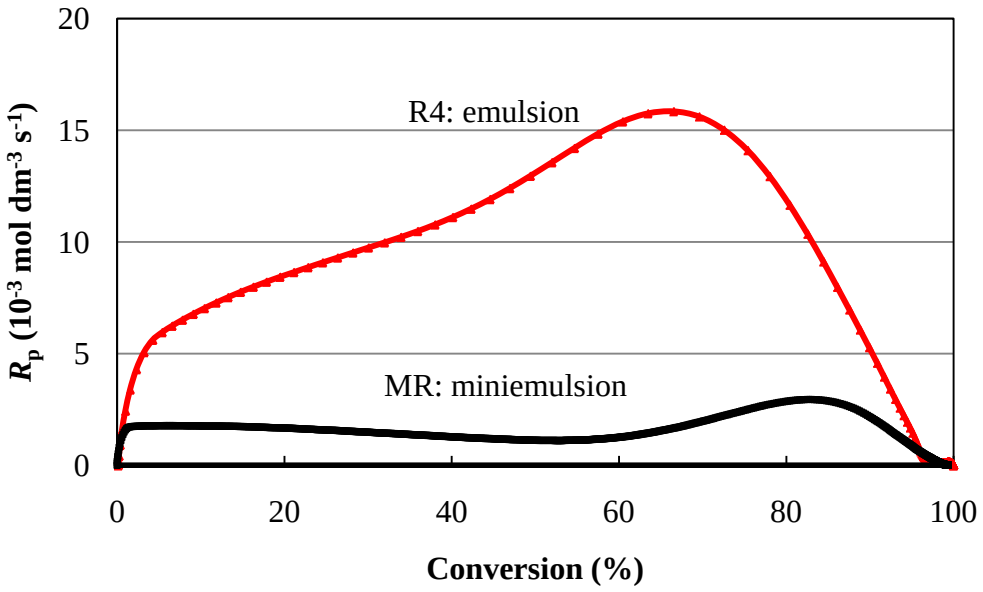

Figure 6.4: *Reaction rates vs. conversion of redox-initiated emulsion polymerization and miniemulsion polymerization at 25 ºC.*

The molecular weight distribution (obtained by GPC) of the KPS-initiated latex and the redox-initiated latex is shown in Figure 6.5. In miniemulsion polymerization, the polymerization occurs within the miniemulsion droplets. Therefore, the molecular weight is lower compared with emulsion polymerization. The high radical flux from redox initiator not only results in smaller particles, but also results in much lower molecular weight of the latex polymer.

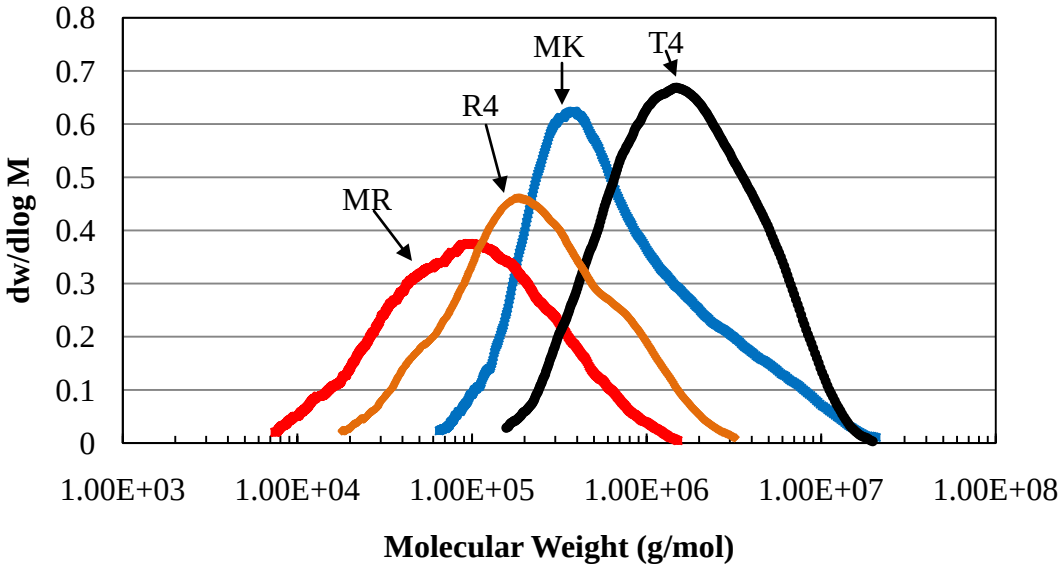

Figure 6.5: *Molecular weight distribution (measured by GPC) of latex (T4: KPS-initiated emulsion polymerization; MK: KPS-initiated miniemulsion polymerization; R4: redox-initiated emulsion polymerization; MR: redox-initiated miniemulsion polymerization).*

6.4 Conclusions

Miniemulsion polymerizations were carried out to study the influence on homogeneous nucleation by the high radical flux resulting from the redox initiator system. Compared with micellar nucleation in the KPS-initiated emulsion system and both micellar and homogenous nucleation in the redox-initiated emulsion system, droplet nucleation is the main nucleation mechanism in miniemulsion polymerization and high radical flux has little influence on the nucleation process. This occurs because the monomer primarily remains within the monomer droplets and the amount

of dissolved monomer present in the aqueous phase is limited during the polymerization. Droplet nucleation in miniemulsion polymerization results in the formation of lower molecular weight polymer compared with emulsion polymerization. In the redox-initiated miniemulsion system, low reaction temperature and high radical flux result in the formation of smaller particles with lower molecular weight compared with the KPS-initiated miniemulsion system.

6.5 References

1 El-Aasser, M. S., Sudol, E. D., in *Emulsion Polymerization and Emulsion* Polymers, Lovell, P. A. and El-Aasser, M. S. Ed., John Wiley and Son, Chichester, p 37&707, (1997)

2 Higuchi, I. and Misra, J., *J. Pharm. Sci.*, **51**, 459 (1962)

3 Ugelstad, J. and Mork, P. C., *Adv. Colloids Interface Sci.*, **13**, 101 (1980)

4 Delgado, J., El-Aasser, M. S. and Vanderhoff, J. W., *J. Polym. Sci. A Polym. Chem.*, **24**, 861 (1986)

5 Zhou, X., Ni, P. and Yu, Z., *Polymer*, **48**, 6262 (2007)

6 Capek, I. and Chern, C. S., *Adv. Polym. Sci*., **155**, 101 (2001)

7 Luo, Y. and Schork, F. J., *J. Polym. Sci. A Polym. Chem.*, **40**, 3200 (2002)

8 Asua, J. M., *Prog. Polym. Sci*., **27**, 1283 (2002)

9 Landfester, K., Bechthold, N., Tiarks, F. and Antonietti, M., *Macromolecules*, **32**, 5222 (1999)

Chapter 7

Fractional Surfactant Surface Coverage and Mechanical Stability of Latex Particles

7.1 Introduction

At the same SLS surfactant concentrations, the redox-initiated latex particles are much smaller than the KPS-initiated latex particles. This indicates that the SLS surfactant surface coverage on the particle surface of redox-initiated latexes is different from that of the KPS-initiated latex, which can significantly influence latex stability. Therefore, the fractional surfactant surface coverage and the latex mechanical stability were studied.

There are three main types of latex stability: mechanical, chemical, and thermal. Only mechanical stability was studied in this research program. Latex mechanical stability can reflect the ability of a latex in withstanding the effects of mechanical forces, such as shearing and agitation [1-3]. Mechanical stability is important for later processing of the latex, such as pumping, transportation, and storage. Although mechanical stability is important in practical processes, it is difficult to define quantitatively. The results obtained from mechanical stability tests are strongly dependent on the experimental conditions and procedures used. The method of measuring the weight of coagulum [4] after a given time of agitation was used to detect

the mechanical stability of a latex, which is described in this chapter. The electrostatic stability is provided by anionic surfactant (SLS) on the surface of latex particles [5-7]. The relationship between the fractional surfactant surface coverage and latex mechanical stability was studied to determine the critical fractional surfactant surface coverage for both KPS-initiated and redox-initiated latexes.

7.2 Experimental

The Du Nouy ring method was used to measure the surface tension of latex. All measurements were carried out at 25 ºC. Calibration curves (surface tension vs. SLS concentration) were obtained for the KPS-initiated and redox-iniated systems with different salt and buffer concentrations. The aqueous phase for a latex sample was obtained using a serum replacement cell with a 50 nm membrane. The polymer particles were retained inside the cell by the membrane, since the particles are larger than the pore size, and only the aqueous phase flowed through the membrane to be collected. Then, the surface tension of the aqueous phase was measured. The free SLS concentration in the aqueous phase can be calculated from surface tension, as described in Chapter 2. Then, the fractional surfactant surface coverage on the surface of the latex polymer particles can be calculated. A Hamilton Beach Blender was used to run the blender test [8] to measure latex mechanical stability. 250 g of latex sample was mixed at ~ 8000 rpm for 5 minutes. A 100 μm nylon mesh filter was used to filter the coagulum out of the latex. 1 liter of DI water was used to wash the foam, coagulum and the blender during the filtration. The coagulum retained by the mesh

was then placed in an aluminum pan and put in an oven (90 ºC) for 48 h to dry and remove entrapped water, and the weight of the dried coagulum was measured. The percent coagulum of these samples was calculated based on the weight of dried coagulum and the total polymer weight in the latex samples. The characterization methods are described in Chapter 2.

7.3 Results and Discussions

The high radical flux in the redox-initiated systems resulted in much smaller particles and higher particle number compared with KPS-initiated systems. However, their particle numbers are significantly different at the same surfactant concentrations for the two systems. The influence of fractional surfactant surface coverage on latex stability is described in this chapter.

The surface tensions at different aqueous SLS concentrations with different salt concentrations are shown in Figures 7.1 and 7.2. Different salt concentrations, which match the salt concentrations used in the recipe for each latex sample, were used to obtain the relationship between the SLS surfactant concentration and surface tension. Due to the difference in ionic strengths, the salt concentrations can significantly influence the surface tensions for the same SLS concentration. Higher salt concentration results in a lower surface tension. Since ascorbic acid is a weak electrolyte, the ascorbic acid concentrations do not influence the surface tension significantly.

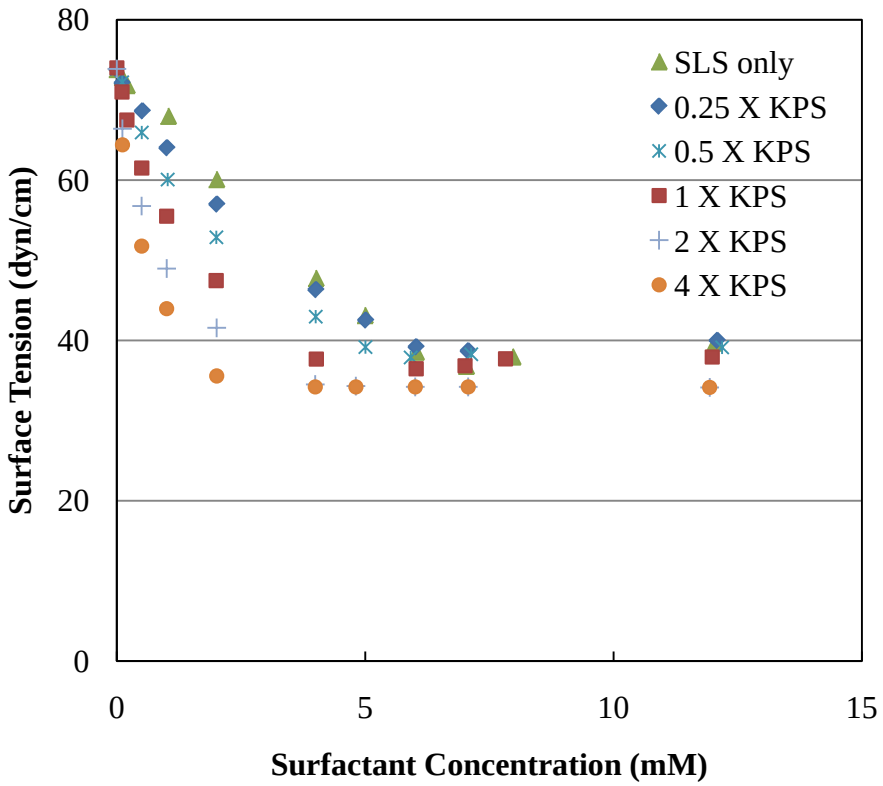

Figure 7.1: *Aqueous surface tension at different SLS concentrations with different salt concentrations of KPS and $NaHCO_3$ (0.43 mM KPS and 0.14 mM $NaHCO_3$ for 0.25 × KPS; 0.86 mM KPS and 0.28 mM $NaHCO_3$ for 0.5 × KPS; 1.7 mM KPS and 0.6 mM $NaHCO_3$ for 1 × KPS; 3.4 mM KPS and 1.2 mM $NaHCO_3$ for 2 × KPS; and 6.8 mM KPS and 2.4 mM $NaHCO_3$ for 4 x KPS).*

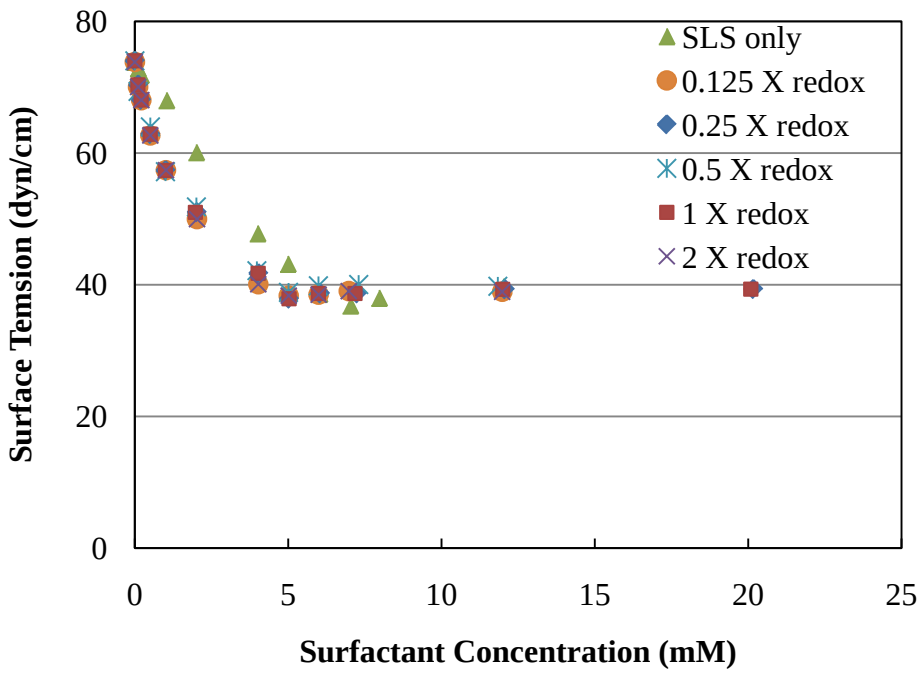

Figure 7.2: *Aqueous surface tension at different SLS concentrations with different NaCl concentrations and ascorbic acid concentrations (7.2 mM NaCl and 0.6 mM ascorbic acid for standards with 0.125 × redox; 7.2 mM NaCl and 1.2 mM ascorbic acid for standards with 0.25 × redox; 7.2 mM NaCl and 2.5 mM ascorbic acid for standards with 0.5 × redox; 7.2 mM NaCl and 5.1 mM ascorbic acid for standards with 1 × redox and 7.2 mM NaCl; and 10.2 mM ascorbic acid for standards with 2 × redox).*

After the relationships between the surface tension and SLS surfactant concentration were obtained, the free SLS surfactant concentration was calculated using the surface tension of the aqueous phase of the latex sample. The free SLS surfactant concentrations for KPS-initiated and redox-initiated latex are shown in Figures 7.3, 7.4 and 7.5 with different surfactant and initiator concentrations, and

solids contents, respectively. Due to the lower total particle surface area, the KPS-initiated latex has higher free SLS surfactant concentrations compared to the redox-initiated latex. The free surfactant concentration increased with higher initial SLS surfactant concentration, lower initiator concentration, and lower solids content, though there was much less effect in the case of the redox-initiated latex compared to the KPS-initiated latex.

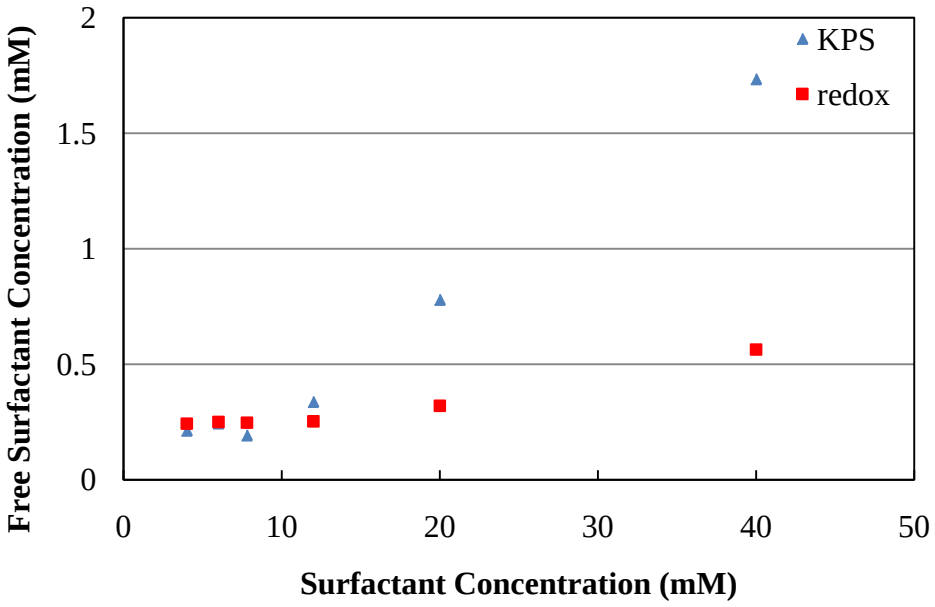

Figure 7.3: *Free SLS concentration in the aqueous phase at different surfactant concentrations in the recipe.*

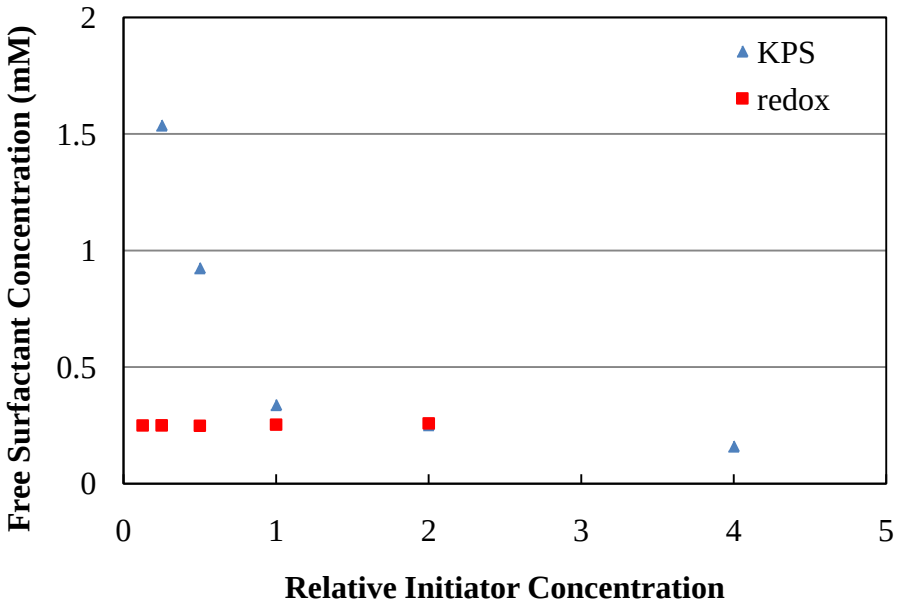

Figure 7.4: *Free SLS concentration in the aqueous phase at different initiator concentrations in the recipe.*

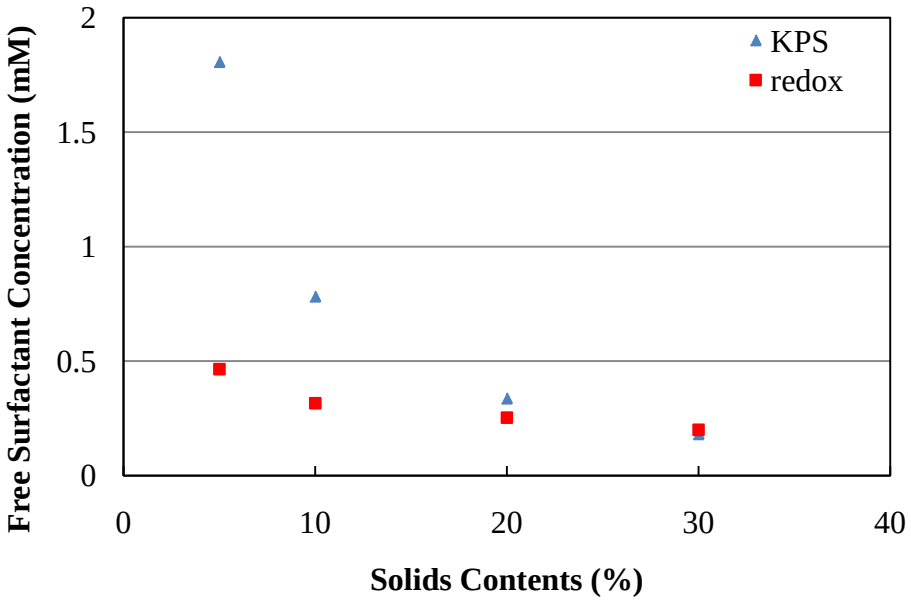

Figure 7.5: *Free SLS concentration in the aqueous phase at different solids contents in the recipe.*

The surface area covered per SLS surfactant molecule at surface saturation, was around 54 $Å^2$/molecule [9] for the PBMA-SLS system. The amount of SLS adsorbed on the surfaces of the latex polymer particles could be calculated from the free SLS concentration in the aqueous phase. Then the fractional surfactant surface coverage of the PBMA particles with adsorbed SLS surfactant molecules present were calculated and are shown in Figures 7.6, 7.7 and 7.8. Due to the much higher particle number in the redox-initiated latex, the total particle surface area is higher and the fractional surfactant surface coverage is lower compared with the same surfactant concentration in the KPS-initiated latex. The fractional surfactant surface coverage increased with higher SLS surfactant concentration, lower initiator concentration, and lower solids contents, and there was less effect for the redox-initiated latex compared with the KPS-initiated latex. A significant difference in the fractional surfactant surface coverage usually indicates a significant difference in the stability of latex. Therefore, a study of the mechanical stability of these latexes was necessary.

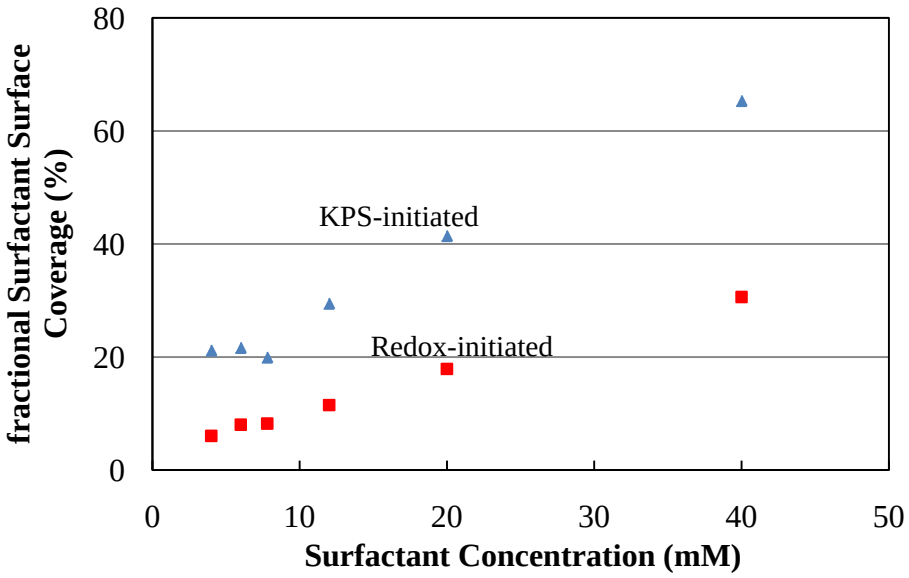

Figure 7.6: *Fractional surfactant surface coverage at different surfactant concentrations in the recipe.*

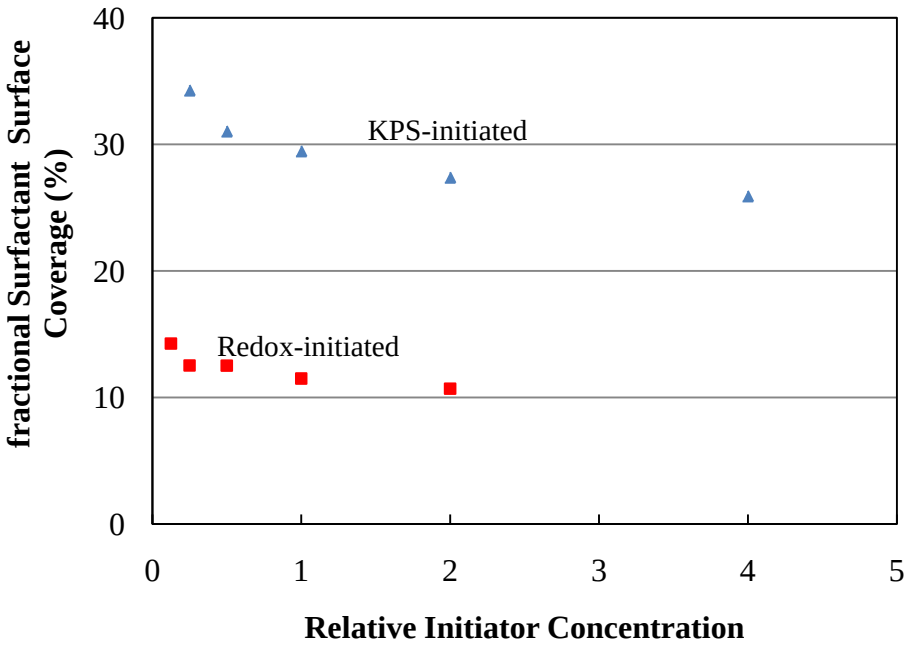

Figure 7.7: *Fractional surfactant surface coverage at different initiator concentrations in the recipe.*

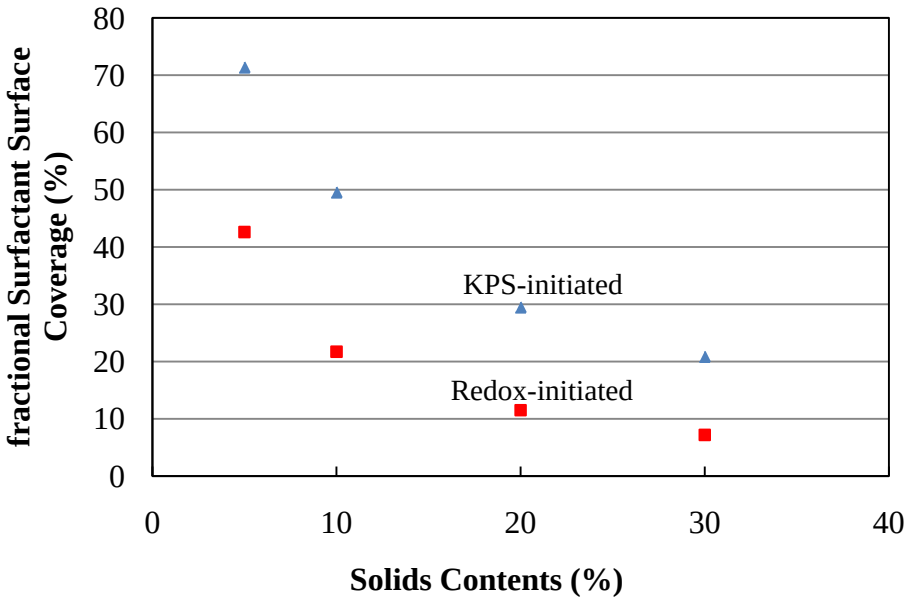

Figure 7.8: *Fractional surfactant surface coverage at different solids contents in the recipe.*

A Hamilton Beach blender was used to carry out the blender test for the latex stability measurements. The coagulum ratio is calculated by dividing the amount of polymer in the coagulum (g) by the total polymer weight in the samples (g). The results of the coagulum ratio versus fractional surface coverage are shown in Figures 7.9 and 7.10 for the redox-initiated and the KPS-initiated systems, respectively. The lower surfactant surface coverage range for the redox-initiated latexes resulted from its much higher particle number. However, the trend in the mechanical stability of the latexes is similar for both systems. Only a few samples with high initial surfactant concentrations and lower solids contents are stable. The critical fractional surfactant surface coverage to maintain latex stability is 19% for redox-initiated latex and 39% for KPS-initiated latex. Compared with the KPS-initiated latex, the redox-initiated latex only needs half of the fractional surfactant surface coverage to attain latex

stability. Electrostatic stability is the main force that imparts stability to the latex in both systems. The fractional surfactant surface coverage is the main source of electrostatic stability, and the charged end groups from initiator decomposition can also contribute to the latex stability. In the KPS-initiated latex, sulfate charged groups (SO_4^{2-}) are present on the particle surface, and in the redox-initiated latex, hydroxyl group (OH) are located on the particle surface. Since the critical fractional surfactant surface coverage is only half in redox-initiated latex compared with KPS-initiated latex, the presence of hydroxyl groups on the particle surface should be the reason for the similarity in stability in both systems. The Zeta potential of KPS-initiated and redox-initiated latexes were measured at solids content of 50 mg/L with 10 mM NaCl, and the results are described in Appendix B. Zeta potential values are similar at around -30 mV for both systems, which indicates the hydroxyl group can contribute to the electrokinetic phenomena, which is important to the stability of the latex particles. The origin of the charge for hydroxyl group can be the result of either the preferential adsorption of hydroxyl group (polarization) or contact electrification between phases (latex polymer and water) [10-12]. Therefore, the stability of redox-initiated latex at low surfactant surface coverage may be enhanced by the higher concentration of hydroxyl groups on the particle surface, which is introduced by high radical flux of the redox initiator (H_2O_2). Therefore, the redox-initiated latex can achieve a similar latex stability with much lower fractional surfactant surface coverage.

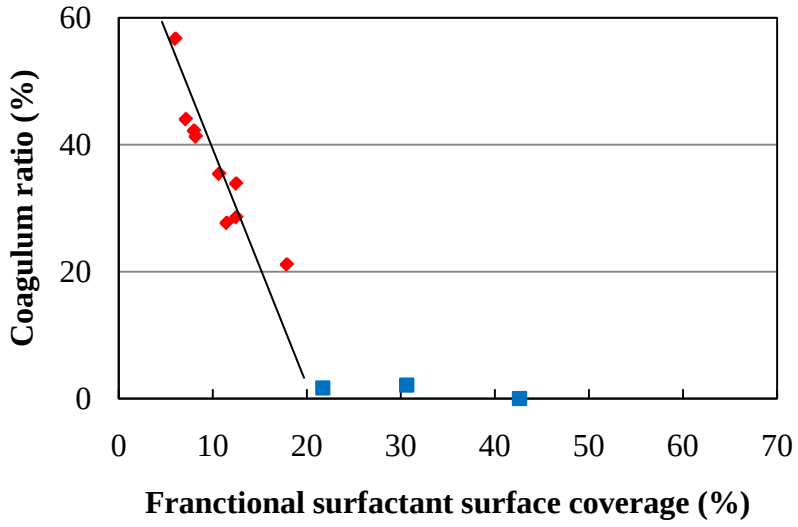

Figure 7.9: *Percentage of coagulum versus fractional surfactant surface coverage for redox-initiated latexes.*

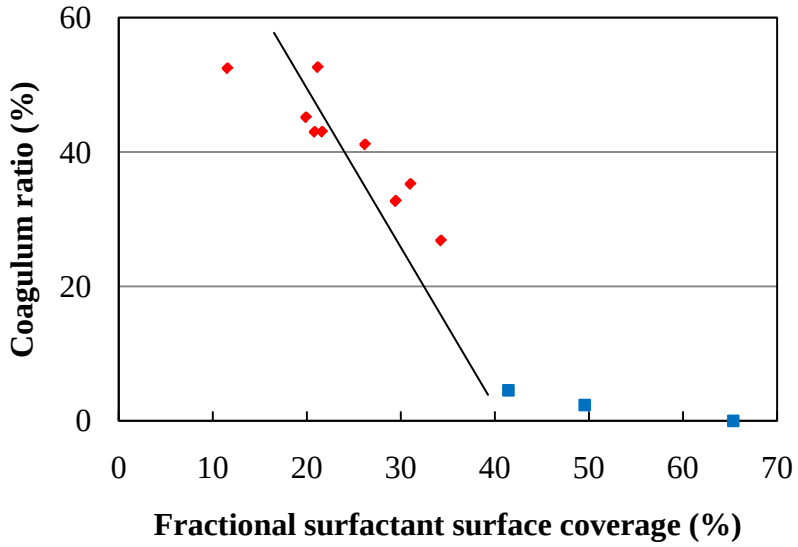

Figure 7.10: *Percentage of coagulum versus fractional surfactant surface coverage for KPS-initiated latexes.*

7.4 Conclusions

The surface tension of the aqueous phase of latex samples was measured and the free surfactant concentration and the fractional surfactant surface coverage on the PBMA particles with adsorbed SLS surfactant molecules were calculated. The free surfactant concentrations and fractional surfactant surface coverage are much lower in the case of the redox-initiated latexes, compared with the KPS-initiated latex, and they increased with higher SLS surfactant concentrations, lower initiator concentrations, and lower solids contents, although the redox-initiated latex is not affected as much compared to the KPS-initiated latex. The stability of the redox-initiated latex was measured by a blender test. The critical surfactant surface coverage needed to maintain latex stability is 19% for the redox-initiated latex and 39% for the KPS-initiated latex. The stability of the redox-initiated latex with low fractional surfactant surface coverage may be enhanced by the presence of extra hydroxyl groups from the decomposition of redox initiator (H_2O_2). Therefore, the redox-initiated emulsion polymerization can result in latex with much smaller particle size and similar stability for the same surfactant concentrations compared with the KPS-initiated systems.

7.5 References

1 Blackley, D. C., in *Polymer Lattices*, Chapman and Hall, Volume 1 (1997)

2 Utracki, L. A., *J. Colloid Interface Sci*., **42**, 185 (1973)

3 Castelvetro, V., De Vita, C., Giannini, G. and Giaiacopi, S., *J. Appl. Polym. Sci*., **102**, 3083 (2006)

4 International Organization for Standardization, 2006-1985

5 Colobie, D., Sudol, E. D. and El-Aasser, M. S., *Macromolecules*, **33**, 7283 (2000)

6 Cummins, P. G., Staples, E. and Penfold, J., *J. Phys. Chem*., 94, 3740 (1990)

7 Sefcik, J., Verduyn, M., Storti, G. and Morbidelli, M., *Langmuir*, **19**, 4778 (2003)

8 American *Standard Test Method* D1417-03D

9 Fitch, R. M. and Sutterlin, N., *Polymer Colloids II*, Plenum, New York, p 583 (1980)

10 Kamel, A. A., Ma, C. M., El-Aasser, M. S. and Micale, F. J., *J. Disper. Sci. Technol*., **2**, 315 (1981)

11 Haydon, D. A., *Biochm. Biophys. Acta*, **50**, 457 (1961)

12 Taylor, A. J. and Wood, F. W., *Trans. Faraday Soc*., **53**, 523 (1957)

Chapter 8

Redox-initiated Adiabatic Batch

Emulsion Polymerization of *n*-Butyl Methacrylate

8.1 Introduction

High-temperature isothermal processes are usually employed in emulsion polymerization to reduce the polymerization cycle time and maintain reaction reproducibility. Reactions using thermal initiator are usually carried out at 60 ºC - 90 ºC, due to the high activation energy (125-160 kJ·mol^{-1}) of the initiators [1]. However, the energy used in these commercial-scale processes is large, and the cost is huge. For example, a 500 m^3 reactor should need more than $3000 to heat up the reactants. Heating of the reactor and its contents also takes a significant amount of time. The heating equipment and heat transfer system are also expensive.

A high radical flux redox initiator (described in Chapter 4) was considered as an alternative to thermal initiators to decrease the reaction temperature of emulsion polymerization. The low activation energy (40-80 kJ·mol^{-1}) of redox initiators [1] allows polymerization at room temperature. Further, these polymerization reactions are highly exothermic and the heat of reaction can be utilized [2-7]. Therefore, the combined use of redox initiators and an adiabatic process is being evaluated to take an advantage of the low reaction temperature and the heat of polymerization [8]. The redox initiator

can start the reaction at room temperature, where no preheating is needed. Under adiabatic conditions, the polymerization heat can be utilized to increase the reactor temperature. The higher reactor temperature can result in a higher reaction rate, where the reaction cycle can be reduced. Due to the surface-to-volume ratio change in the reactor during the isothermal scale up process, the heat transfer rate can not be consistent, and this influences the reactor temperature profile during the polymerization. It can significantly influence the properties of the product at different scales, such as conversion, particle size and molecular weight. Under adiabatic conditions, the heat transfer between the reactor and jacket is negligible, which would not be influenced by the surface-to-volume ratio of the reactor. Therefore, the reactor temperature can be better maintained at a consistent value during the scale up process, which result in less effect in product's properties during scale up process. Adiabatic processes were carried out in the Mettler RC1 reactor with minimal heat loss (~10%). Hydrogen peroxide (H_2O_2) and ascorbic acid (AA), in conjunction with Fe^{2+} ion, were used as the redox initiator components in the emulsion polymerization of BMA to study the differences between isothermal and adiabatic conditions.

8.2 Experimental

Recipes used for redox-initiated emulsion polymerizations under different conditions are shown in Tables 8.1 and 8.2. Table 8.1 shows the variation of the starting reaction temperatures and Table 8.2 shows the variation in solids contents. The Mettler RC1 reactor was equipped with a pitched-blade impeller with one baffle

and the agitation speed was 400 rpm. The distillation mode (D_i) of the Mettler RC1 was used to maintain adiabatic conditions. The two redox initiator components (ascorbic acid and H_2O_2) were separately dissolved in 5 g water and fed into the reactor in one shot at the beginning of the redox-initiated process. H_2O_2 solution was fed into the reactor first and ascorbic acid solution was fed one minute later. The redox-initiated polymerizations were predominantly carried out with a starting temperature of 25 ºC, except for several polymerizations that were carried out at 40 ºC or 55 ºC. The recipes used for isothermal conditions with different starting reaction temperatures and solids contents were shown previously in Tables 4.9 and 4.10 (Chapter 4).

Table 8.1: Recipes for Redox-initiated Emulsion Polymerizations where the Staring Polymerization Temperature was Varied

Reactions	**AD1**	**AD2**	**AD3**
BMA (g)	125.0		
DI water (g)	500.0		
SLS (g) *	1.733 (12mM)		
$FeSO_4$ (g) *	0.0125 (0.09 mM)		
NaCl (g) *	0.209 (7.2 mM)		
Starting Polymerization Temperature (ºC)	25	40	55
AA (g) *	0.45 (5.1 mM)		
H_2O_2 (30%) (g) *	0.45 (7.9 mM)		

* Molar concentrations based on water

Table 8.2: Recipes for Redox-initiated Emulsion Polymerizations where the Solids Content was Varied, with a Starting Polymerization Temperature of 25 ºC

Reactions	**AD4**	**AD5**	**AD1**	**AD6**
BMA (g)	26.3	55.5	125.0	214.3
DI water (g)	500.0			
SLS (g) *	1.733 (12mM)			
$FeSO_4$ (g) *	0.0125 (0.09 mM)			
NaCl (g) *	0.209 (7.2 mM)			
A A (g) *	0.45 (5.1 mM)			
H_2O_2 (30%) (g) *	0.45 (7.9 mM)			

* Molar concentrations based on water

The Mettler RC1 reaction calorimeter was used to obtain the continuous reaction rate, conversion, and reactor temperature during the polymerization. The final solids content and conversion were measured gravimetrically. The molecular weight was measured by GPC and TEM imaging with a negative staining technique was used for particle sizing to obtain accurate particle sizes. The characterization methods are described in Chapter 2.

8.3 Results and Discussions

With the use of the Mettler RC1 reactor calorimeter, time-dependent reaction rates, indicating different polymerization stages, can be accurately calculated from the reaction heat measured by the reactor. The reactions were carried out using redox initiator (H_2O_2 and ascorbic acid with $FeSO_4$) at different solids contents and different reaction temperatures. The results for the redox-initiated reactions are shown in Table 8.3.

Table 8.3: Results of Redox-initiated Emulsion Polymerization Reactions

Sample	**AD1**	**AD2**	**AD3**	**AD4**	**AD5**	**AD6**
Solids	19.91%	20.15%	19.95%	5.26%	10.12%	29.67%
Conversion	98.4%	99.8%	99.6%	97.8%	97.4%	99.8%
Coagulum	0.4%	0.5%	1.4%	0.0%	0.0%	1.7%
M_N (g/mol)	100,600	98,600	63,400	143,900	89,300	134,700
M_W (g/mol)	353,300	351,700	256,300	732,500	793,900	390,200
MW PDI	3.51	3.57	4.04	5.09	8.89	2.90
D_n (nm)	45.8	42.9	47.7	34.4	37.5	49.7
D_v (nm)	46.1	43.2	47.8	34.7	38.4	50.2
D_w (nm)	46.5	43.9	48.2	35.2	40.4	51.2
SD (nm)	3.3	3.6	2.6	2.8	6.2	4.8
PDI (D_w/D_n)	1.02	1.02	1.01	1.02	1.07	1.03

Polymerizations were carried out under adiabatic conditions in the Mettler RC1 reactor, which eliminates the temperature difference between the reactor and

jacket to minimize heat transfer. There were slight differences in reaction rate and conversion between the isothermal and adiabatic conditions of redox-initiated polymerizations (shown in Figures 8.1 and 8.2). When the polymerization is carried out under adiabatic conditions, the reaction heat can be utilized to increase the reactor temperature. This can result in a faster reaction rate at the same reaction time and the total reaction time can be reduced. The use of adiabatic conditions can reduce the reaction cycle. However, the reaction rate under isothermal conditions is higher than that under adiabatic conditions at same conversion until it reaches 70% conversion (shown in Figure 8.2). Under adiabatic conditions, the reactor temperature increases with conversion. Aggregation may occur during the homogenous nucleation process of redox-initiated polymerization due to insufficient amount of surfactant in the aqueous phase. The high reactor temperature can result in a larger amount of aggregation, which reduces the particle number, and further results in a lower reaction rate. This was confirmed by the larger latex particle sizes in adiabatic systems, which is compared with isothermal systems. After 70% conversion, a higher reactor temperature was achieved for the adiabatic systems, and the higher reaction rate constant of BMA at higher reaction temperature results in a higher reaction rate. Therefore, the reaction rate for the polymerization carried out under isothermal conditions is lower than those under adiabatic conditions after 70% conversion. In order to eliminate the influence of the nucleation process, seeded emulsion polymerization experiments will be described in Chapter 9 to further study the influence of adiabatic conditions. Under adiabatic conditions, the reaction temperature increases with conversion and can be well maintained after the reaction is complete.

The reactor temperature increase is ~ 20 °C for reaction AD1 and the heat loss is about 10 %, which is compared with a theoretical temperature increase (~ 22°C). The heat loss results primarily from the reactor inserts, such as the shaft, the impeller and the probes, which indicates negligible heat loss in this system (shown in Figures 8.3 and 8.4).

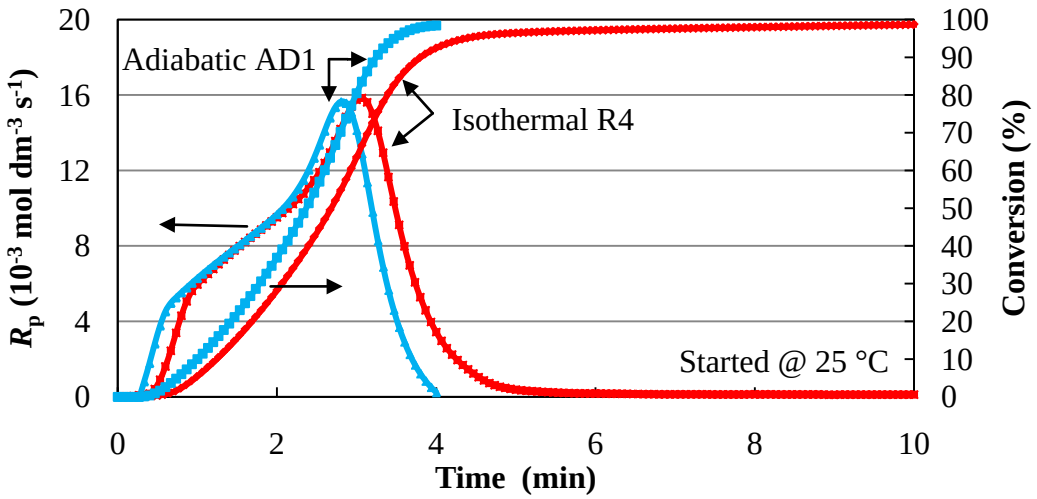

Figure 8.1: *Reaction rates and conversion of redox-initiated emulsion polymerizations under isothermal and adiabatic conditions.*

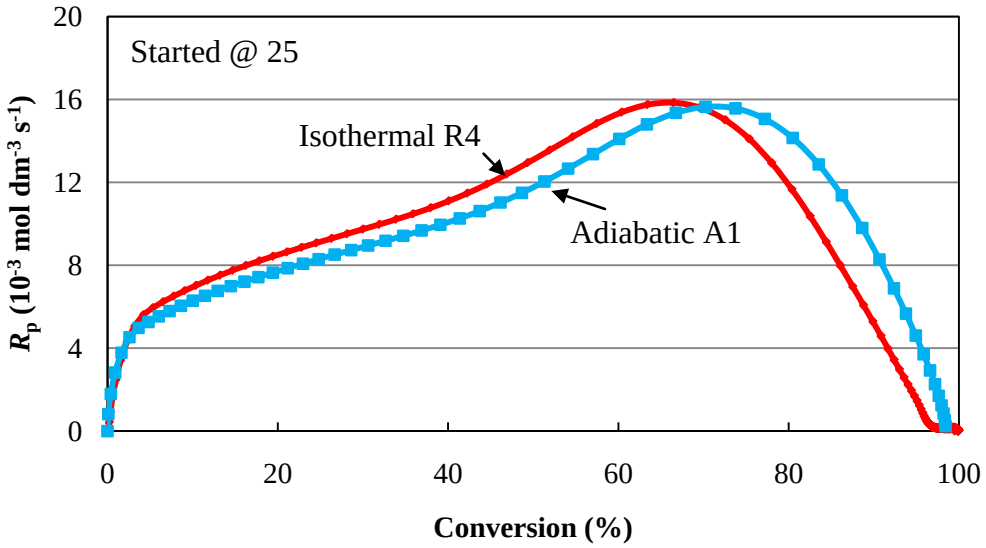

Figure 8.2: *Reaction rates vs. conversion of redox-initiated emulsion polymerization under isothermal and adiabatic conditions.*

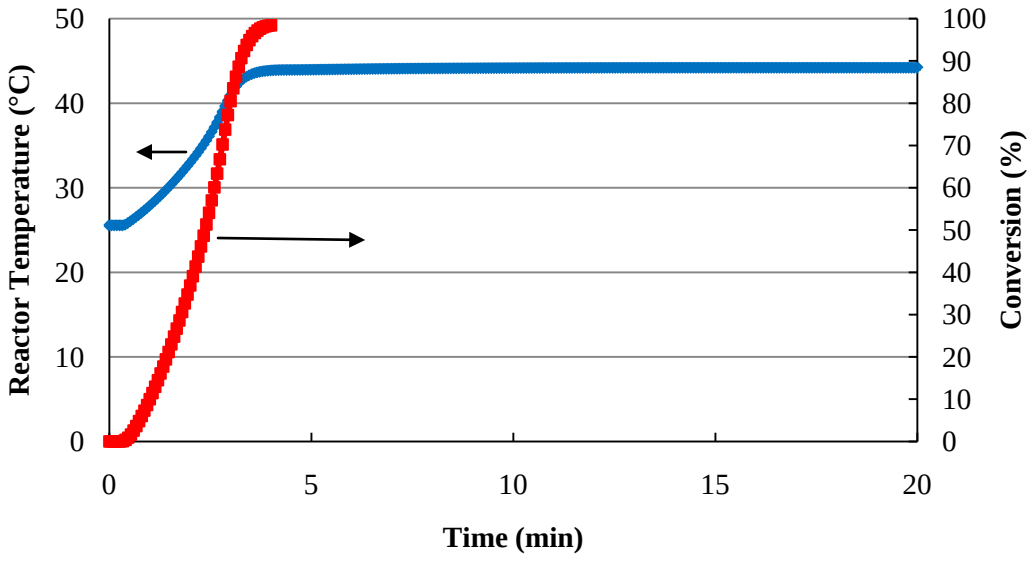

Figure 8.3: *Reactor temperature and conversion of redox-initiated emulsion polymerization under adiabatic conditions.*

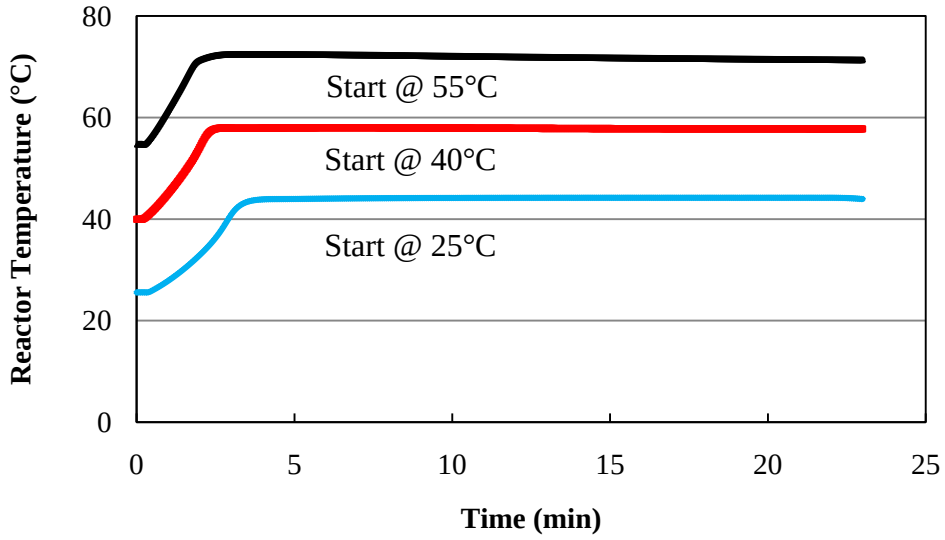

Figure 8.4: *Reactor temperature of redox-initiated emulsion polymerization under adiabatic conditions.*

The reaction rates of redox-initiated polymerizations at different starting reaction temperatures under adiabatic and isothermal conditions are shown in Figures 8.5 and 8.6. The reaction rate is higher with a higher reaction temperature, because the reaction rate constant is higher at a higher temperature. There is a fast increase in the reaction rate at the beginning of the reaction (~ 5% conversion), which represents the nucleation process (Interval I). The reaction rate increases with a slower slope, until ~ 70% conversion is attained (Interval II). This continuing slower reaction rate increase indicates the presence of homogenous nucleation, which is described in Chapter 4. After that, the reaction rate decreases, due to the disappearance of monomer droplets (Interval III). The shapes of three intervals of emulsion polymerization are almost the same for the two processes (isothermal and adiabatic), indicating that the increase of the reactor temperature during the polymerization is not a key factor for the

continuous increase of the reaction rate in Interval II. Under adiabatic conditions, the latex particle size is larger than that under isothermal conditions as shown in Figure 8.7. This is caused by the instability of the particles at higher temperature. At higher reaction temperature, the radical generation rate from the redox initiator is higher, and therefore results in the formation of more nuclei. However, the particle size is not significantly affected by the reaction temperature. This is caused by the instability of the particles at higher temperature, which result in a larger particle size than expected. The molecular weight is unaffected by adiabatic conditions compared with isothermal conditions, which results from a combination of the influence of reaction rate constant, radical generation rate, and particle size (shown in Figure 8.8).

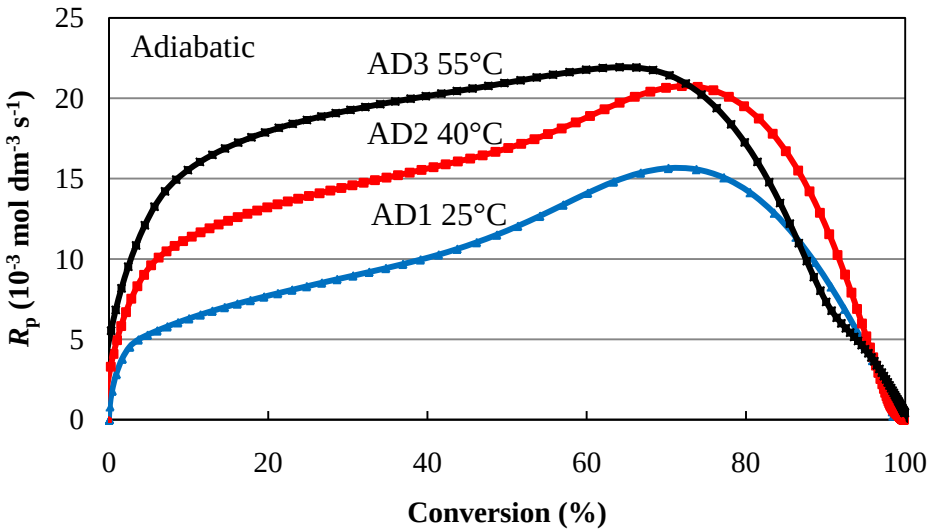

Figure 8.5: *Reaction rates vs. conversion of redox-initiated emulsion polymerizations carried out at different reaction staring temperatures (adiabatic).*

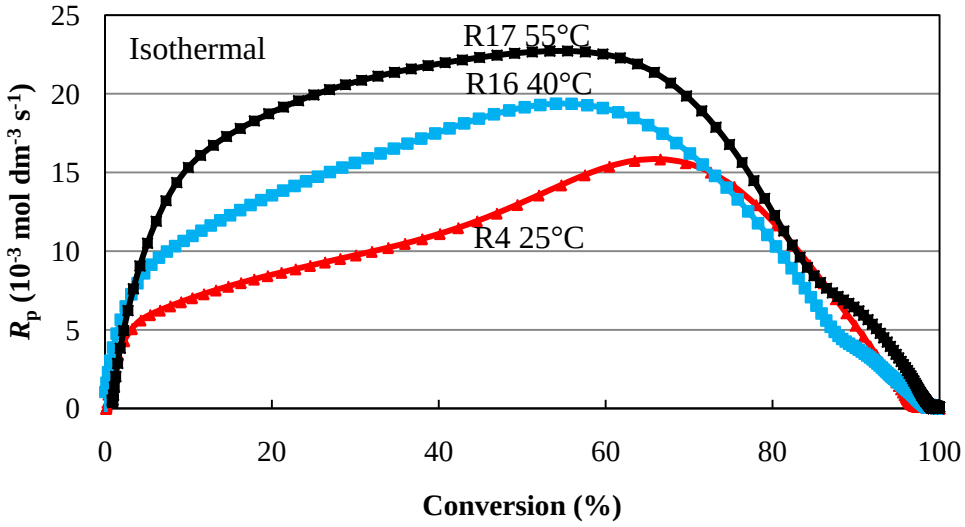

Figure 8.6: *Reaction rates vs. conversion of redox-initiated emulsion polymerization at different reaction temperatures.*

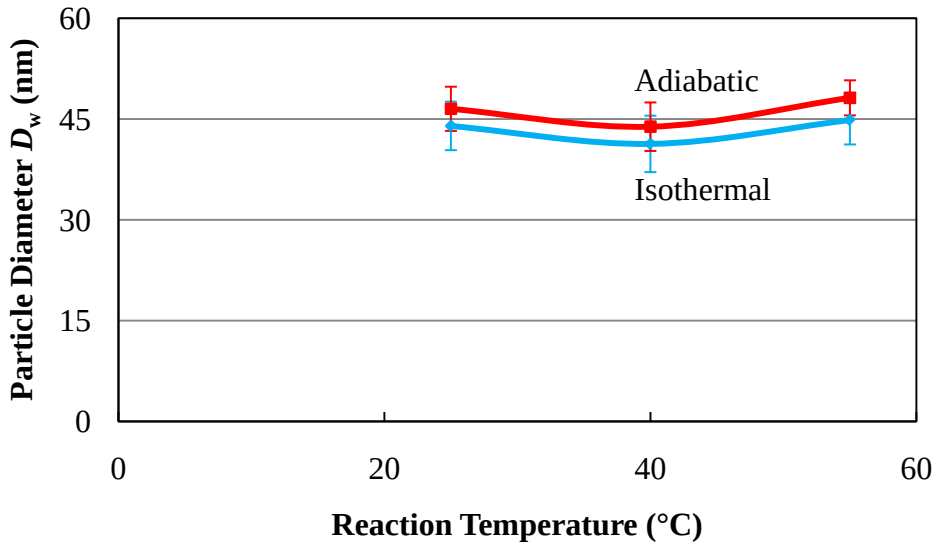

Figure 8.7: *Particle diameter (D_w) versus reaction temperatures for isothermal and adiabatic redox-initiated latexes.*

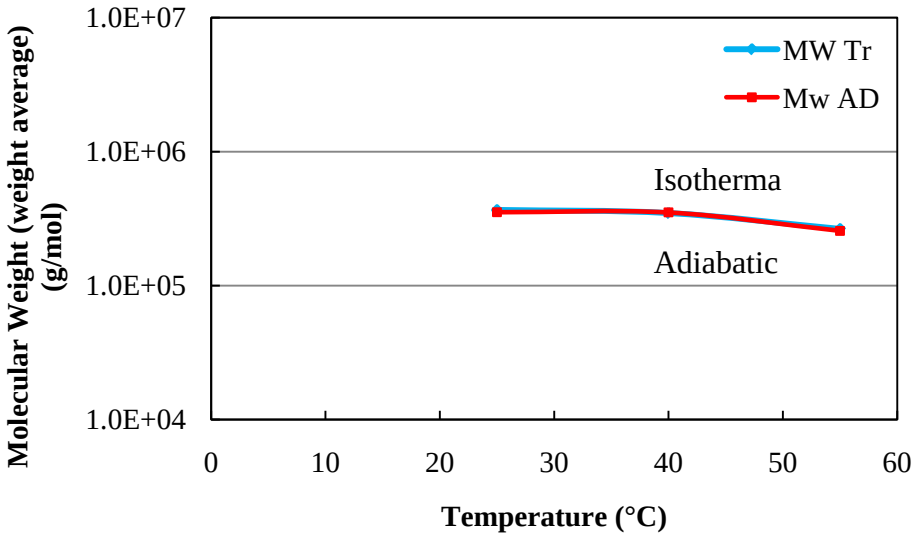

Figure 8.8: *Relation between molecular weight (weight-average) versus reaction temperature for isothermal and adiabatic redox-initiated latexes.*

The reaction rates of redox-initiated polymerizations at different solids contents under adiabatic and isothermal conditions are shown in Figures 8.9 and 8.10. The reaction rate is higher with higher solids content, which is caused by more homogeneous nucleation at higher solids content, which is described in Chapter 4. The three intervals of emulsion polymerization are almost the same for both isothermal and adiabatic processes, except for the polymerizations at 30% solids content (AD6 and R15). Under adiabatic conditions, the reaction temperature increases during the reaction. At the same solids contents, the reaction rate curves are similar during Interval II under both isothermal and adiabatic conditions, which indicate that the temperature increase during the polymerization is not the key factor for the reaction rate increase during Interval II. At 30% solids content (isothermal), the fluctuation of the reaction rate in recipe R16 is caused by the high viscosity of the latex (described in

Chapter 4), which results in limited mass transfer of the radicals and monomers. For recipe AD6 (30% solids under adiabatic conditions), the reactor temperature increased during the polymerization, and the higher reaction temperature improved the extent of mass transfer. Therefore, the fluctuation of the reaction rate is not as significant as in R16. The particle size is larger with higher solids content under both conditions, which is shown in Figure 8.11. With the same recipes, emulsion polymerization under adiabatic conditions resulted in a higher reactor temperature during the polymerization. Under adiabatic conditions, the particle sizes are larger compared with the isothermal process, which indicates instability of the particles at higher temperature. The molecular weight is almost unaffected by adiabatic conditions compared with the isothermal conditions for different initial solids contents, which results from a combination of the influence of the reaction rate constant, radical generation rate, and particle size (shown in Figure 8.12).

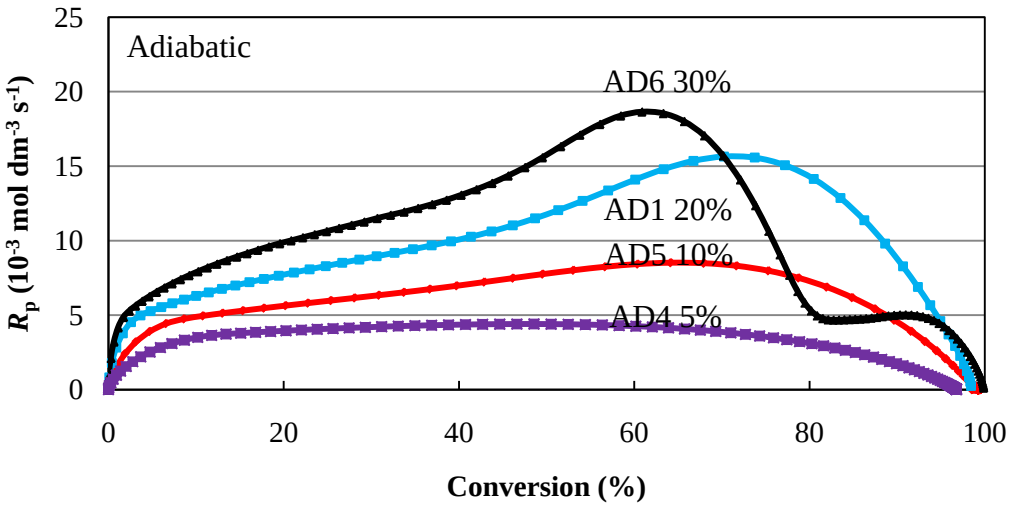

Figure 8.9: *Reaction rates vs. conversion of redox-initiated emulsion polymerizations carried out at different solids contents (adiabatic).*

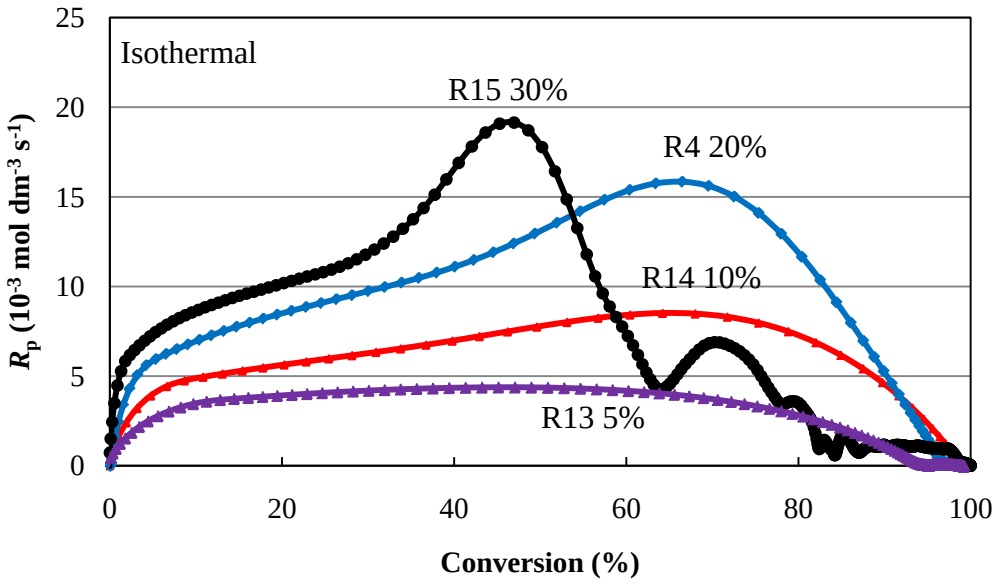

Figure 8.10: *Reaction rates vs. conversion of redox-initiated emulsion polymerizations carried out at different solids contents.*

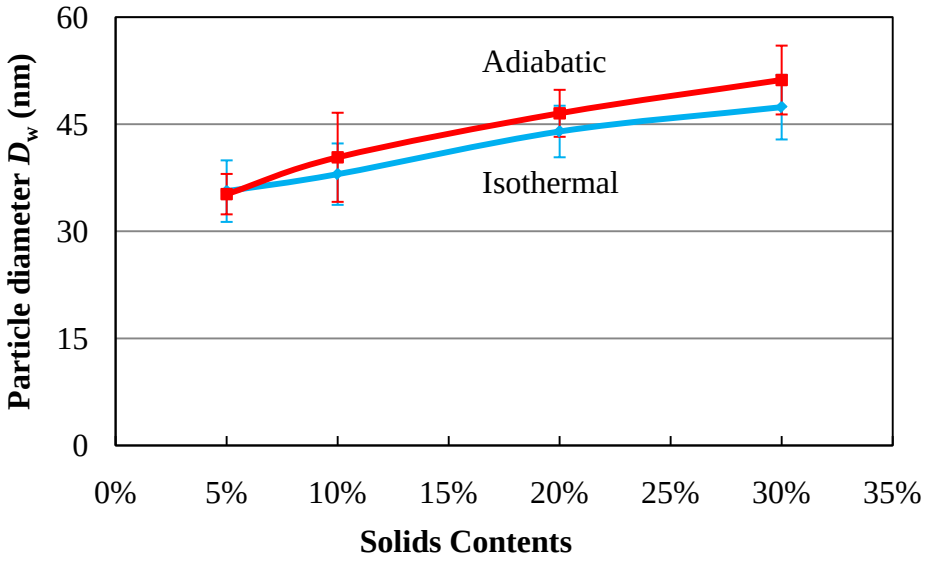

Figure 8.11: *Particle diameter (D_w) versus solids contents for isothermal and adiabatic redox-initiated latexes.*

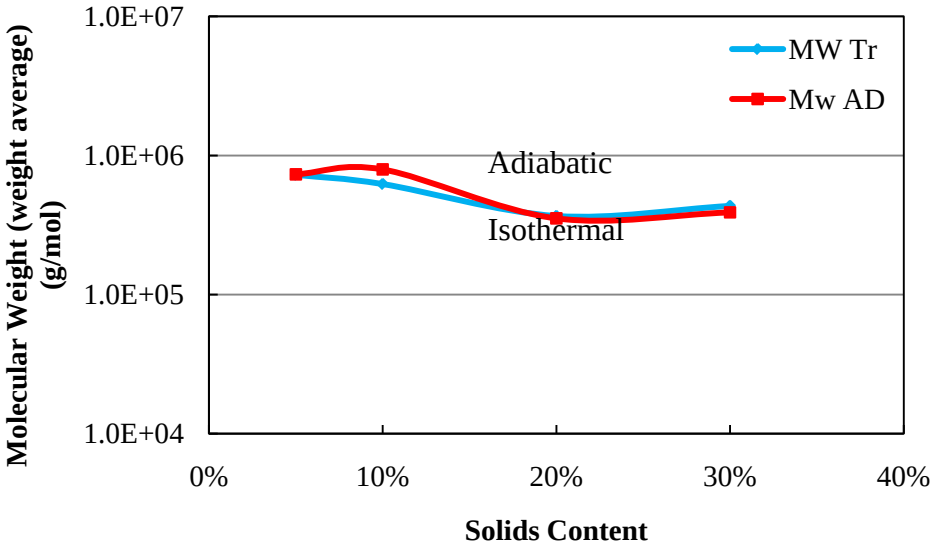

Figure 8.12: *Relation between molecular weight (weight average) versus solids contents for isothermal and adiabatic redox-initiated latexes.*

8.4 Conclusions

'Adiabatic' redox-initiated emulsion polymerization has been investigated as a process to produce latexes with a shorter production cycle and improved scalability, compared to the isothermal process. 'Adiabatic' processes were carried out in the Mettler RC1 reactor, and there was minimal heat loss (~10%) in this reactor under adiabatic conditions. The reactor temperature increased with conversion during the polymerization and the reaction time is shorter under adiabatic conditions compared with isothermal conditions. Under adiabatic conditions, the higher starting reaction temperature and higher solids content can result in a faster reaction rate, which is the

same as under isothermal conditions. However, the differences in the reaction rates under isothermal and adiabatic conditions are not significant. This result is caused by the larger particle size and higher temperatures under 'adiabatic' conditions. Therefore, the reaction rates are affected by a combination of reduced particle number and the increased reaction rate constant at higher reaction temperature under adiabatic conditions. The difference between the molecular weights obtained under the isothermal and adiabatic conditions are negligible.

8.5 References

1 Sarac, A. S., *Prog. Polym. Sci*., **24**, 1149 (1999)

2 Nomura, M., Tobita, H., Suzuki, K., and Lee, D. I., *Polymeric Microspheres: Science and Technology*, Kyoto University Press, Kyoto, Japan, p. 181 (2007)

3 Mosebach, M. and Reichert, K., *J. Appl. Polym, Sci*., **66**, 673 (1997)

4 Zhang, C., Du, Z., Li, H. and Ruckenstein, E., *Polymer*, **43**, 2945 (2002)

5 Ballweber, E. G., US Patent 4,335,237 (1982)

6 Platkowski, K. and Reichert, K., *Polymer*, **40**, 1057 (1999)

7 Yashoda, M. P., Sherigara, B. S. and Venkateswaran, G., *Polymer*, **41**, 7381 (2000)

8 Goikoetxea, M., Heijungs, R., Barandiaran M. J. and Asua, J. M., *Macromol. React. Eng*., **2**, 90 (2008)

Chapter 9

Seeded Semi-batch Emulsion Polymerization of *n*-Butyl Methacrylate

9.1 Introduction

Seeded emulsion polymerization is a type of emulsion polymerization with preformed latex introduced into the reaction mixture at the beginningof the polymerization, where the nucleation is heterogeneous. Seeded emulsion polymerization processes are important for an industrial large-scale production of synthetic polymer latexes [1-6], and have been used particularly when the composition, structure and size of the latex particles need to be controlled. Since the 1940s, semi-batch emulsion polymerization processes have been developed for a variety of products using different reactor configurations. There are many advantages for seeded semi-batch emulsion polymerizations, such as: economical production of large-volume latex, uniform product quality, less coagulation, controlled heat generation rate, and controlled composition and structure of the resulting latex.

Adiabatic seeded semi-batch emulsion polymerization processes have been considered as alternatives to the usual isothermal process to utilize the heat of polymerization [7-10]. Under adiabatic conditions, the reactor temperature increases,

whereby a faster reaction rate is achieved and the cycle time is reduced. In this way, the time and energy costs of heating the reactor can be reduced. The adiabatic process can therefore be regarded as a 'green' process resulting in a smaller environmental impact compared to the normal isothermal emulsion polymerization process. Redox initiator can be used to initiate the polymerization at lower temperatures.

Monomer-starved feeding conditions were used in the seeded semi-batch processes, where the monomer feed rate is less than the maximum rate of polymerization. In this situation, there is no monomer build-up in the reactor and the reaction rate is controlled by the monomer feed rate. Polymerization processes were carried out in the Mettler RC1 reactor. KPS was used as thermal initiator at 70 ºC under isothermal conditions, and hydrogen peroxide (H_2O_2) and ascorbic acid (AA), in conjunction with Fe^{2+} ion, were used as the redox initiator system with a starting temperature at 25 ºC under both adiabatic and isothermal conditions.

9.2 Experimental

Recipes used for seeded semi-batch emulsion polymerizations under different conditions are shown in Table 9.1. The Mettler RC1 reactor was equipped with a pitched-blade impeller with one baffle and the agitation speed was 400 rpm. The semi-batch processes were carried out by feeding BMA monomer, SLS surfactant solution and redox initiator components with syringe pump separately. The seed was obtained from the redox-initiated polymerization (R4; recipe shown in Table 4.6, Chapter 4).

200 g of latex (R4: 20% solids content) and 200 g of DI water were mixed to generate the 10% solids seed for the seeded semi-batch polymerization. In redox-initiated semi-batch polymerization, BMA monomer, SLS surfactant (dissolved in 5 g DI water), ascorbic acid (dissolved in 5 g DI water) and H_2O_2 (dissolved in 5 g DI water) were fed by a syringe pump over 2 hours period under isothermal and adiabatic conditions. In KPS-initiated semi-batch polymerization, KPS solution (dissolved in 5 g DI water) was fed into the reactor in one shot 5 minutes before monomer feeding began. BMA monomer and SLS surfactant (dissolved in 10 g DI water) were fed into the reactor using a syringe pump over 2 hours under isothermal condition. The redox-initiated polymerizations were carried out with a starting temperature of 25 ºC and KPS-initiated polymerization was carried out at 70 ºC. The latex samples were taken out of the reactor every 20 minutes for particle sizing, conversion and molecular weight measurement. 1 gram of 1 % hydroquinone solution was added to each latex sample to prevent further reaction. Dialysis membrane tubing (3500 Daltons) was used to clean the latex to eliminate the influence of residual monomer on particle sizing.

Table 9.1: Recipes for Seeded Semi-batch Emulsion Polymerizations of BMA

Reactions	**S1**	**S2**	**S3**
Seed (g)	200.0 (R4)		
DI water (g)	200.0		
Feed	Feeding Time (2 h)		
BMA (g)	85.1 (feeding)		
SLS (g) *	0.50 (4.6 mM) (feeding)		
H_2O (g)	15.0 (feeding)		
Temperature (ºC)	25		70
Conditions	Isothermal	Adiabatic	Isothermal
KPS (g) *	-		0.175 (1.7 mM) (one shot)
A A (g) *	0.40 (6.0 mM) (feeding)		-
H_2O_2 (30%) (g) *	0.40 (9.4 mM) (feeding)		-

*Based on water

The Mettler RC1 reaction calorimeter was used to obtain the continuous reaction rate, conversion, and reactor temperature. The solids contents and conversions were measured gravimetrically after removing samples periodically from the reactor during the polymerization. The molecular weight was measured by GPC and TEM imaging with a negative staining technique was used for particle sizing to obtain accurate particle sizes. UV spectroscopy (Spetronic Genesys2) was used to detect the

monomer level present in the aqueous phase. The characterization methods are described in Chapter 2.

9.3 Results and Discussions

Time-dependent reaction rates and conversions can be accurately calculated from the heat of reaction measured with the Mettler RC1 reactor calorimeter. Batch emulsion polymerizations were described in the previous chapters, where the nucleation process is critical and can significantly influence the polymerization process and final particle properties. Therefore, a seeded semi-batch emulsion polymerization is described in this chapter, which can eliminate the influences of the nucleation process. The results for the seeded semi-batch reactions are shown in Table 9.2.

Table 9.2: Results of Seeded Semi-batch Emulsion Polymerization Reactions of BMA

Sample	R4	S1	S2	S3
Solids	20.24%	24.98%	24.89%	24.89%
Conversion	99.6%	99.5%	99.0%	97.5%
Coagulum	0.3%	0.3%	0.1%	0.1%
M_N (g/mol)	132,000	159,100	227,000	150,200
M_W (g/mol)	367,100	1,965,800	1,790,800	632,200
MW PDI	2.78	12.36	7.89	4.21
D_n (nm)	43.1	61.0	59.8	59.7
D_v (nm)	43.4	61.5	60.2	60.0
D_w (nm)	44.0	62.5	60.9	60.8
SD (D_n) (nm)	3.6	5.6	4.6	4.8
PDI	1.02	1.02	1.02	1.02
Particle No (L^{-1})	2.48×10^{18}	2.50×10^{18}	2.64×10^{18}	2.67×10^{18}
N_p Ratio (Seed/Final)	-	1.01	1.06	1.08

The reaction rates of redox-initiated isothermal and adiabatic polymerizations (starting at 25 ºC) and KPS-initiated isothermal polymerization (70 ºC) are shown in Figure 9.1. Under monomer-starved feed conditions, monomer diffuses directly to the polymer particle through the aqueous phase and is polymerized. The low monomer concentration and limited surfactant concentration in the aqueous phase results in

negligible secondary nucleation. Since no new particles were formed during this process (refer to the particle number ratio of seed to final latex in Table 9.2, ~1:1 ratio), the reaction rate only depends on the monomer feed rate, rather than the concentration of initiator or particle number. Therefore, those three reaction rates all have similar values during the 2-hour feeding period because of the same monomer feed rates. From the reaction rate data, it is seen that the reactions are well-controlled under monomer-starved feed conditions, and they had high fractional conversion during the polymerization (shown in Figure 9.2). The reaction temperatures during the polymerization are shown in Figure 9.3. S1 and S3 are under good isothermal control, where the reaction temperatures are well maintained at 25 °C and 70 °C, respectively. S2 is well maintained under adiabatic conditions, where the reaction temperature increased with the monomer feed.

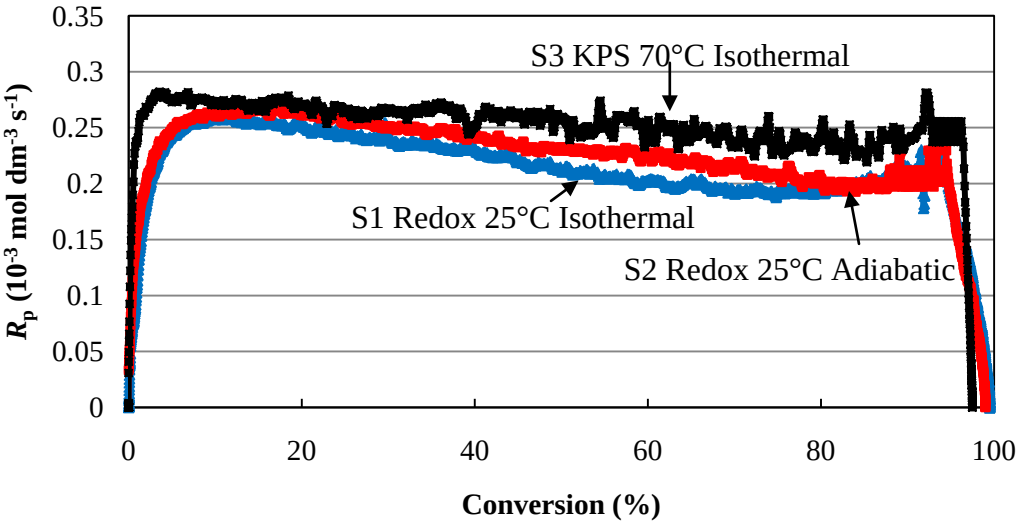

Figure 9.1: *Reaction rates vs. conversion of seeded semi-batch emulsion polymerizations of BMA.*

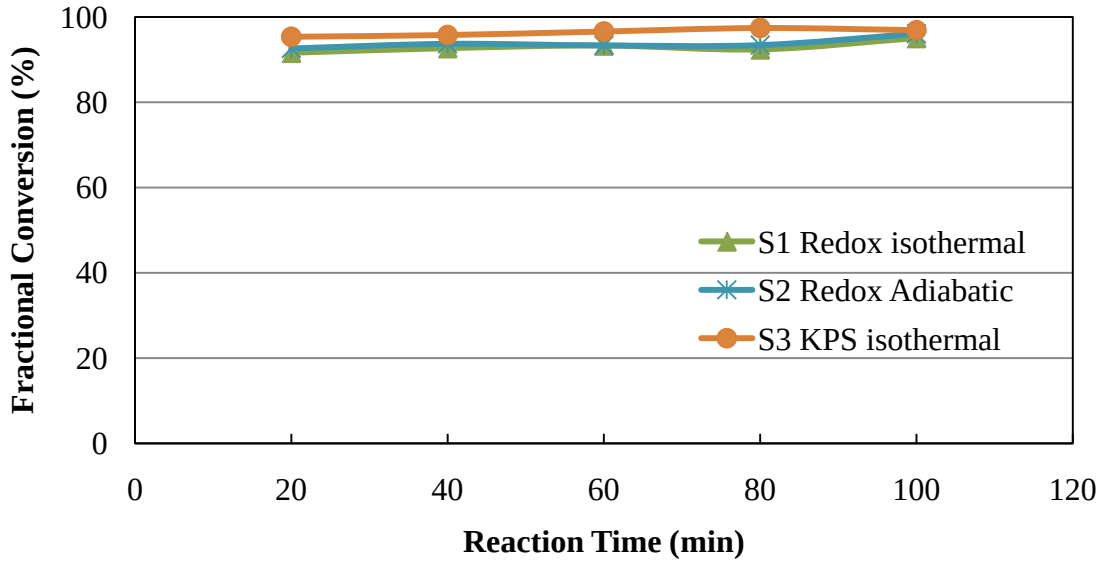

Figure 9.2: *Fractional conversion vs. reaction time of seeded semi-batch emulsion polymerizations of BMA.*

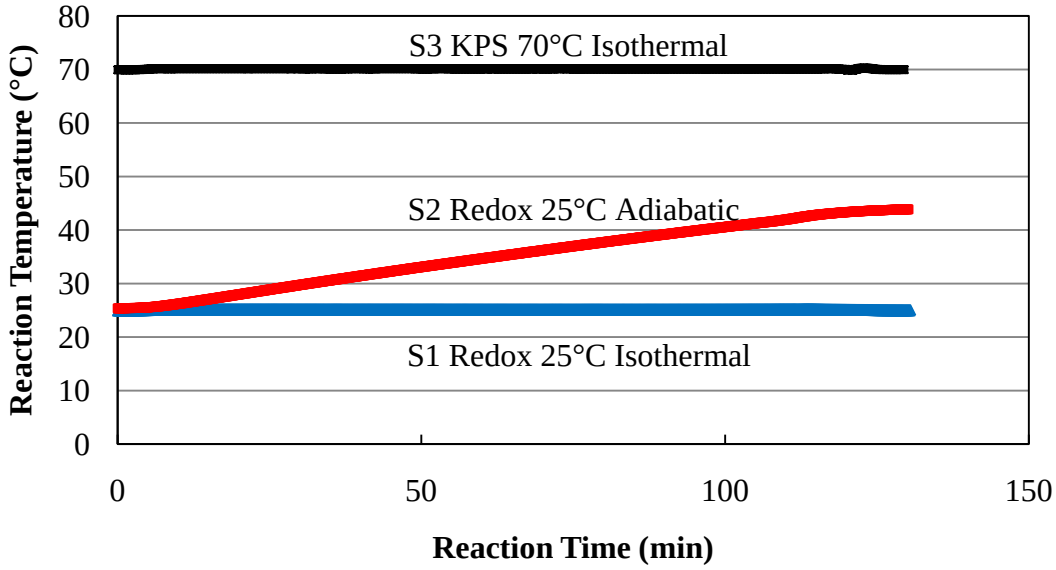

Figure 9.3: *Reaction temperature vs. reaction time of seeded semi-batch emulsion polymerizations of BMA.*

The final particle sizes were measured by TEM imaging, and the results are shown in Figures 9.4 and 9.5. The final particle sizes are larger than the seed particle size, and are similar for the three reactions. From calculations, the final particle number is almost in a one-to-one ratio from the initial seed to the final latex product (S1: 1.01, S2: 1.06 and S3:1.08), demonstrating that the final particles are formed from the initial seed particles. The difference in the total number of particles may be caused by a broadening of the particle size distribution. A slight difference in the latex particle size can result in a huge difference in the calculated particle number. Homogenous nucleation is limited by using the monomer-starved feed method, where insufficient monomer is present in the aqueous phase. Micellar nucleation is limited by the low free surfactant concentration (below cmc), where no micelles are present. The molecular weight is higher in the final latex than the seed (shown in Figure 9.6). The redox-initiated polymerizations are carried out at lower temperature (25 °C) and the radicals (OH•) are different, compared to the KPS-initiated process (70 °C and $SO_4\bullet^-$). The different temperatures result in different propagations and termination rates [8]. The different radicals may result in different radical capture rates and location of the radical in the particles. Therefore, the redox-initiated latex has higher molecular weight and broader molecular weight distribution compared to the KPS-initiated latex, probably resulting from the combination of the influences of different reaction temperatures and radical types.

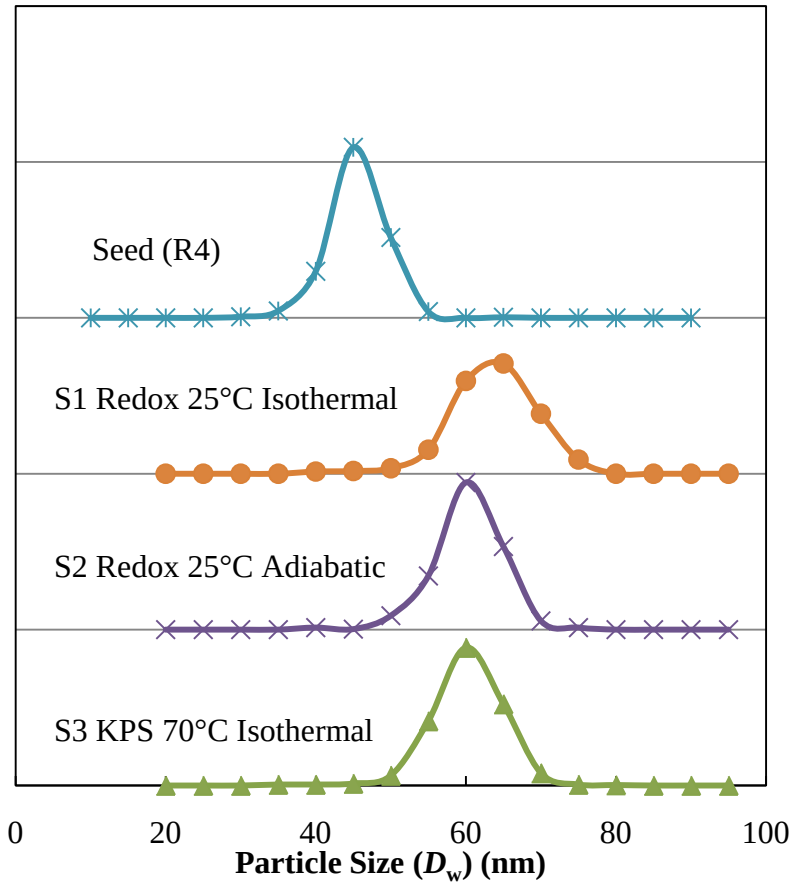

Figure 9.4: *Particle size and particle size distribution of seed latex and seeded semi-batch final latex.*

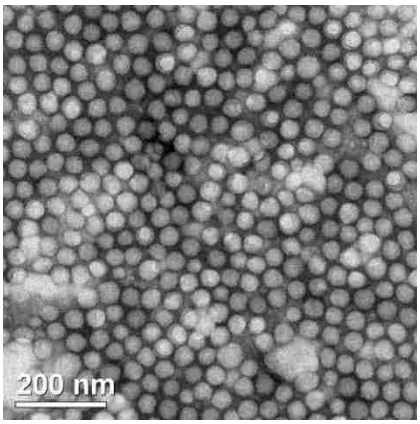

Seed (R4)

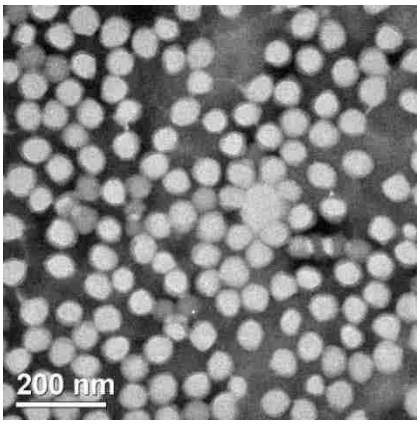

S1 (redox-initiated isothermal)

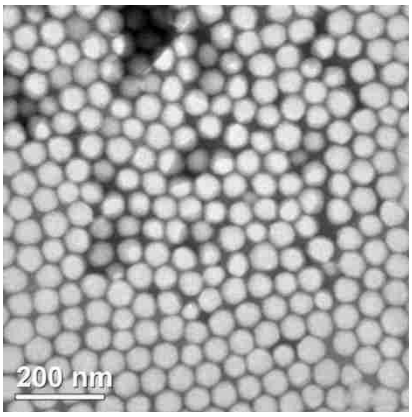

S1 (redox-initiated adiabatic)

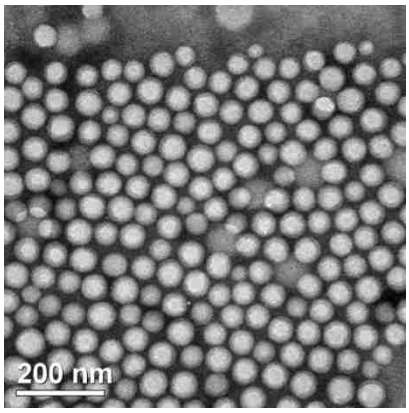

S3 (KPS-initiated isothermal)

Figure 9.5: *TEM images of latex particle of seed latex and semi-batch final latex.*

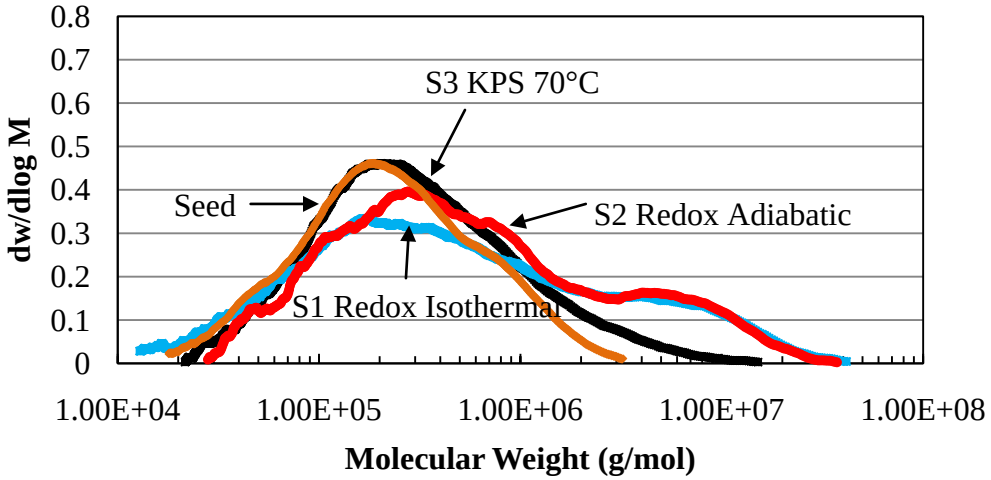

Figure 9.6: *Molecular weight of the latex obtained from seeded semi-batch emulsion polymerizations.*

The particle sizes and molecular weight of the latex polymer obtained during the polymerizations are shown in Figures 9.7, 9.8 and 9.9. In all three reactions (S1, S2 and S3), the latex particle size increased as monomer was fed into the reactor during the polymerization and exhibited similar final particle sizes. The molecular weights also increased as the monomer was fed into the reactor for all three reactions. In reaction S3, the molecular weight slightly increased during the polymerization. However, in the redox-initiated reactions S1 and S2, the molecular weight significantly increased during the first half hour of feeding, and then the molecular weight remained at a similar value with a slight increase during the next one and half hour of feeding monomer. During the polymerization, the reaction temperature was held constant (25 °C) under isothermal conditions (S1) and increased under adiabatic conditions (S2). Therefore, the reaction temperature may not be a key factor that

influences the molecular weight change in redox-initiated system. Higher and broader molecular weights in the redox-initiated polymerizations compared to the thermally-initiated system, may result from the influences of different radical types. It needs further investigation to study.

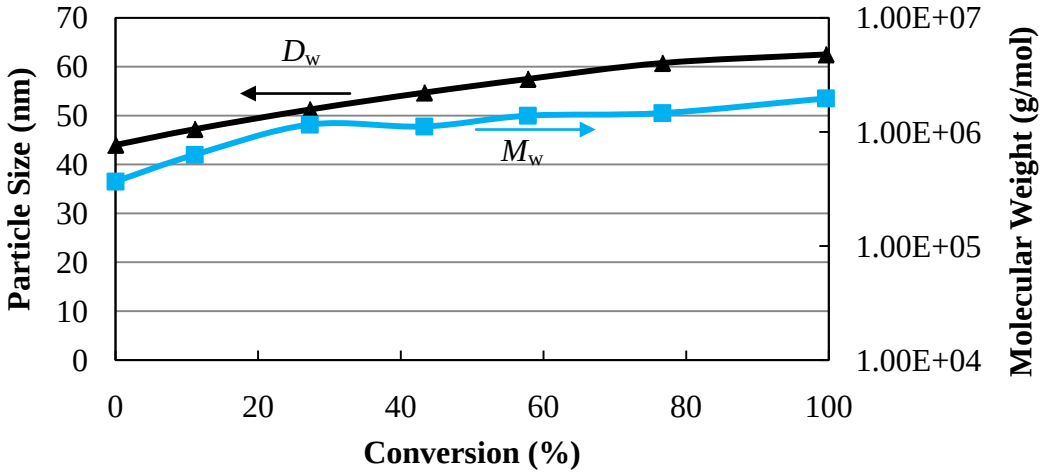

Figure 9.7: *Particle size and molecular weight of latex obtained during redox-initiated semi-batch emulsion polymerizations under isothermal conditions at 25 ºC (S1).*

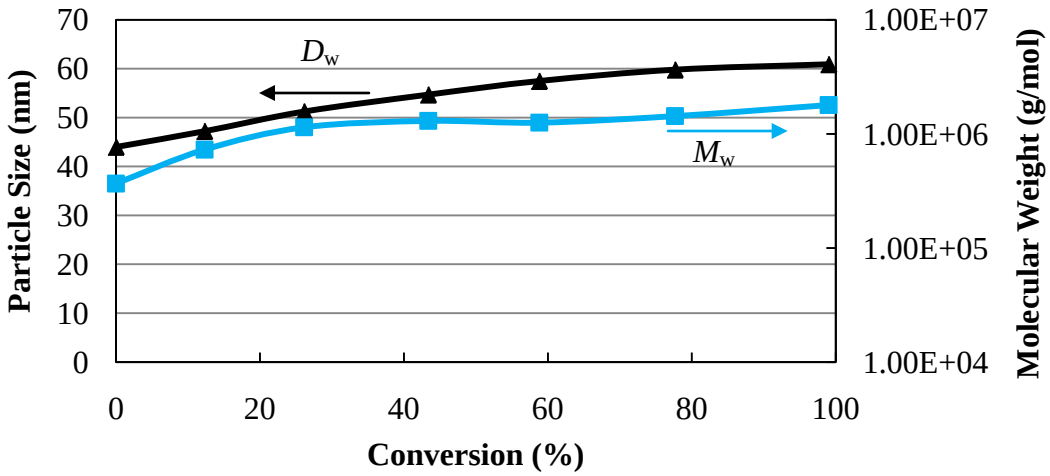

Figure 9.8: *Particle size and molecular weight of latex obtained during redox-initiated semi-batch emulsion polymerizations under adiabatic conditions with a starting temperature of 25 ºC (S2).*

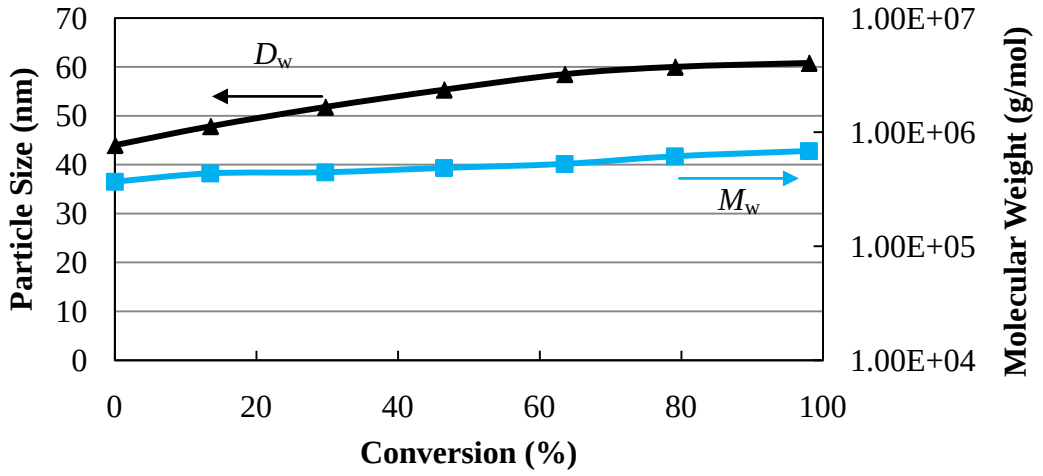

Figure 9.9: *Particle size and molecular weight of latex obtained during KPS-initiated semi-batch emulsion polymerizations under isothermal conditions at 70 ºC (S3).*

In the previous seeded semi-batch emulsion polymerizations, the monomer feeding rates are same, where the reactions have the same reaction rate and the same reaction time. Therefore, reactions with different monomer feeding rates are considered and theoretical calculations were carried out for comparisons between the isothermal and the adiabatic systems, and between the KPS-initiated and redox-initiated systems. Since the polymerization occurs primarily in the polymer particles, the rate of polymerization can be calculated from Eq. (9-1):

$$R_p = \frac{k_p [M]_p \bar{n} N_p}{N_A} \tag{9-1}$$

where k_p ($dm^3 \cdot mol^{-1} \cdot s^{-1}$) is the propagation rate constant, $[M]_p$ (mol/dm^3) is the concentration of monomer in the polymer particles, $\bar{n}$ is the average number of free-radicals per particle, N_p (dm^{-3}) is the number of particles per unit volume of water, and N_A is the Avogadro's number.

A zero-one system [11] was used to estimate the value of $\bar{n}$. In this system, a radical enters a particle, where either contains a growing chain or does not. If the particle contains a growing chain, the entry of a radical results in very rapid termination. If the particle does not contain a growing chain, the entry of a radical results in a growing chain. In this case, the steady-state value of the average number of radicals per particle ($\bar{n}$), is around 0.5.

The saturation concentration of BMA monomer in PBMA polymer particles [12] is 3.8 mol/dm^3. The BMA propagation rate constant is high (1241.6 $dm^3 mol^{-1} s^{-1}$ at 70 °C and 369.7 $dm^3 mol^{-1} s^{-1}$ at 25 °C) [13], which can be calculated from Eq. (9-2)

$$k_p = 10^{6.58}\,\mathrm{L\cdot mol^{-1}\cdot s^{-1}}\exp\left(\frac{-22.9\mathrm{kJ\cdot mol^{-1}}}{RT}\right) \quad (9\text{-}2)$$

Assuming that the reaction rate is the limiting step, the monomer diffusion time is negligible, sufficient radicals are present and fractional conversion is near 100%. Therefore, under monomer-starved conditions, the maximum monomer feed rate is the reaction rate at a saturation concentration of BMA in the PBMA particles. The conditions used for the calculation are as follows: 400 g latex with 10% solids content, 2.5×10^{18} L^{-1} as the particle number, 85 g BMA as monomer feed. The maximum feed rate under monomer-starved feed conditions can be calculated for isothermal conditions (25 °C and 70 °C) and adiabatic conditions (starting temperature 25 °C), which is shown in Figure 9.10. Under adiabatic conditions, the reaction heat can be utilized to increase the reactor temperature in reaction S2 (as shown in Figure 9.11). With a higher reactor temperature, the reaction rate is higher and the monomer feed rate can be higher. Under the maximum feed rate, the total reaction time is S1: 570 seconds, S2: 415 seconds, and S3: 170 seconds. Reaction S3 has the fastest reaction rate and the shortest reaction time, due to the highest reaction temperature. Therefore, the redox-initiated adiabatic seeded semi-batch emulsion polymerization can start the reaction at 25 °C (saving energy), and reduce the feed cycle (saving time).

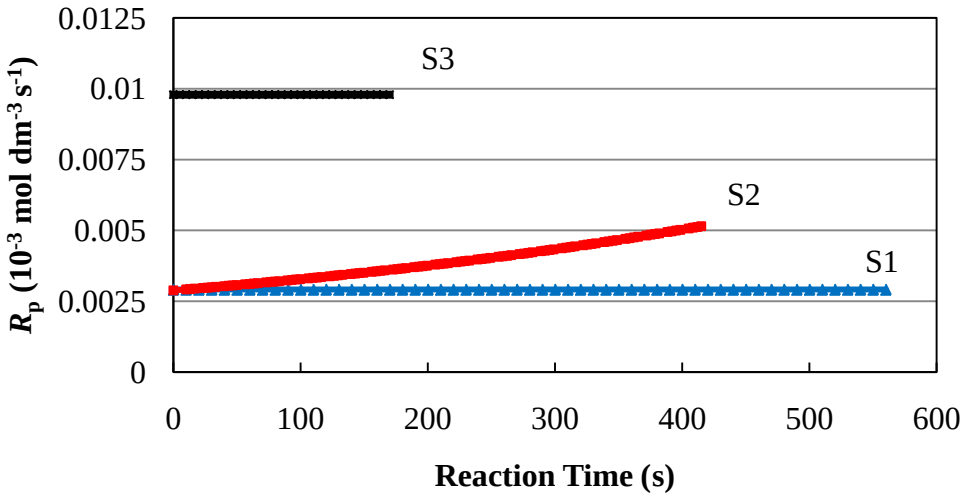

Figure 9.10: *Reaction rates during seeded semi-batch emulsion polymerizations of BMA (S1: under isothermal conditions at 25 ºC; S2: under adiabatic conditions starting at 25 ºC; and S3: under isothermal conditions at 70 ºC).*

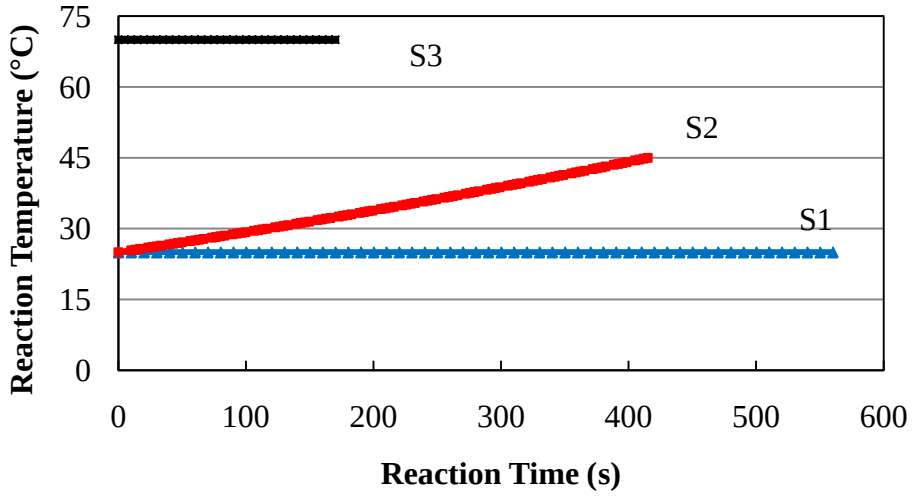

Figure 9.11: *Reaction temperatures during seeded semi-batch emulsion polymerizations of BMA (S1: under isothermal conditions at 25 ºC; S2: under adiabatic conditions starting at 25 ºC; and S3: under isothermal conditions at 70 ºC).*

9.4 Conclusions

Monomer-starved seeded semi-batch emulsion polymerizations have been investigated as a process to eliminate the influence of the nucleation process, compared to the batch emulsion polymerization. The particle size and conversion increased during the feed process, with a high fractional conversion. The particle number remains constant during the polymerization, where secondary nucleation is eliminated. The particle size difference between the redox-initiated latex and KPS-initiated latex are negligible. In the redox-initiated processes, the molecular weights are similar between isothermal and adiabatic conditions. The radicals (OH•) in redox-initiated polymerizations are different from the radicals ($SO_4•^-$) in the KPS-initiated process. The different radicals result in different radical capture rate and location of the radical in the particles. Therefore, the difference in molecular weight between the redox-initiated latex and KPS-initiated latex may be caused by the different reaction temperatures and different radicals. The seeded semi-batch redox-initiated emulsion polymerization can be carried out at room temperature to save energy. Under adiabatic conditions, the reactor temperature can be increased by reaction heat, where higher reaction rates can be achieved and reaction time can be shortened.

9.5 References

1 Hawkett, B. S., Napper, D. H. and Gilbert, R. G., *J. Chem. Soc., Faraday Trans.*, **76**, 1323 (1980)

2 Okubo, M., Ando, M., Yamada, A., Katsuta, Y. and Mastsumoto, T., *J. POLYM. SCI. POL. LETT*., **19**, 143 (1981)

3 Okubo, M., Katsuta, Y. and Mastsumoto, T., *J. POLYM. SCI. POL. LETT*., **20**, 45 (1982)

4 Nomura, M., Tobita, H. and Suzuki, K., *Adv. Poly. Sci*., **175**, 1 (2005)

5 Pohelein, G., in *Emulsion polymerization and emulsion polymers*. Lovell, P. A., El-Aasser, M. S. Ed., John Wiley and Son, Chichester, p 277 (1997)

6 Chern, C. S., *Prog. Poly. Sci*., **31**, 443 (2006)

7 Nomura, M., Tobita, H., Suzuki, K., and Lee, D. I., *Polymeric Microspheres: Science and Technology*, Kyoto University Press, Kyoto, Japan, p. 181 (2007)

8 Goikoetxea, M., Heijungs, R., Barandiaran, M. J. and Asua, J. M., *Macromol. React. Eng*., **2**, 90 (2008)

9 Mosebach, M. and Reichert, K., *J. Appl. Polym, Sci*., **66**, 673 (1997)

10 Zhang, C., Du, Z., Li, H. and Ruckenstein, E., *Polymer*, **43**, 2945 (2002)

11 Hawkett, B. S., Napper, D. H. and Gilbert, R.G., *J. Chem. Soc. Faraday Trans 1*, **76**, 1323 (1980)

12 Halnan, L. F., Napper, D. H. and Gilbert, R.G., J. *Chem. Soc. Faraday Trans 1*, **80**, 2851 (1984)

13 S. Beuermann, M. Buback, T. P. Davis, R. G. Gilbert, R. A. Hutchinson, A. Kajiwara and B. Klumperman, Macromol Chem. Phys., **201**, 1355 (2000)

Chapter 10

Conclusions and Recommendations

10.1 Conclusions

In this dissertation research, ‘adiabatic’ redox-initiated emulsion polymerization has been studied as a green process: the heat of polymerization can be utilized to increase the system temperature, enhance the reaction rate, and reduce the cost for the heating process compared to conventional emulsion polymerizations. TEM imaging was used to measure the latex particle diameter. The Mettler RC1 reactor was used to study the details of the polymerization process. KPS was used as the thermal initiator, and H_2O_2 and ascorbic acid was used as the redox initiator. In the redox-initiated systems, ferrous sulfate was added as catalyst for the redox initiator and NaCl was added as electrolyte to control the latex viscosity. Emulsion polymerizations were carried out in batch or as seeded semi-batch emulsion processes under isothermal and adiabatic conditions. The nucleation mechanism and polymerization kinetics were investigated. Miniemulsion polymerizations were further carried out as a comparison to conventional emulsion polymerization. The fractional SLS surfactant surface coverage was calculated and the mechanical stability of latex was measured.

In the batch emulsion polymerization, the thermal-initiated latexes have a larger particle size and higher molecular weight compared to the redox-initiated

latexes. Employing higher surfactant concentrations can decrease the particle size and increase the molecular weight. Higher initiator concentrations can decrease the particle diameter as well as the molecular weight. Higher solids content can increase the particle size, but had no significant influence on the molecular weight. The reaction rate, which was measured with the Mettler RC1 reactor, exhibits a large difference between the KPS-initiated and the redox-initiated process. Three intervals are observed in the KPS-initiated process. However, different shapes of intervals are observed in the redox-initiated process with much higher reaction rate. From the differences in particle number and reaction rate, micellar nucleation is the main nucleation mechanism for the KPS-initiated polymerization, and both homogeneous nucleation and micellar nucleation are significant in the redox-initiated polymerization. Homogenous nucleation rates were investigated based on the Fitch-Tsai theory and the Ugelstad-Hansen theory. The Fuchs stability factor for latex particles during the polymerization and the oligmer radical concentrations in water are calculated, which agree with the Fitch-Tsai theory, but are not compatible with the Ugelstad-Hansen theory, due to the inaccuracy of Fuchs stability factor for a charged radical colliding with a latex particle.

.

Miniemulsion polymerizations were carried out to study the influence of the high radical flux resulting from the redox initiator system. Compared with micellar nucleation in the KPS-initiated emulsion system and both micellar and homogenous nucleation in the redox-initiated emulsion system, droplet nucleation is the main

nucleation mechanism in miniemulsion polymerization and high radical flux has little influence on the nucleation process.

The surface tensions of the aqueous phase of the latex samples were measured and the free surfactant concentration and the fractional surfactant surface coverage on the PBMA particles with adsorbed SLS surfactant molecules were calculated. The mechanical stability of the redox-initiated latex was measured with a blender test. The critical surfactant surface coverage needed to maintain latex stability is 19% for the redox-initiated latex and 39% for the KPS-initiated latex. The redox-initiated latex particles require less surfactant surface coverage compared to the KPS-initiated latex particles to maintain the same mechanical stability for the reason that extra hydroxyl groups were introduced on the latex particle surface by redox initiator (H_2O_2) decomposition and improved the latex stability.

Redox-initiated adiabatic batch emulsion polymerizations have been investigated as a process to produce latexes with a shorter cycle time and improved scalability, compared to the isothermal process. Adiabatic batch processes were carried out in the Mettler RC1 reactor with minimal heat loss. The reactor temperature increased with conversion during the polymerization and reaction time is shorter under the adiabatic conditions compared with the isothermal conditions. Higher starting reaction temperature and higher solids content can result in a higher reaction rate under the adiabatic and the isothermal conditions. The difference in the molecular weights of latexes obtained under the isothermal and adiabatic conditions is negligible.

Compared to the batch emulsion polymerization, monomer-starved seeded semi-batch emulsion polymerization has been investigated as a process to eliminate the influence of the nucleation process. The particle size and conversion increased during the feeding process, with a high fractional conversion. The particle numbers remain constant during the polymerization indicating that secondary nucleation is eliminated. However, there is a significant difference in the molecular weights between the redox-initiated latex and the KPS-initiated latex because that the radicals are different in those two systems. The seeded semi-batch emulsion polymerization under the adiabatic condition can also save the energy and reduce the time.

10.2 Recommendation

1 Anionic surfactant (SLS) was the only surfactant used in this work. Nonionic surfactant (i.e., Triton X-100) can be considered as an alternative in the redox-initiated system with less dependence on the electrolyte concentration. Further, the combination of anionic surfactant and nonionic surfactant can result in higher latex stability, and deserves more investigation.

2 *n*-Butyl methacrylate is the only monomer used in this work. Monomers with different reaction rate constants (i.e., styrene) and water solubilities (i.e., methyl methacrylate) compared to BMA, and copolymerization of different monomers should be considered in the future to study the influence on homogeneous nucleation.

3 Hydrogen peroxide and ascorbic acid are the only redox initiator system used in this work. Different redox initiators should be considered in the future to study the effect of different end groups.

4 The hydroxyl group and sulfate group concentrations on the latex particles can be determined by titration methods. Zeta potential on the redox-initiated and KPS-initiated latex particles at different pH values can be measured. Those data can be used to further study the latex stability.

5 Different strategies using the redox initiator and adiabatic conditions can be considered in future studies, such as the combination of a seed stage using the redox-initiated adiabatic condition and a feed stage using the KPS-initiated isothermal condition.

Appendix A

Reduction-oxidation Reaction between Hydrogen Peroxide and Ascorbic Acid

The reduction-oxidation reaction between hydrogen peroxide and ascorbic acid is very complicated. The main reactions generating radicals [1, 2] are shown in Eq. (A-1) and (A-2). The radical generation rate was discussed in Chapters 4 and 5.

$$Fe^{2+} + H_2O_2 \rightarrow Fe^{3+} + OH^- + OH\bullet \quad \text{(A-1)}$$

$$2Fe^{3+} + 2OH^- + AA \rightarrow 2Fe^{2+} + DHA + 2H_2O \quad \text{(A-2)}$$

However, there are many side reactions that occur in this redox reaction. The reactions between ferrous ions and hydrogen peroxide are shown in Eq. (A-3) to Eq. (A-7) and the reactions between hydrogen peroxide [3] itself are shown in Eq. (A-8) and Eq. (A-9). The reactions between ferrous ions and ascorbic acid [4] are shown in Eq. (A-10) to Eq. (A-15), where AA is dehydroascorbic acid. Many of those side reactions can generate radicals. The radical generation rate calculation in this study is based on the main reactions only, and side reactions are not considered. Therefore, the real radical generation rate may be different from the calculation results.

$$OH\bullet + Fe^{2+} \rightarrow Fe^{3+} + OH^- + Fe^{3+} \quad \text{(A-3)}$$

$$H_2O_2 + Fe^{3+} \rightarrow FeOOH^{2+} + H^+ \quad \text{(A-4)}$$

$$FeOOH^{2+} \rightarrow Fe^{2+} + HO_2\bullet \quad \text{(A-5)}$$

$$Fe^{2+} + HO_2\bullet \rightarrow Fe^{3+} + HO_2^- \quad \text{(A-6)}$$

$$Fe^{2+} + HO_2\bullet \rightarrow Fe^{3+} + H^+ + O_2 \quad \text{(A-7)}$$

$$OH\bullet + H_2O_2 \rightarrow H_2O + HO_2\bullet \quad \text{(A-8)}$$

$$OH\bullet + OH\bullet \rightarrow H_2O_2 \quad \text{(A-9)}$$

$$AAH_2 \rightarrow AAH^- + H^+ \quad \text{(A-10)}$$

$$AAH \rightarrow AA\bullet^- + H^+ \quad \text{(A-11)}$$

$$AAH^- + Fe^{2+} \rightarrow FeAAH^+\bullet \quad \text{(A-12)}$$

$$FeAAH^+\bullet \rightarrow Fe^{2+} + AAH\bullet \quad \text{(A-13)}$$

$$Fe^{2+} + AA\bullet^- \rightarrow AA + Fe^{2+} \quad \text{(A-14)}$$

$$FeAAH^+\bullet \rightarrow FeAA\bullet + H^+ \quad \text{(A-15)}$$

References

1 Jellinek, H. G., *Pure Appl. Chem.*, **4**, 419 (1962)

2 Deutsch, J. C., *Anal. Biochem.*, **255**, 1 (1998)

3 Malik, P. K. and Saha, S. K., *Sep. Purif. Technol.*, **31**, 241 (2003)

4 Grinstead, R. R., *J. Am. Chem. Soc.*, **82**, 3464 (1960)

Appendix B

Zeta Potential of KPS-initiated and Redox-initiated Latex from Batch Emulsion Polymerization

Zeta potential is a term for the electrokinetic potential in colloidal systems, which is the electric potential in the interfacial electrical double layer at the location of the slipping plane versus a point in the bulk fluid away from the interface. The value of zeta potential is very important, because that it can indicate the stability of colloidal dispersions. Therefore, the zeta potential of the KPS-initiated and the redox-initiated latexes from batch emulsion polymerization was measured by Malvern Zetasizer Nano. The solids content of the samples for measurement was diluted to 50 mg/L with a background electrolyte concentration of 10 mM NaCl. The results for the KPS-initiated latexes with different recipes are shown in Tables A.1, A.2, and A.3. The results for the redox-initiated latexes with different recipes are shown in Tables A.4, A.5, and A.6.

Table A.1: Zeta Potential of KPS-initiated Latex

with Different Surfactant Concentrations

Samples	SLS (mM)	Zeta Potential (mV)
T1	4.0	-38.3
T2	6.0	-38.3
T3	7.8	-34.5
T4	12.0	-38.8
T5	20.0	-40.5
T6	40.0	-48.7

Table A.2: Zeta Potential of KPS-initiated Latex with Different KPS Concentrations

Samples	KPS (mM)	Zeta Potential (mV)
T7	4.0	-39.6
T8	6.0	-37.4
T4	7.8	-38.8
T9	20.0	-38.2
T10	40.0	-39.0

Table A.3: Zeta Potential of KPS-initiated Latex with Different Solids Contents

Samples	Solids Content (%)	Zeta Potential (mV)
T11	5	-42.8
T12	10	-37.7
T4	20	-38.8
T13	30	-31.7

Table A.4: Zeta Potential of Redox-initiated Latex

with Different Surfactant Concentrations

Samples	SLS (mM)	Zeta Potential (mV)
R1	4.0	-42.2
R2	6.0	-39.9
R3	7.8	-39.9
R4	12.0	-37.9
R5	20.0	-41.0
R6	40.0	-25.8

Table A.5: Zeta Potential of Redox-initiated Latex with Different H_2O_2 Concentrations

Samples	H_2O_2 (mM)	Zeta Potential (mV)
R7	1.0	-35.8
R8	2.0	-36.0
R9	4.0	-42.4
R4	7.9	-37.9
R10	15.8	-35.4

Table A.6: Zeta Potential of Redox-initiated Latex with Different Solids Contents

Samples	Solids Content (%)	Zeta Potential (mV)
R13	5	-28.0
R14	10	-28.9
R4	20	-37.9
R15	30	-36.4

From the zeta potential results of KPS-initiated and redox-initiated latex, they have similar absolute values, which are around ~ 30 mV to ~ 40 mV. At this level of zeta potential, the latex particles can be considered as moderately stable. Since the samples are diluted during the measurement, the surfactants can be considered to be all detached from the particle surface at this situation. Therefore, only the end groups,

which were introduced by radicals, on the particle surface contribute to the values of the zeta potential. In the KPS-initiated latex, the charged group (SO_4^{2-}) is located on the particle surface, and in the redox-initiated latex, the hydroxyl group (OH) is on the particle surface. The dissociation of the counterions of the charged group (SO_4^{2-}) can contribute to the zeta potential greater than the hydroxyl group (OH). However, the values of zeta potential for KPS-initiated and redox-initiated latex particles are similar (~ 30 mV). This indicates that the hydroxyl groups (OH) also have a strong contribution to the electrokinetic phenomena, which can improve the stability of redox-initiated latex. The origin of the charge for hydroxyl group can be the result of either the preferential adsorption of hydroxyl group or contact electrification between phases (latex polymer and water) [1-3].

Preferential Adsorption of Hydroxyl Group

The reason for this preferential adsorption on a neutral surface is caused by polarization, which is the interaction of the ion-induced dipoles. When an ion is near a surface, it will induce a separation of charge (dipole) in the atoms of surface, and those dipoles exert an attraction force on the ions. Therefore, the stabilizing charge can be attributed to the hydroxyl group on the surface.

Contact Electrification between Phases

Two phases in contact may have different affinities for electrons, and then the flow of electrons from one phase to the other can lead to a potential difference between the two phases. The contact charge exchange is attributed to the presence of local intrinsic molecular states in polymers and water. The presence of both acceptor and donor states provides a definition for the polymer chemical potential, Fermi level, where the energy is divided into two states. Since the Fermi levels of the polymer and water are close, electron transfer will take place.

References

1 Kamel, A. A., Ma, C. M., El-Aasser, M. S. and Micale, F. J., *J. Disper. Sci. Technol.*, **2**, 315 (1981)

2 Haydon, D. A., *Biochm. Biophys. Acta*, **50**, 457 (1961)

3 Taylor, A. J. and Wood, F. W., *Trans. Faraday Soc*., **53**, 523 (1957)

VITA

Shi Wang was born on June 11, 1980 in Shenyang, China. He is the only child of Xiaoxu Shi and Lihong Deng. He received his Bachelor's and Master's degrees in Chemical Engineering from Tianjin University, Tianjin, China in 2002 and 2005, respectively. In 2006, he arrived at the Department of Chemical Engineering at Lehigh University to study for his Ph.D. and joined the Emulsion Polymers Institute (EPI). His research focused on adiabatic redox-initiated emulsion polymerization processes. Shi also completed several side projects besides his thesis research, including a two year polymerization scale-up project, in cooperation with Dynalene Inc. He gave presentations at the 2010 AIChE annual meeting and at the 2012 ACS annual meeting. He was awarded with the Best Poster Award at the 2011 International Polymer Colloids Group Conference and the Excellence in Polymer Science & Engineering Award by the Society of Plastic Engineers in 2011 for his excellent work in the emulsion polymer area.

Shi Wang has contributed to many community services. He has worked as a coordinator in the Lehigh Chinese Students and Scholars Association in 2007, and as the vice president of the same association in 2008 and earned the Multicultural Life in Lehigh Award in 2009.

Shi Wang married Aishuang Xiang in 2011 and they have a lovely son, Elwin Wang.